UNIVERSITÀ DEGLI STUDI DI PARMA

Dottorato di ricerca in Scienze Chimiche

Ciclo XXV (2010-2012)

Innovative materials and approaches for mass spectrometry: advances and applications

Coordinatore
Prof. G. Predieri

Tutori
Prof. M. Careri
Prof. A. Rossi

Dottorando
Andrea Penna

2013

To my family

Science is the belief in the ignorance of experts.

Richard Phillips Feynman

Index

Introduction **page 9**

Chapter 1.
Surface modifications for desorption electrospray ionization-mass spectrometric investigations **page 13**

1.1. Investigation of novel sol-gel hydrophobic surfaces for desorption electrospray ionization-mass spectrometry analysis page 21

1.2. Synthesis and characterization of xerogel hydrophobic surfaces on flat SiO_2 for an in-depth investigation on reaction mechanisms page 35

1.3. Synthesis and characterization of thin films on SiO_2 flat surfaces by adsorption of alkylsiloxanes in non-polar solvents page 49

1.4. Synthesis and characterization of tailored surfaces as supports for surface effects investigations in desorption electrospray ionization-mass spectrometry page 65

1.5. Investigation on pneumatic aspects in desorption electrospray and electrospray ionization page 79

Chapter 2.
Novel applications of MS in proteomics: development of analytical methods for multi-allergen determination in food by liquid chromatography-tandem mass spectrometry **page 87**

2.1. Particle-packed column versus silica-based monolithic column for liquid chromatography–electrospray-linear ion trap-tandem mass spectrometry multi-allergen trace analysis in foods page 89

2.2. A rapid size-exclusion solid phase extraction step for enhanced sensitivity in multi-allergen determination in dark chocolate and biscuits by liquid chromatography tandem mass spectrometry page 101

Introduction

Anyone who doesn't take truth seriously in small matters
cannot be trusted in large ones either.
Albert Einstein

Mass spectrometry (MS) was born in the mid-19th century within studies involving gas discharges. In that context the ability of converting light into positive ions and electrons and the further development in the separation of those ions lead to the construction of the first mass spectrometers. The use of mass spectrometry began with study of isotopes, also in the Manhattan Project for the development of the atomic bomb. From that time this technique has gained importance in physics and chemistry, but a great step forward was after the introduction, in the mid-20th century, of electrospray ionization (ESI)[1] and matrix-assisted laser desorption ionization (MALDI)[2] interfaces, which gave the possibility of analyzing biomolecules and large organic molecules, practically impossible by conventional ionization techniques for that time. The ability of these ion sources of producing intact ions in vacuum from large and complex species in solution is widely known and was quickly recognized by awarding the Nobel Prize to Fenn and Tanaka in 2002 “for the development of methods, for identification and structure analyses of biological macromolecules [...] for their development of soft desorption ionisation methods for mass spectrometric analyses of biological macromolecules”. In the past decade, MS has experienced consistent instrumental improvements that enable research applications unheard of before. So far ESI has been recognized as great additional tool for scientific development of a huge range of different disciplines, ranging from physics to materials science, to chemistry and biological sciences. The great abilities of gaining huge insights into large and often fragile polar molecules, such as polymers and biomolecules like nucleotides and proteins has drawn huge investments, as these techniques can be used in completely different fields of application. Given the potentiality of gaining further knowledge in life sciences, the popularity of ESI and MALDI interfaces has led to huge technological developments, in term of new interfaces, analyzers, detectors as well as calculators and software. Furthermore, coupling MS with chromatographic techniques has ensured its widespread use taking advantages from such reliable separation techniques.

Taking inspiration from the aforementioned interfaces, in the last decade ionization techniques called “ambient ionization” has raised their diffusion for the possibility of generating ions from outside the mass spectrometer without or with little sample preparation or separation. The most important progenitor of those techniques is the atmospheric pressure (AP) version of MALDI developed by Laiko *et al.*[3], with the

possibility of coupling both electrospray and MALDI spectral measurements on the same instrument. In this context, the possibility of combining advantages from in-solution ionization, happening in ESI ionization, to those of desorption ionization (DI) techniques has been widely investigated and a wide list of ambient desorption ionization techniques have been recently reviewed and listed in order of publication by Venter *et al.*[4] It was demonstrated how it was possible to combine ESI and laser-based techniques, as well as plasma, atmospheric pressure chemical and photoionization to carry out a reliable "ambient" analysis. Among them, by far the most studied and used, being defined an atmospheric pressure version of SIMS, was desorption electrospray ionization-mass spectrometry (DESI-MS),[5] proposed for the first time in 2004 by Cooks' group. This ion source will be further discussed in the next pages as a predominant topic of this Ph.D. work.

This Ph.D. work has been divided into two main parts. The first part is composed in turn by five chapters concerning application of surface modifications to address surface and pneumatic phenomena occurring in a DESI ion source. The second part states about innovative approaches for proteomics in food: in particular, novel high-performance liquid chromatography (HPLC)-MS methods for the quantitative analysis of hidden allergenic proteins in food were devised.

In detail, in the first chapter it is explained how a sol-gel mixture of tetraethoxysilane (TEOS) and octyltriethoxysilane (OTES) was used to prepare dip-coated hydrophobic xerogel films and then characterized by means of atomic force microscopy (AFM) and surface free energy measurements. It is showed how different analytical responses were observed when different solvent mixture deposition procedures and solvent spray compositions were investigated.

The second chapter describes an in-depth examination of surface modifications by sol-gel aqueous chemistry presented in the first chapter of this manuscript. Surface modifications were carried out by hydrolysis and polycondensation of silicon alcoxyde precursors, i.e. TEOS and OTES followed by xerogel film synthesis on Si(100) wafers covered by an oxide layer, in order to gain insights into the surface chemistry related to the film synthesis. Conclusions were drawn on the possibility of comparing DESI-MS results by using surfaces obtained by different reaction pathways.

In the third chapter a preliminary investigation was carried out to evaluate the possibility of tailoring surface free energy in a wider range with respect to that obtained by using the xerogel films above described, by depositing different alkylsilanes with self-assembling procedures. It was shown how it was possible to obtain morphologically homogeneous and thickness-controlled films in the nm-range, as demonstrated by instrumental surface characterizations, such as AFM, ellipsometry and contact angle goniometry.

The fourth chapter presents for the first time the use of functionalized glasses as supports for DESI-MS investigations. Surface effects in term of DESI efficiency were carried out by using functionalized surfaces obtained depositing three different silanes (3-mercaptopropyltriethoxysilane, MTS,

octyltriethoxysilane, OTES and 1H,1H,2H,2H-perfluorooctyltriethoxy-silane, FOTES) from toluene solution onto standard glass slides. Surface characterization was carried out by contact angle goniometry, atomic force microscopy and X-ray photoelectron spectroscopy (XPS). Low-molecular weight compounds were used as analytes and surface effects are discussed together with those of sprayer potential in term of ion formation yield.

In the fifth chapter, which completes the first part of the thesis, a study of pneumatic effects was carried out with ESI and DESI interfaces by setting the sprayer potential in order to no ESI ionization occurs. Further confirmation about the physico-chemical processes involved in the ion formation mechanism were obtained by exploring ESI parameters effects on the analyte ionization. It was confirmed that DESI phenomenon is mainly pneumatically driven and it is related to analyte solubility in the sprayed solvent. At last, it was confirmed that in a DESI interface, like in ESI, ion formation is ruled by thermodynamics and proton transfer is preferred toward the species with the highest gas phase basicity.

The second part of this manuscript is divided into two more chapters (sixth and seventh) and the development of analytical methods for the analysis of five hidden allergens in foodstuff, i.e. cashew-nut, hazelnut, almond, peanut and walnut is presented. In detail, the sixth chapter describes, for the first time in literature, an innovative buffer-based extraction method for the simultaneous analysis of five nut allergens in cereals and biscuits using liquid chromatography-electrospray-linear ion trap-tandem mass spectrometry (LC-ESI-LIT-MS). Reversed-phase (RP) chromatography was used for the analytical separation and selected reaction monitoring (SRM) MS as detection technique. Chromatographic and mass spectrometric performances were evaluated in term of Eurachem validation guidelines.

In the seventh and last chapter of this manuscript it is presented how it was possible to enhance sensitivity for the simultaneous determination of the aforementioned five nut allergens in biscuit and in dark chocolate by a LC-ESI-MS^2 approach. A very fast and efficient separation of marker peptides with selected reaction monitoring detection was obtained.

1 Surface modifications for desorption electrospray ionization-mass spectrometric investigations

The introduction of innovative methods, expanding application of mass spectrometry to diverse scientific areas has amounted impressive progresses in chemistry, extending the types of samples and compounds that can be analyzed. However, an awkward feature of MS is that sample must be introduced into vacuum or into an inaccessible region closely coupled to the vacuum system to obtain ions suitable for mass analysis. Electrospray ionization was the first technique that gave the possibility of analyzing liquid-phase sample in an atmospheric pressure interface.

As far as the analysis of condensed phases is concerned, DI methods have been developed and have reached so far a great scientific impact, because molecules, rather than nebulized from a solution typical for an ESI experiment, are embedded in a substrate. All DI methods involve the impact on condensed-phase samples of projectiles, which include photons (matrix assisted laser desorption ionization, MALDI), translationally excited atoms (fast atom bombardment, FAB),[6] and energetic ions (secondary ion mass spectrometry, SIMS),[7] that usually require a high-vacuum environment. Vacuum conditions may be a great limiting factor, as they can alter native conditions of a sample.

After the introduction of AP-MALDI in 2000, in the last decade a huge variety of soft techniques has been proposed, taking advantage from the use of an atmospheric interface to generate gas-phase ions. The possibility of combining advantages from in-solution ionization, occurring in ESI ionization, to those of DI techniques has been widely investigated and a wide list of ambient desorption ionization techniques have been reviewed and listed in order of publication by Venter *et al.*,[4] having ability to record mass spectra of ordinary and not treated samples in their native environment, making MS qualitatively more valuable and open to many new areas of application. Ambient desorption ionization techniques successfully bridge the gap between the ambient environment, where condensed-phase samples are present, and the vacuum system, where analysis takes place, without either none or minor sample manipulation and preparation.

Among ambient DI interfaces so far the most studied is DESI-MS,[5] proposed in 2004 by Cooks' group. This direct probe exposure method, based on ESI, can be used on samples under ambient conditions with little or no sample preparation. The principle is illustrated in Figure 1. An ionized stream of solvent

that is produced by an ESI source is sprayed on the surface of the sample under investigation. The exact mechanism has yet to be completely elucidated, but from literature it is accepted that charged droplets and ions of solvent desorb and extract some sample material and bounce off the surface towards the inlet capillary of an atmospheric pressure interface of a mass spectrometer. In detail, the surface is commonly exposed to a pneumatically-assisted ESI flow, in presence of a heated nebulizer gas, normally nitrogen. The analytes undergo jets of charged solvent droplets with diameters less than 10 µm, commonly at velocities typically in excess of 100 m/s. As analytes are usually present in the solid state on the surface they are thus solubilized into a thin solvent layer at the interface, a process which takes place in a time scale of hundreds of milliseconds.[8,9]

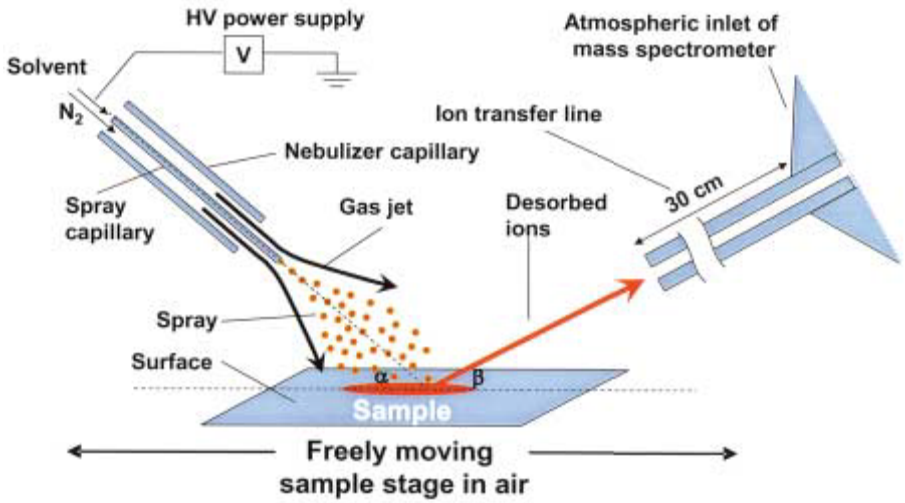

Figure 1. Schematic of a typical DESI experiment: the sample solution is deposited from solution and dried onto a standard PTFE surface and then sprayed with a mixture of solvents for the MS analysis. Reproduced from Takàts *et al.*[5] with kind permission

Desorption of analyte species into the gas phase takes place by subsequent off-spring droplets ejection by the solvent layer.[10] Dissolution of the analyte in a thin liquid film of solvent charged droplets is strongly suggested by investigations on samples of peptides or proteins which produce multiply charged ions,[11] as well as experiments on DNA nucleobases.[12] Furthermore, from measurements of droplet size and velocity distributions, isolated gas-phase ions are accepted to be formed after a droplet pick-up mechanism, akin to what observed relative to the ion formation in an ESI interface.[13,14] Further studies concerning DESI mechanism confirmed the hypothesis of a surface pre-wetting by initial droplets and surface analytes dissolution or collection in this localized solvent layer. Later-arriving droplets impact this surface solvent-layer and break it up, creating numerous off-spring droplets containing the material originating from the solvent layer including the dissolved analytes. Thus, analyte desorption occurs by momentum transfer in the form of charged sub-µm droplets that are then ionized by ESI mechanisms.[15,16]

This aspect is confirmed by similarities in MS spectra with respect to ESI, including multiply charged ions, non-covalent complexes and metal adducts.[17]

In a DESI ion source sample may be exposed as such or deposited on a sample holder, which may be made of any material, conducting or non-conducting, provided that it does not contribute to background. Interesting features are the possibility of introducing reactive substances in the sprayer, to react with the sample (known as reactive-DESI),[18] the possibility of using DESI with thin-layer chromatography[19] and, finally, the most important, to be used to map the position of analytes on native surface sample, to generate multivariate chemical maps from hyperspectral data.[20] A wide range of molecules can be analyzed by the use of these techniques, ranging from small non-polar to large ones, like proteins. A huge range of applications has recently been reviewed by Cooks' group.[4]

In this first part of the manuscript it is presented a thorough study on fundamental physico-chemical processes in a DESI ion source, concerning how pneumatic and surface effects affect ion formation yield, to improve basic knowledge of such a versatile new soft ionization technique. It is laid out how it was possible to carry out different surface modifications by the use of sol-gel and self-assembly methods, in order to obtain tailored materials for MS investigations.

The sol-gel process

The sol-gel process is nowadays one of the most studied approaches to obtain high-quality glassy and ceramic materials. Interest in this topic has grown so far for the possibility of obtaining high purity materials in a controlled environment, with several advantages with respect to traditional methods in such a way to control porosity, mechanical rigidity, refractive index, dielectric constant, optical clarity, hydrophobicity, and chemical and optical functions.[21] The whole process relies on the hydrolysis and polycondensation of alkoxide precursors evolving from a dispersion of colloidal particles, i.e. a sol to an interconnected rigid network, i.e. a gel, which then undergoes aging and drying.[22] Alcoxydes, namely chemicals with the general formula $M(OR)_n$ are often used in this process, where R is an alkyl moiety and M is a metal or a semi-metal. Alcoxyde molecules undergo reactions of hydrolysis and condensation (Scheme 1.1) and the rate constants of the two simultaneous reactions are known to strongly affect the quality of the final product. Thus the colloidal solution evolves through an increase of viscosity, due to increase in M-O-M bonds. The cross-linking of M-O-M bonds increase in the gelation step and afterwards, when the gel ages and a volume contraction takes place, due to the solvent evaporation (syneresis). Finally, an annealing step is often carried out to eliminate residuals of solvent and to complete condensation reactions in the polymeric network. So far the most used precursors are aluminum, titanium and silicon alcoxydes, and for this reason part of this Ph.D. work is dedicated to the development of suitable materials by using silicon alcoxydes.

This chemical process is influenced by several factors, the most studied of which are:

- solvent and concentration of reactive species
- use of complexing agents, such as β-diketons and organic acids, to slow down the hydrolysis constant rate
- catalyzers, to increase the overall reaction rate. The most used catalyzers are acids and bases, to favour the hydrolysis or the condensation reaction respectively, particularly important in either film or small particle synthesis
- amount of water, which determine the hydrolysis degree, and therefore the final texture of the gel network.

$$M(OR)_n + H_2O \rightarrow M(OR)_{-1}(OH) + ROH$$

$$M(OR)_n + M(OR)_{n-1}(OH) \rightarrow (RO)_{n-1}M\text{-}O\text{-}Si(OR)_{n-1} + ROH$$

(elimination of alcohol)

$$M(OR)_{n-1}(OH) + M(OR)_{n-1}(OH) \rightarrow (RO)_{n-1}M\text{-}O\text{-}Si(OR)_{n-1} + H_2O$$

(disidratation)

Scheme 1.1 Hydrolysis and condensation reactions characteristic of the sol-gel process

Hydrolysis and condensation

Hydrolysis takes place as a consequence of nucleophilic attack by water on the alcoxyde molecule. The hydrolysis constant rate mainly depends upon the amount of water, the chemistry of R groups. Without any catalyst the hydrolysis rate is quite slow, therefore the use of catalysts is often taken into account, the most important being acid and basic. In acidic catalysis an oxygen atom of an alcoxyde group is protonated, giving a five-substituted intermediate. On the other hand, in a basic environment the hydrolysis goes through the addition of a hydroxyl ion to an alcoxyde molecule via a S_N2 mechanism.

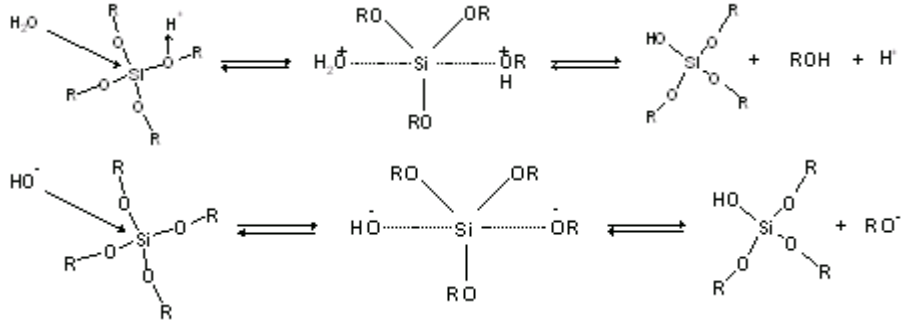

Figure 1.1. Hydrolysis mechanisms in acid and base-catalyzed conditions

Condensation

Silanol groups that are formed in the hydrolysis step can polymerize with the formation of an M-O-M bridge. Accepted mechanisms of condensation are through either the elimination of alcohol or water molecule with consequent formation of an M-O-M bond.

The sol-gel process in this Ph.D. work was chosen as a wet-chemical technique for the fabrication of organic-inorganic hybrid films. The application of this process for protective coatings is widely known in the literature, mainly produced by spin or dip coating procedures.[23-25] The sol-gel procedure was used for xerogel film syntheses with the aim of tuning surface wettability for subsequent applications as supports for DESI-MS investigations.

Self assembled monolayers

Self-assembled monolayers (SAMs) are, from definition, an evolution from adsorption and consequent spontaneous assembly of surfactants on solid surfaces.[26] In general, one functional group within the surface active molecule, often referred to as the "head-group", has a high affinity for the surface, while the "backbone" extends away from it. The molecular assemblies generated in this way represent a facile tool for tailoring and controlling interfacial properties such as adhesion, wettability or friction. The design flexibility of surface-active molecules, for instance the introduction of functionalized terminating or "tail" groups, allows for the tailoring of surface properties on a molecular scale. Hence, depending on the chemical structure of the adsorbates as well as on the adsorption parameters, monolayers with distinct structural and chemical properties can be generated, as schematically depicted in Figure 1.2.

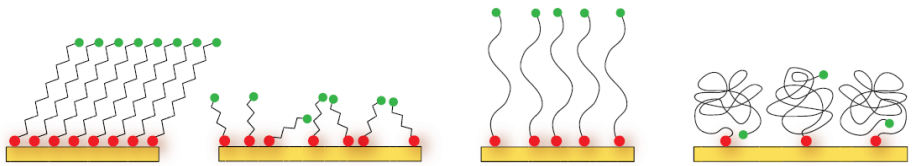

Figure 1.2. Possible structural conformations of self-assembled monolayers (SAMs) on a substrate surface

While the first self-assembled monolayer system was observed for silanes on glass by Zisman in 1946,[27] the interest of the research community in SAMs only grew tremendously after SAMs from alkanethiols on gold surfaces were discovered by Nuzzo et al. in 1983.[28] To date, alkanethiolate SAMs on gold surfaces represent the most studied self-assembly systems, while SAMs from silanes are of considerable technological importance, mainly because of their affinity to oxide surfaces. Monolayers of organosilicon molecules on oxide surfaces have reached considerable technological importance during the last decades. So-called "silane coupling agents" have found widespread use as adhesion promoters.[29 30] In contrast to thiol SAMs, the formation of silane monolayers requires an oxide surface with the most prominent substrates being silicon oxide, glass, aluminum oxide, quartz or mica.

Adsorption of silane SAMs-methods and mechanism

The formation of silane SAMs on oxide surfaces can be achieved by adsorption from a liquid or from the vapor phase. For the generation of silane SAMs from solution, there are a number of parameters that need to be controlled, including the type of solvent, water concentration, pH and temperature.[31] From this viewpoint, vapor phase adsorption appears to be more convenient. However, the adsorption kinetics from the vapor phase might be slower compared to adsorption from solution and not all molecules are eligible for vapor-phase adsorption, especially if they have a high molecular weight. Such molecules are not conveniently vaporized in a sufficiently high concentration, which can result in incomplete monolayers. Yet, for molecules that are suitable for vapor-phase adsorption, this technique is highly attractive since there are fewer parameters to control during the adsorption and the reported SAMs appear to be well structured and dense.[32] Figure 1.3 illustrates the basic steps involved in the adsorption of alkoxysilanes together with chlorosilanes, the most commonly employed organosilicon derivatives.[33]

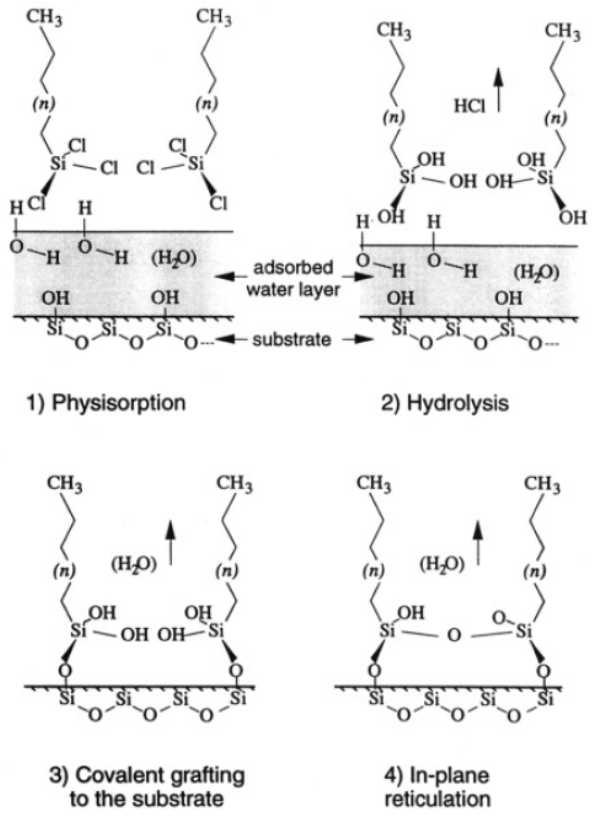

Figure 1.3. General scheme proposed for the silanization reaction. From Brozska *et al.*with kind permission[33]

The first step involves the hydrolysis of alkoxy groups (most often trimethoxy- or triethoxy-) to silanols in the presence of water. This water may either come from the surface-adsorbed hydration layer, from the atmosphere or it may be necessary

to add water in some cases to increase the degree of hydrolysis.[34] The subsequent formation of hydrogen bonds with surface silanol groups (step 2 in Figure 1.3) is followed by a condensation reaction in which water is liberated to form covalent siloxane bonds to the substrates. In the case of trimethoxy- or trichloro-terminated silanes, lateral condensation of silanol groups with neighboring chains, i.e. step 4, generates a SAM with a unique stability. Due to steric restrictions it is not possible for all three silanol groups to bind to the surface.[35] Silane SAMs, in case of alkoxy- or chlorosilanes with a trifunctional headgroup as depicted in Figure 1.3, could form three-dimensional structures, since all three silanols can condense with hydroxyl moieties. This could prevent the formation of a full monolayer, i.e. partial coverage or multilayers are feasible.[36] It is therefore believed that the water content in the system is of fundamental importance. An overabundance of water was found to induce polycondensation of silane molecules prior to adsorption, whereas a lack of water is known to result in incomplete monolayers.[37] Silane SAMs are thus more prone to defects in comparison to thiol monolayers, unless all adsorption parameters are carefully controlled. A further source for defects inside the monolayer is the low mobility of covalently immobilized silanes, which also leads to the picture of silane SAM formation from isolated islands to which single or groups of molecules couple via condensation of free silanols.

Therefore molecular self-assembly processes were taken into account for the ability of forming organized structures or patterns as a consequence of specific, local interactions among the components themselves, without external direction. The process induces a high molecular order, in particular higher than that expected by chemical reactions (like sol-gel), where an ordered state may proceed towards a disordered state depending on thermodynamic parameters. Given that surface functionalizations with a high degree of perfection can be achieved under ambient conditions,[38,39] DESI-MS investigations by using self-assembly at solid surfaces were carried out and results are presented in this Ph.D. work.

1.1

Investigation of novel sol-gel hydrophobic surfaces for desorption electrospray ionization-mass spectrometry analysis

Introduction

Several recent publications report the applications of ambient ionization techniques, such as direct analysis in real time-MS and DESI-MS, as useful approaches for the high-throughput investigation of a variety of samples. These techniques are successfully exploited for qualitative purposes in the chemical, forensic, pharmaceutical and clinical fields.[4,40-43] As for quantitative purposes, even if the capability to produce linear calibration curves has been already reported, reliability and reproducibility of the methods developed using these two techniques are still under investigation.[44-46]

Focusing on the DESI-MS technique, very fast ionization of several classes of molecules in a condensed phase can be achieved without sample preparation. Water-soluble and non-polar compounds, like small drugs, lipids or cholesterol have been successfully analyzed in biological samples with detection limits in the low ng ml^{-1} range.[47,48] Organic molecules were also identified on intact surfaces opening the potential of this technique to perform MS imaging. In such a context, lipid and drug spatial distributions in mammalian tissue sections were recently evaluated with a lateral resolution in the hundreds of micrometers.[49-53]

By using this source, samples are directly impacted with ionized solvent droplets generated from a pneumatically-assisted ESI probe. After desorption, ionization of the analytes occurs through interactions with the charged droplets, depending on the polarity and the reaction solvent, or, under some operating conditions, with impacting gas-phase ions generated by the primary electrospray. The analyte/ion desorption and transmission efficiency depend upon various parameters such as spray composition, source geometry and surfaces used for sample deposition. Quality of the final result in terms of sensitivity and repeatability is determined by surface wettability and consequent expulsion of charged offspring droplets and pick-up process. Different surfaces, such as glass, polymethylmethacrylate (PMMA), polytetrafluoroethylene (PTFE) and more recently mesh materials were tested to improve signal sensitivity and stability.[54,55] Among these supports, the PTFE super-hydrophobic surface is one of the most widely used materials, allowing compatibility with almost all solvents (except 100% H_2O), high ion currents and long lasting signals. In addition, the low surface energy (wettability) of this surface controls the droplet behaviour demonstrating that super-hydrophobic materials have excellent potentials as DESI substrates.[56]

However, the best results on PTFE were demonstrated only for polar analytes desorbed by polar spray mixtures. On the basis of these features, the capabilities of PTFE surface for DESI analysis represent an attractive approach for the development of surfaces having different hydrophobic properties. In such a context, the versatility of sol-gel materials could be exploited to obtain a variety of supports with different chemical properties and selectivity, or to include reacting species, such as trypsin, in order to obtain active surfaces. Many advantages are related with the use of the sol-gel process, such as potentially highly pure and homogeneous materials, extremely high versatility, stability and relatively cheap methods. A number of hybrid silica gels containing perfluoroalkyl or alkyl chains has been proposed leading to supports with a variety of controlled hydrophobic properties.[57-59]

In the past sol-gel supports have been successfully applied in mass spectrometry to obtain matrix-free mass spectra from the matrix assisted laser desorption ionization (MALDI) process.[60] Differently doped sol-gel materials were further developed to overcome the challenge to perform sensitive MALDI analysis of small molecules. In this study sol-gel materials were investigated for the first time as novel surfaces for DESI-MS analysis with the aim of emphasizing basic research on the influence of surface properties on the DESI process, and consequently improving DESI-MS analytical work. Attention was focused to the study of the physico-chemical features of each surface, since it is known that they influence the DESI process efficiency.[55,56] Considering that the chemistry of the sol-gel materials gives the opportunity to tailor the properties of the surfaces in such a way to enhance DESI analytical performances, we studied the behaviour of sol-gel materials at three different hydrophobic degrees as solid supports in a variety of solvents. A dip-coating procedure was used to obtain homogeneous, thickness-controlled films of acid catalyzed sol-gel layers on glass supports. The morphology of these surfaces was characterized and their behaviour was tested for different solvent spray solvent mixtures. Melamine, Sudan I, Sudan III and reserpine were the analytes under investigation. Finally, the results obtained for the sol-gel supports were compared with those obtained on PTFE surfaces.

Experimental

Materials

Tetraethoxysilane (TEOS) and octyltriethoxysilane (OTES) were purchased from Acros (Acros Organics, Geel, Belgium). Hydrochloric acid was purchased from Merck (Darmstadt, Germany). Acetonitrile (ACN), ethanol (EtOH), acetone, dichloromethane (DCM), tetrahydrofuran (THF), methanol (MeOH), formic acid (FA), reserpine, Sudan I, Sudan III and melamine were from Sigma Aldrich (St. Louis, MO, USA). All commercially available chemicals were of analytical grade. Figure 1 displays the chemical formulas of the analytes melamine, Sudan I, Sudan III and reserpine. Aqueous solutions were prepared in deionized water purified to

18.2 MΩ·cm using a Milli-Q water purification system (Milli-Q element A10 System, Millipore, San Francisco, CA, USA).

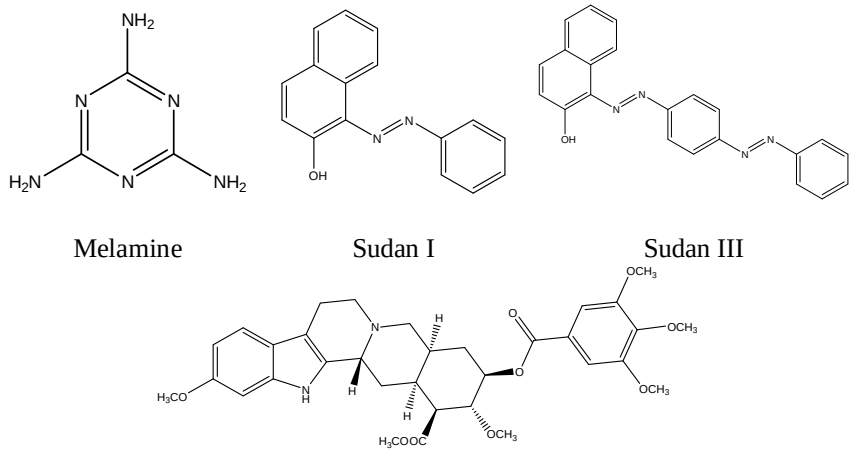

Melamine Sudan I Sudan III

Reserpine

Figure 1.1.1. Chemical formula of the compounds investigated

Instruments

Experiments were performed using a linear ion trap LTQ Orbitrap XL™ mass spectrometer (Thermo Fisher Scientific, San Josè, CA, USA) equipped with a DESI ion source (Prosolia Inc., Indianapolis, IN, USA). The source parameters were set as follows: spray voltage, 3.5 kV; solvent flow-rate, 2 µL min^{-1}; capillary voltage, 40 V; capillary temperature, 270°C; tube lens voltage, 80V; injection time, 500 ms; tip-to-surface distance, 2 mm; tip-to-inlet distance, 3 mm; surface rate, 250 µm s^{-1}; incidence angle, 54°. Solvent spray compositions: (a) ACN: water:FA (50:49.9:0.1); (b) MeOH:DCM:FA (50:49.9:0.1); (c) THF:DCM:FA (50:49.9:0.1). PTFE slides (26 x 76 mm) were purchased by Prosolia.

Sol-gel substrate preparation

Starting sol consisted of 2.2 mL of water (molar ratio Si/H_2O=0.25), and 30 µL of 1 M hydrochloric acid (final $[H^+]$=0.01 M). Four different sol−gel derivative supports were prepared by keeping a Si final concentration (1.2 M) constant and reacting various molar percentage (20% (S2), 40% (S4), 60% (S6) and 80% (S8)) of OTES (MW 276.49, density 0.88 g ml^{-1}) and TEOS (MW 208.33, density 0.934 g ml^{-1}) in the starting sol. The mixture was stirred for about 12 hours at room temperature before use. The dip-coating process involves dipping and removing a common glass substrate (26 x 76 mm) from the starting solution at a controlled speed; three different withdrawal rates were tested: 2, 10 and 22 cm min^{-1}. After each immersion, the surfaces were dried at room temperature for 1 hour before annealing at 120°C for 60 minutes. A schematic of the synthesis of sol-gel based surfaces developed is reported in Figure 1.1.2. The sol gel substrates were stored at room temperature when not immediately used and their efficiency was tested over

three months. Film morphology was characterized using a Park XE-100 atomic force microscope (AFM, Park Systems Corp., Suwon, Korea).

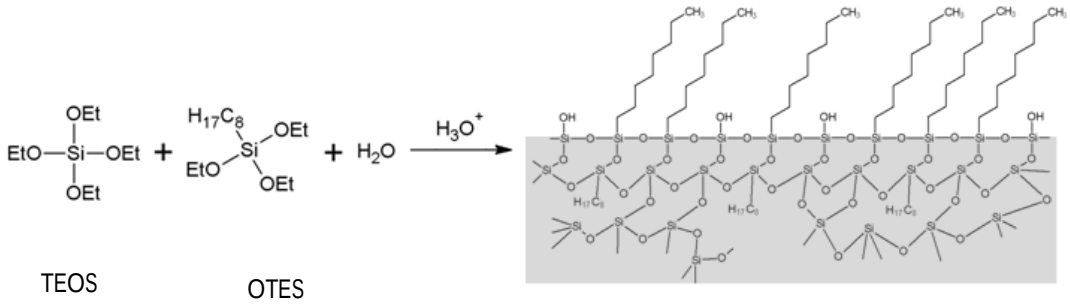

Figure 1.1.2. Schematic of the synthesis of sol-gel based materials developed for DESI-MS analysis

Scotch tape test for coatings adhesion

A Scotch tape test was used to evaluate the adhesion strength of silica sol gel coatings to the glass substrate. The typical procedure was given as follows:[61] first, the surface of the sample was cut by a razor to make grid lines. The total test area was about 1 cm^2 with each square grid dimension of 1×1 mm. The Scotch tape (18 mm width, 3M, Milan, Italy) was applied firmly to cover the grid area of the coating at room temperature. After around 1 min, the Scotch tape was stripped off with one quick peeling. The adhesion strength of the coatings can be estimated by counting the number of squares peeled off compared to the total number of squares. Each test was repeated at least three times an all surfaces.

Surface free energy measurements

The values of the surface free energy were measured at 293 K using a Cahn Dynamic Contact Angle analyzer (DCA-312, Cahn Instruments Inc, Cerritos, USA). The test liquid, i.e. water, was placed in a 25 mL beaker on a platform under the plate. The platform speed was set at 150 μm s^{-1}. All samples were tested five times. The surface energy values of the solid materials were calculated using the Wu's equation.[62]

Sample preparation

Reserpine 100 μM standard solutions were prepared in a H_2O:ACN (50:50, v/v) mixture; a mixture of the three analytes (Sudan I, Sudan III, melamine) was prepared in MeOH, acetone and THF at the final concentration of 100 μM. For DESI-MS experiments, 1 μL of the analyte solutions was spotted on the sol-gel surfaces and dried at room temperature.

Results and discussion

Film preparation and characterization

To obtain a high homogeneous coating, the chemistry of each step of the sol-gel process was carefully controlled in terms of silicon concentration, water/silicon molar ratio (*R*) and acid concentration. Silicon was used at the concentration of about 1 mol L^{-1}, the acid concentration was 0.01 mol L^{-1} and *R* was 4.0.[22]

Four different OTES-based sol-gel derivatives were synthesized to obtain surfaces with different hydrophobic features; however, it has to be noted that using the 80% fraction of OTES, the sol-gel derivative becomes too lipophilic, and this turns into a worse adhesion of the sol on the glass surface with a formation of inhomogeneous gel coatings, that result inadequate for DESI-MS applications. This behaviour can be explained by the formation of a significant amount of polyhedral oligosilsesquioxanes (POSS) containing 6, 8, 10 and/or 12 Si atoms. It is known that high concentrated OTES enriched sols, particularly when not aged, show difficulties in obtaining homogeneous gel films owing to non-equilibrium mixture of products [63]. As a consequence of these findings, only the 20%, 40% and 60% octyl sol-derivatives were used for gel coatings to obtain the S2, S4 and S6 surfaces.

With the aim of examining the adhesion strength between the interface of silica hybrid coatings S_2, S_4 and S_6 and glass surface, the Scotch tape test was used. The absence of stripped areas demonstrated the excellent adhesion strength of all the silica hybrid coatings to the glass surface. Finally, the surface morphologies were characterized by non-contact-mode AFM. Images were recorded for S2, S4, S6 medium thickness gels (withdrawal rate 10 cm min^{-1}, Figure 1.1.4 a-c).

AFM line profiles, related to approximately 25 μm^2 surface area, demonstrated excellent homogeneous coatings (rounded up thickness 1.8 µm); according to Degarmo *et al*,[64] the profile roughness parameter (R_a) was calculated for each surface and it was always found to be smaller than 1 nm, confirming the successful synthesis of very smooth supports. Surface homogeneity plays a fundamental role to carry out successful DESI-MS experiments. In order to evaluate the effect of the gel thickness on the surface homogeneity, three different withdrawal rates were tested on the S6 surface (see Experimental). AFM topography images of the S_6 coating at the minimum, medium and maximum thickness were recorded. Figure 1.1.4 a-b display a homogeneous coating for the minimum (rounded up thickness 1 µm) thickness substrate, whereas in the case of the maximum thickness (approx. 4 µm) a non-homogeneous surface presenting 50 nm peaks and craters was observed.

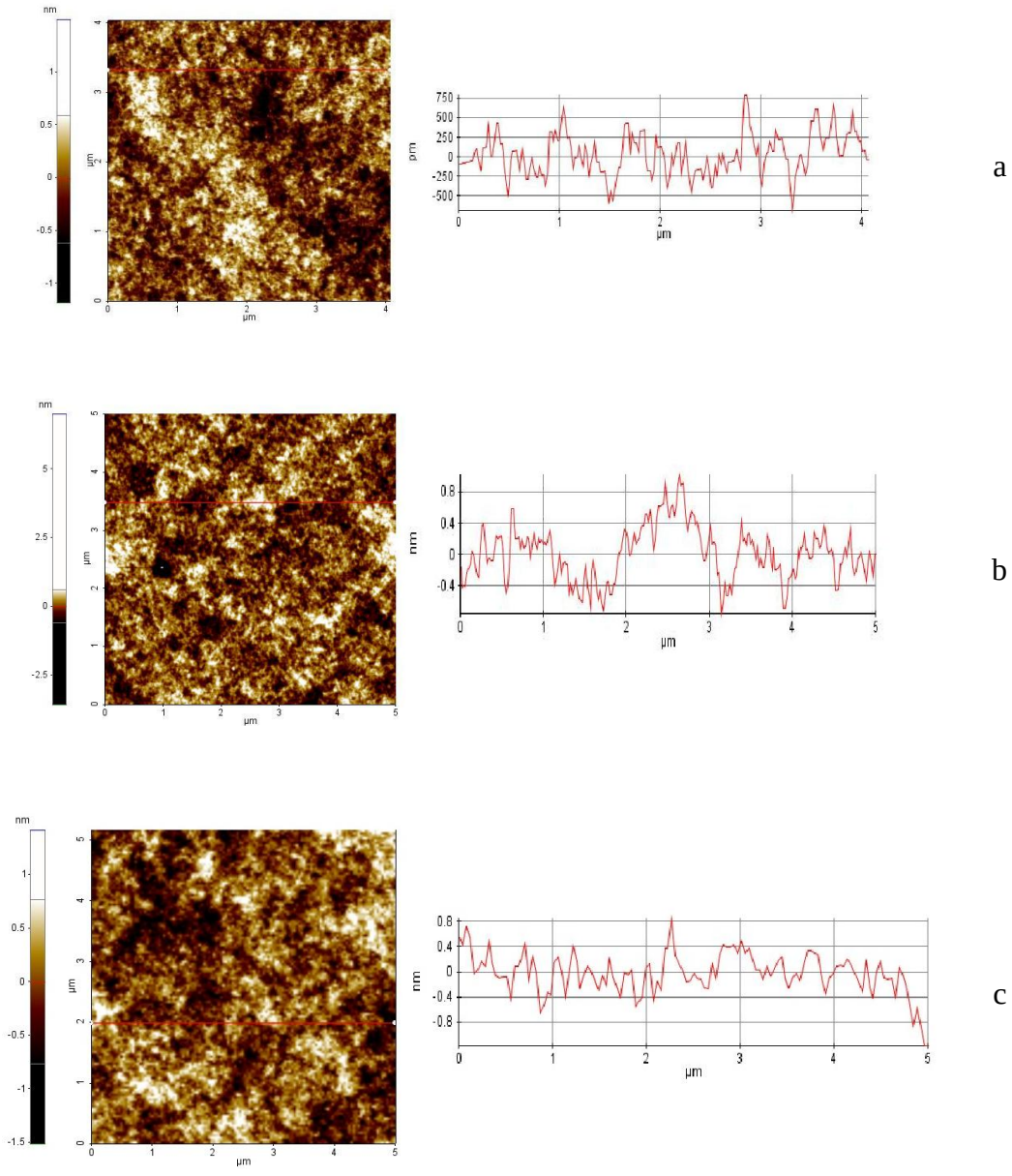

Figure 1.1.3. AFM topography images and line profiles related to approximately 25 µm^2 surface area of the (A) S2 (OTES:TEOS 1:5, molar ratio), (B) S4 (OTES:TEOS 2:5, molar ratio) and (C) S6 (OTES:TEOS 3:5, molar ratio) substrate at medium thickness (approximately 1.8 µm)

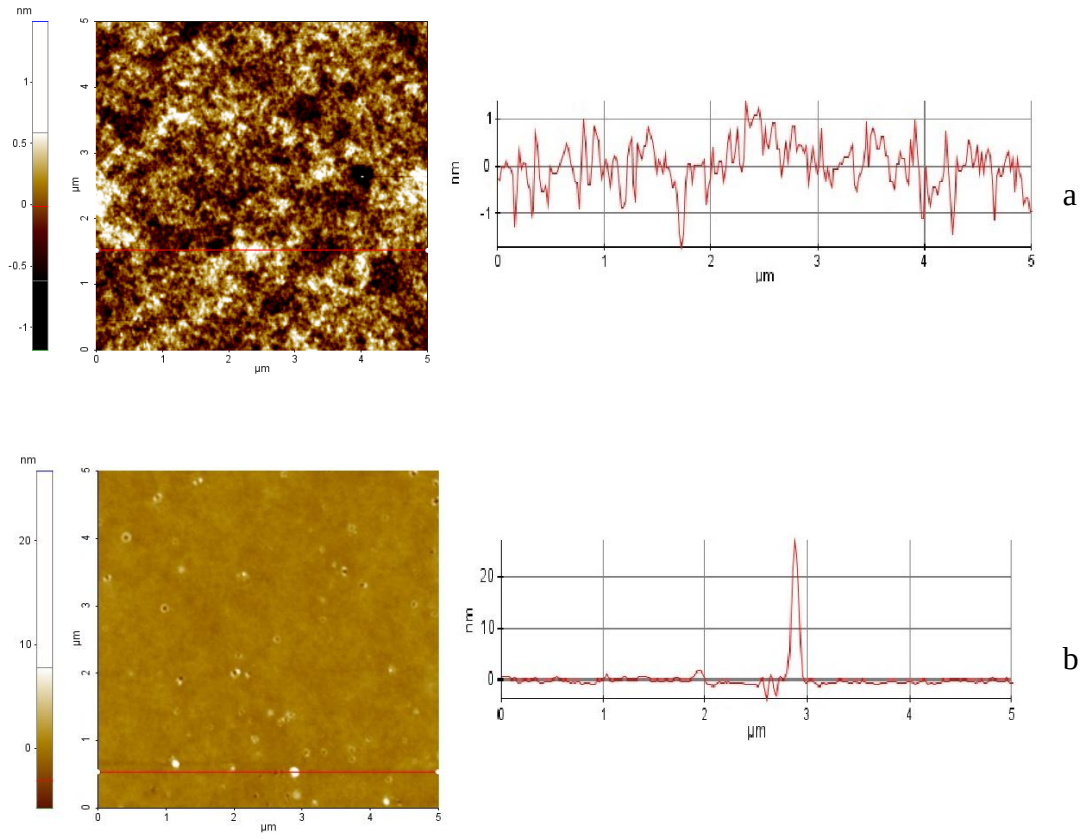

Figure 1.1.4. AFM topography images and line profiles of the S6 (3:5 OTES:TEOS) coating at the (A) minimum (approximately 1 µm) and (B) maximum thickness (approximately 4 µm)

These S6 surfaces having different thickness were tested for DESI-MS experiments by spotting on 1 µL of a reserpine standard solution (100 µM, final amount 100 pmol) dissolved in a H_2O:ACN (50:50, v:v) mixture. The one-way analysis of variance (ANOVA) (α=0.05) results obtained (average value, n=5) demonstrated a significant decrease of ion current for the surface at the maximum thickness (7.8±4.5e5 cps) with respect to those obtained for the minimum (2.0±1.0e6 cps) and medium thickness (1.4±0.4e6 cps). These results demonstrate the importance of the film homogeneity on the DESI signal intensity. For these reasons all the further experiments of the S2, S4 and S6 surfaces were carried out at the medium thickness coating.

The shelf-life of the three substrates was tested with a standard solution of reserpine over three months, and no differences in terms of sensitivity or background were observed in the mass spectra.

At last, to evidence differences in hydrophobic properties, surface free energy measurements were carried out for each silica-based surface and PTFE. It

was evidenced an increase of this parameter from S2 to S6, the values referred to S2 and S4 being closer and similar to that referred to PTFE (Table 1.1.1). This behaviour reveals a decreasing hydrophobicity in the series S2, S4, S6, thus suggesting that the effective surface exposition of the C_8 alkyl chains decreases in the series S2 > S4 > S6. The significant lower hydrophobicity of S6 could be due to the auto-aggregation of the octyl chains,[65] which are present to a large extent in this material, causing a reduction of their effective exposition.

Table 1.1.1. Surface free energy measurements for the PTFE, S2, S4 and S6 surfaces

Surface type	Surface free energy / mJ m^{-2}
PTFE	16.0±0.2
S2	17.1±0.2
S4	18.6±0.2
S6	24.7±0.2

Evaluation of S2, S4 and S6 surfaces for DESI experiments

Initially, charging and discharging behaviour of the four hybrid silica-based surfaces was tested for the S2, S4 and S6 surfaces by spotting a standard solution of reserpine (100 pmol in H_2O:ACN 50:50, v:v), and the results were compared with those obtained with a PTFE surface. In this study, reserpine was chosen as reference compound, being a common standard for calibration of ESI-MS instruments. For all the three sol-gel surfaces the ion current reaches a maximum value and drops to zero within one minute, whereas in the case of the PTFE surface, the signal decreases slowly within ten minutes. As a consequence, the new hybrid silica-based surfaces resulted to display a worse ability to stabilize charge accumulations on the surface during a DESI-MS experiment when compared to PTFE. Nonetheless, with PTFE and all the three hybrid silica-based surfaces ion currents of the same order of magnitude were obtained.

In the second part of the work, the DESI-MS behaviour of a mixture of three analytes (melamine, Sudan I and Sudan III) exhibiting different polarity was investigated on the three different substrates. In particular, signal intensity and ion current stability were tested by varying solvent mixture deposition and solvent spray compositions. As for DESI source parameters, the spray flow-rate was kept constant at 2 μL min^{-1} for all the experiments, whereas the tip-to surface distance was varied as a function of the solvent spray composition. Ion current stability exhibited a similar behavior for all the hybrid silica-based surfaces, analogously to that observed in the case of reserpine.

Extracted ion currents for each analyte were compared with a three-way ANOVA (α=0.05), considering solvent mixture deposition, solvent spray composition and surface type as the factors (data not shown). In all cases, $\log_{10}$ data transformation was applied to ensure variance homogeneity among samples. As

expected, the highest currents were obtained by using polar spray solvent mixtures for all analytes, owing to a more efficient solvent ionization.

A similar trend was obtained by measuring ion current values of the three compounds as a function of the surface free energy (Figure 1.1.5). Namely, the highest value of ion current of melamine, the most polar compound, was obtained using low energy surfaces, i.e. PTFE and S2, whereas the lowest current values were observed performing DESI experiments on higher energy surfaces, i.e. S4 and S6. These results evidenced that the most efficient DESI process is obtained for polar analytes using high hydrophobic surfaces (Figure 1.1.5a). By contrast, a less hydrophobic surface like S_6 is more indicated for the DESI-MS analysis of low-polar compounds, as evidenced in the case of Sudan III (Figure 1.1.5b). Finally, for the analysis of Sudan I, which exhibits intermediate polarity, surface type did not evidence any significant differences in average ion current (Figure 5c), thus proving that surface properties do not influence its DESI-MS response.

To better elucidate analytes/surface interactions in the DESI process for melamine and Sudan III, the ion currents were studied under the best analytical conditions corresponding to a MeOH:DCM:FA spray mixture (Figure 1.1.6). Taking into account the same electrical behaviour of the three hybrid silica-based surfaces, as previously described in the case of reserpine, it may be inferred that the differences displayed in average ion currents using S2, S4 and S6 supports are due to differences in surface chemistry. DESI-MS mass spectra of a mixture of the investigated compounds show that the highest ion current of melamine was observed on PTFE and a decreasing trend was observed in the S2 – S6 series (Figure 1.1.7), as described above. By contrast, in the case of Sudan III the best response was observed on the S_6 surface with an opposite trend. In addition, as can be seen in Figure 1.1.7, background signals are comparable among the four surfaces. Therefore, it is reasonable to assume that the best analytical response can be obtained when the softest interaction between analytes and surface takes place, which turns on a more efficient desorption step.

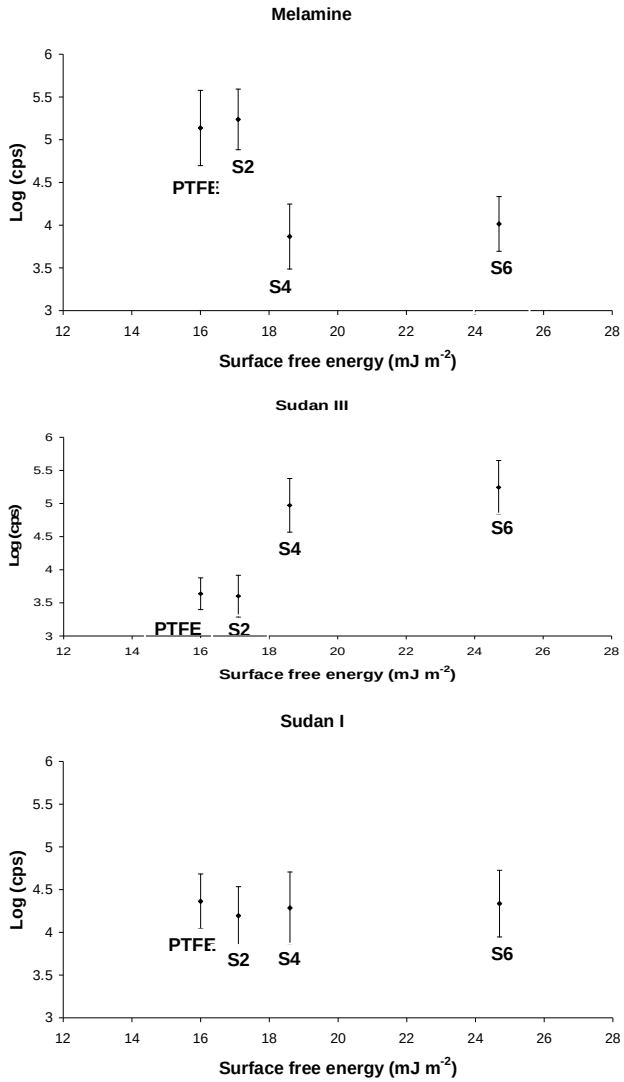

Figure 1.1.5. Extracted ion current signals (n=10) of (a) melamine, (b) Sudan III, (c) Sudan I as a function of surface free energy

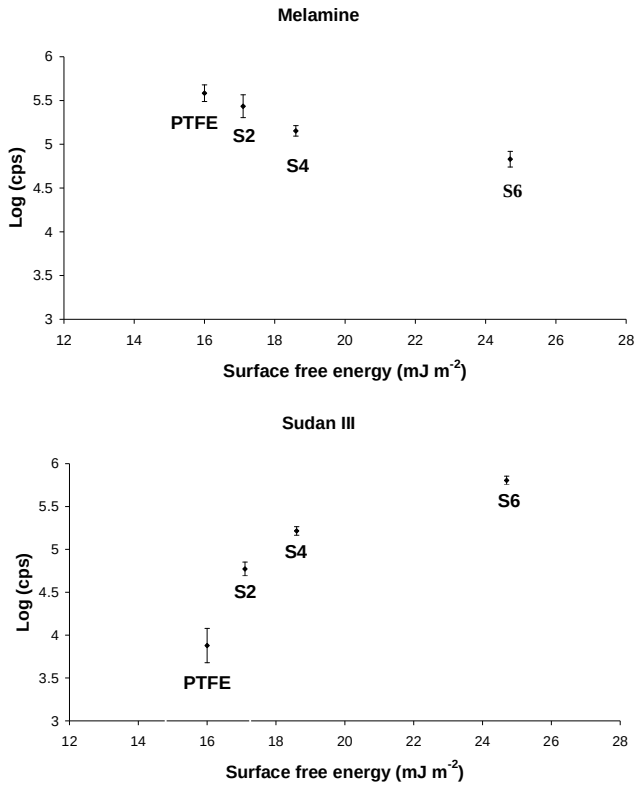

Figure 1.1.6. Extracted ion current signals (n=4) of (A) melamine and (B) Sudan III as a function of surface free energy. Experimental conditions: MeOH : DCM : FA spray mixture

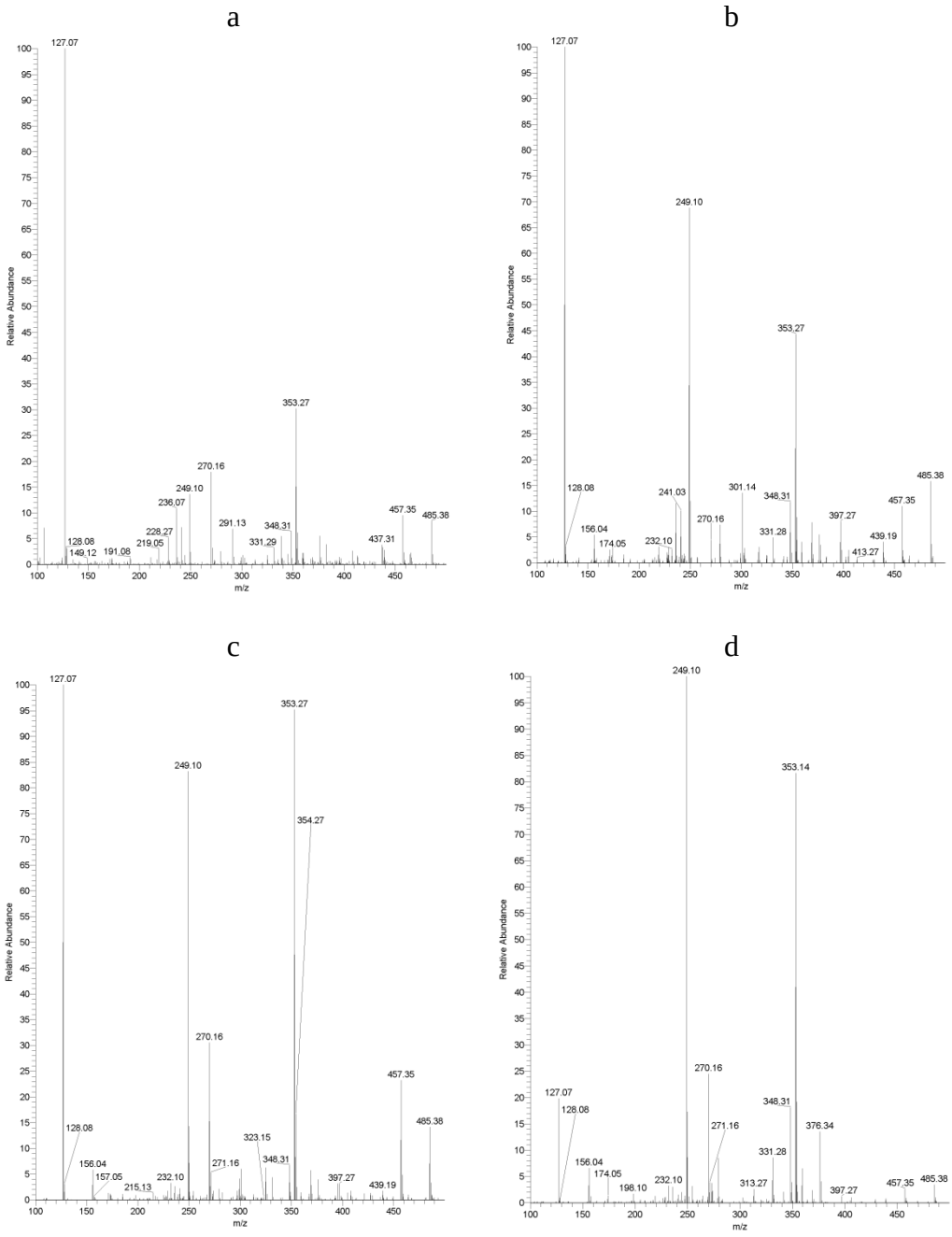

Figure 1.1.7. Full scan DESI-MS mass spectra (m/z 100-500) of a mixture of 100 pmol of melamine (m/z 127.07), Sudan I (m/z 249.10) and Sudan III (m/z 353.27) recorded on PTFE coated slides (a), S2 (b), S4 (c) and S6 surface (d)

Conclusions

Hydrophobic sol-gel supports were successfully prepared as solid supports for DESI-MS experiments. The preparation of the surfaces under controlled conditions allows us to obtain reproducible thickness and excellent homogeneity. The supports present long shelf-life and they are not expensive to produce. Physico-chemical properties of the surface were proved to play an important role in desorption/ionization process of compounds as a function of their polarity. Further investigations concerning surface morphological properties and surface chemistry of the materials will be carried out in order to gain deeper insights into the DESI process.

Acknowledgments

The facilities of the Centro Interdipartimentale Misure (CIM) “Giuseppe Casnati” (University of Parma) were used to perform AFM investigations. We are grateful to Dr. Carlo Vignali for skilful assistance. Thanks also to Dr. Andrea Lorenzi and to Dr. Marco Rocchetti for helpful discussions and suggestions.

1.2

Synthesis and characterization of xerogel hydrophobic surfaces on flat SiO_2 for an in-depth investigation on reaction mechanisms

Introduction

Interest in the sol-gel processing of inorganic ceramic and glass materials began in the mid-1800s' studies on silica gels. These investigations showed that the hydrolysis of tetraethyl orthosilicate (TEOS) under acidic conditions yielded SiO_2 in the form of a "glass-like" material.[22] The possibility of achieving very high levels of chemical homogeneity was recognized for the synthesis of a large number of novel ceramics that could not be synthesised by traditional methods. A variety of coatings and films have also been developed by using sol-gel methods, in particular in glass processing technologies. The motivation for sol-gel processing is primarily the potentially higher purity and homogeneity and the lower processing temperatures associated with sol-gels compared with traditional glass and ceramic processing. Milder processing conditions can also be achieved by using appropriate catalysts, e.g. acid or bases, as well as fluorites.

It is reported in the literature the possibility of obtaining homogeneous coatings by acidic catalysis. In this Ph.D. chapter it is presented how xerogel films were obtained after mixing different silanes, i.e. TEOS and OTES in different molar ratio, by working in aqueous acidic conditions.These conditions were adopted assuming that the proton is attracted by the oxygen atom of an OEt group. This should result in a shift of the electron cloud of the Si-O bond toward the oxygen atom and in an increase of the positive charge on the silicon atom. In this conditions a water molecule might attack the silicon atom, and a transition state should be formed.[66] Linkage of additional Si-OH tetrahedra occurs as a poly-condensation reaction, resulting in a 3D network. When sufficient interconnected Si-O-Si bonds are formed in a region, they respond as colloidal submicrometer particles. The size of these particles and the cross-linking within them depend upon several parameters such as nature and/or concentration of the electrolytes (in this case the acid), nature of the solvent, type of the alcoxyde, temperature. Temperature, nature of the solvent and the acid were not changed for the film synthesis in order to simplify the understanding of the overall panorama of the reactions.

Taking into account previous results in terms of tailoring surface properties for enhanced DESI analytical performances, insights in surface chemistry of the synthesized different xerogel films showing three different hydrophobic degrees were gained, in order to deeply explain surface chemical features observed so far.

Synthesis of hybrid-silica xerogel films was carried out in different experimental conditions and the characterization of the films was performed by means of different instrumental techniques, such as AFM, ellipsometry, profilometry and contact angle (static and dynamic) measurements.

Experimental

Materials

Tetraethyl orthosilicate (TEOS), octyltriethoxysilane (OTES) and toluene were purchased from Acros (Acros Organics, Geel, Belgium). Hydrochloric acid was purchased from Merck (Darmstadt, Germany). Ethanol was from Scharlau (analytical grade, Spain). Aqueous solutions were prepared in deionized water purified to 18.2 MΩ·cm using a Milli-Q water purification system (Milli-Q element A10 System, Millipore, San Francisco, CA, USA).

Experimental procedure

Four batches of syntheses were carried out. The first group (R1) consisted of 2.2 mL of water (molar ratio $Si/H_2O=0.25$) and 30 μL of 1 M hydrochloric acid (final $[H^+]=0.01$ M). Three different sol−gel derivative supports were prepared by keeping a Si final concentration (1.2 M) constant and reacting various molar percentage (20% (S2), 40% (S4) and 60% (S6)) of OTES (MW 276.49, density 0.88 gmL^{-1}) and TEOS (MW 208.33, density 0.934 gmL^{-1}) in the starting sol. The mixture was stirred for about 12 hours at room temperature before use.

The second group (R2) was prepared with the same solutions, but without any stirring.

The third set of reactions (R3) was carried out with a 1:10 silicon concentration dilution with respect to the first group, i.e. 0.12 M.

The fourth batch (R4), as for the second one, was without any stirring step (0.12 M). Single-side-polished silicon wafers (Si(100), Si-Mat Silicon Materials, Germany) of dimensions 10 x 30 mm^2 were used as supports for each film synthesis. All wafers were cleaned by ultra-sonication, first for 10 min in toluene (HPLC grade), then twice 10 min in ethanol to remove glue residues from the cutting and then blown dry in a stream of nitrogen. Subsequently, the silicon wafers were cleaned for 2 min in oxygen plasma (Harrick Plasma, USA) at the pressure of 0.03 mbar.

The coating procedure was carried out in two different modes: (I) dipping and withdrawing of clean silicon wafer substrates from the starting solution at the controlled rate of 2 cm min^{-1} and (II) dipping of clean silicon wafer substrates into the starting sols and removal after 1 hour. A rinsing procedure with 100 mL of water was applied since physisorption of silica particles on the surface might also take place.

The surfaces were then rinsed with 100 mL of water as to remove eventually physisorbed nanoparticles or unreacted silanes on the surface and then dried at room temperature at the open atmosphere before annealing at 120 °C for 60 min.

Methods for characterizing hybrid-silica xerogel films

Contact-angle measurements

The equilibrium contact angle (CA, static) of a sessile drop (5 µL) was measured with a contact-angle goniometer (Rame´ Hart model 100, Rame´ Hart, Inc., Mountain Lakes, NJ) for each surface treatment. The average contact angle was determined by measurement of 5 drops. The contact angles were measured using water.

Dynamic contact angle measurements were performed with the DSA100 (Krüss GmbH, Germany), by using water as solvent, and evaluated by the tangent-method-2 of the DSA3 software. Contact angles were then exported into Excel (Microsoft, USA) for further evaluation (calculation of the mean value, standard deviation, removal of artefacts occurring from faulty profile detection). First, a drop of 3 µl of solvent was set onto the substrate, with the syringe still within the drop. Then, the drop was enlarged to 9 µl at the constant flow-speed of 15 µl min^{-1}. Two different sampling points were taken into account for the measurements for each surface. To investigate changes on the surfaces due to aging, dynamic contact angles of on dip-coated hybrid-silica xerogels (reaction, R1, dip-coating, I) were measured 0, 24 and 48 hours after the annealing step.

Ellipsometry measurements

The thickness of the hybrid-silica xerogel films was determined by a variable-angle spectroscopic ellipsometer (VASE, M-2000F, LOT Oriel GmbH, Darmstadt, Germany) at the incidence angle of 70° under the assumption that the film has a refractive index of 1.45. Measurements were fitted with the WVASE32 analysis software using a three-layer model for an organic layer on a SiO_2/Si substrate. Eight different sampling points were used for the measurements at the relative linear distance of 5 mm from each other. The uncertainty in the measurements was estimated to be in the order of 0.1 nm, on the basis of the imperfections of silica wafers.

Atomic force microscopy investigations

Morphologies of hybrid-silica films were investigated by a DI Dimension controller (Digital Instrument, Santa Barbara, CA) in tapping mode at room temperature with a silicon nitride cantilever (Olympus, Japan), which has a resonant frequency of 265 kHz and a spring constant of 25.5 N m^{-1}.

Results and discussion

In this work acidic conditions were adopted for all reactions. Under these conditions a silica 3D network in the liquid phase is formed. In order to investigate how the formation of sub-micrometer particles interacts with the surface with consequent adsorption and formation of chemical bonds TM-AFM, ellipsometric investigation and contact angle measurements were carried out.

The silica xerogel film obtained following procedure R1 (1.2 M sols, 12 hours stirring) and dip-coated following the procedure I, without a rinsing step with water, was visually observed. An example of non-rinsed surfaces is provided in Figure 1.2.1. This procedure turned out in a highly inhomogeneous coating, with estimated thickness-variation of hundreds of nm along the glass slide.

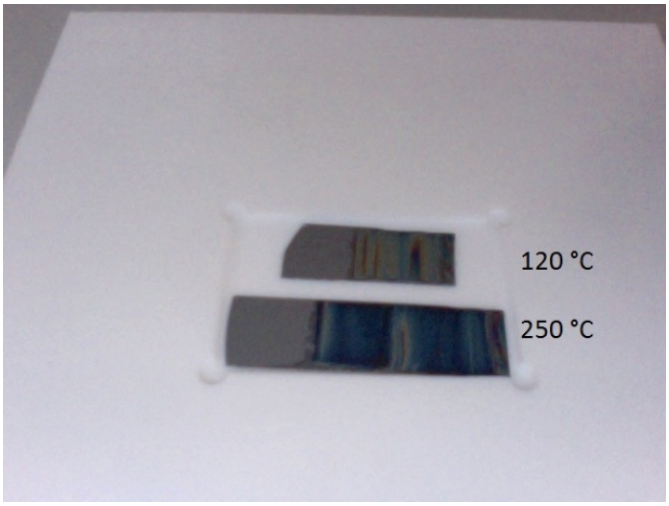

Figure 1.2.1. Example of film formed on silicon wafers after heating at 120°C and 250°C before rinsing with distilled water

The rinsing step is important since it might also happen that silica nanoparticles are physisorbed on overlapped layers and also this might contribute to form a very inhomogeneous film having different thickness in the different points. Figures 1.2.2 a-c show the AFM results obtained when using as coating solutions: 20% (S2), 40% (S4) and 60% OTES (S6); the root mean square roughness (Rq) values together with the contact angle measured on these samples are given in the figures. It is possible to observe that from 20% OTES to 60% OTES an increase in Rq from 2 to 64 nm and morphological inhomogeneity were observed. It is evident from these pictures that by increasing the alkyl chain content, at this concentration level, silanes create islands on the surface, probably because of a lack of adherence – in particular for the S6 sol – on the surface during the dip-coating procedure and a washing step with 100 mL of water.

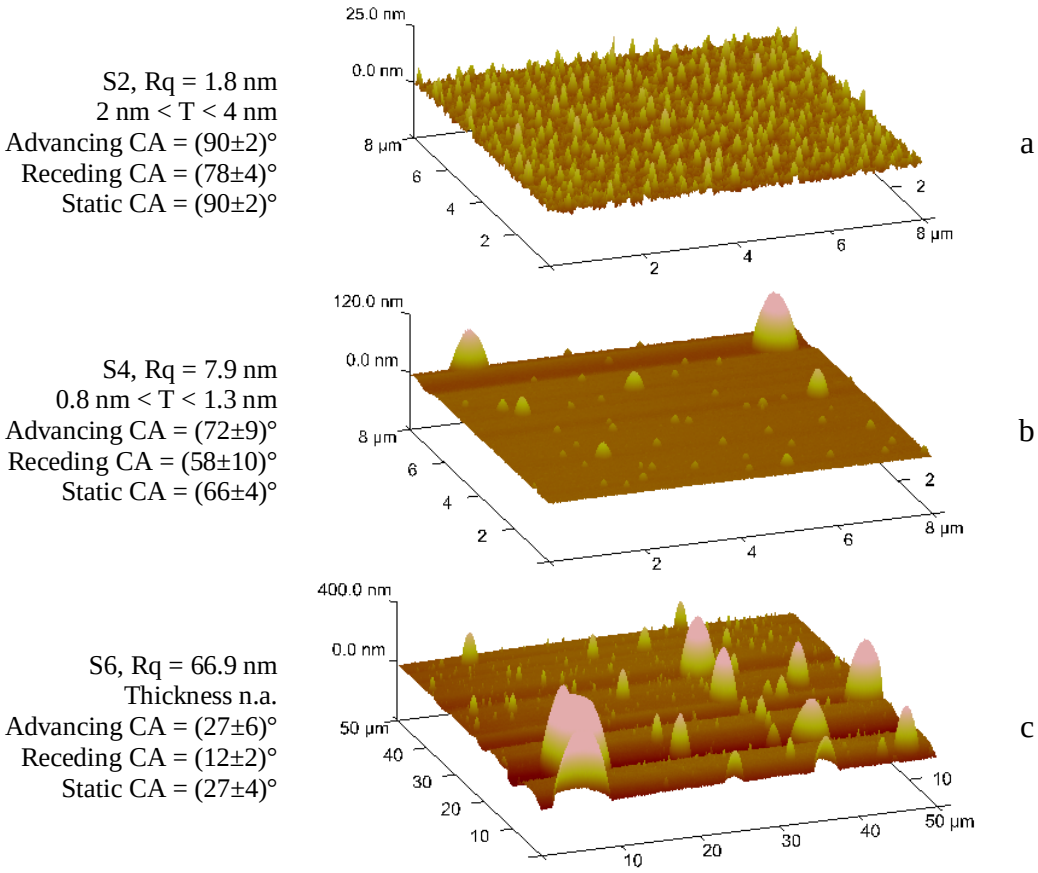

Figure 1.2.2. Three-dimensional TM-AFM pictures of dip-coated (rate of 2 cm min^{-1}) xerogel films obtained by 1.2 M sols in ethanol (a-c). Stirring time 12 h. Samples were rinsed with water. Static contact angles were recorded by using water as solvent

The thickness of the film measured by ellipsometry along the glass slide is shown in figure 1.2.3 for the two solutions S2 and S4. Green and red markers are used for distinguishing the two replicas. Film thickness changes in dependence of the measuring position; these changes are not ascribable to a failure of the ellipsometer used for these measurements; the accuracy is estimated to be ± 0.1 nm.

As for S6, obtained by using [Si] = 1.2 M, the sample roughness resulted to be too high to fit data with an adequate ellipsometric layered model (reflectance mode), as in the cases of the other surfaces. For these reasons, as to address shape and height of islands observed by AFM, a profilometric investigation was carried out. The top picture (Figure 1.2.4a) is referring to a 250x200 μm^2 area and islands were found to be in the order of hundreds of nm in the *z* direction.

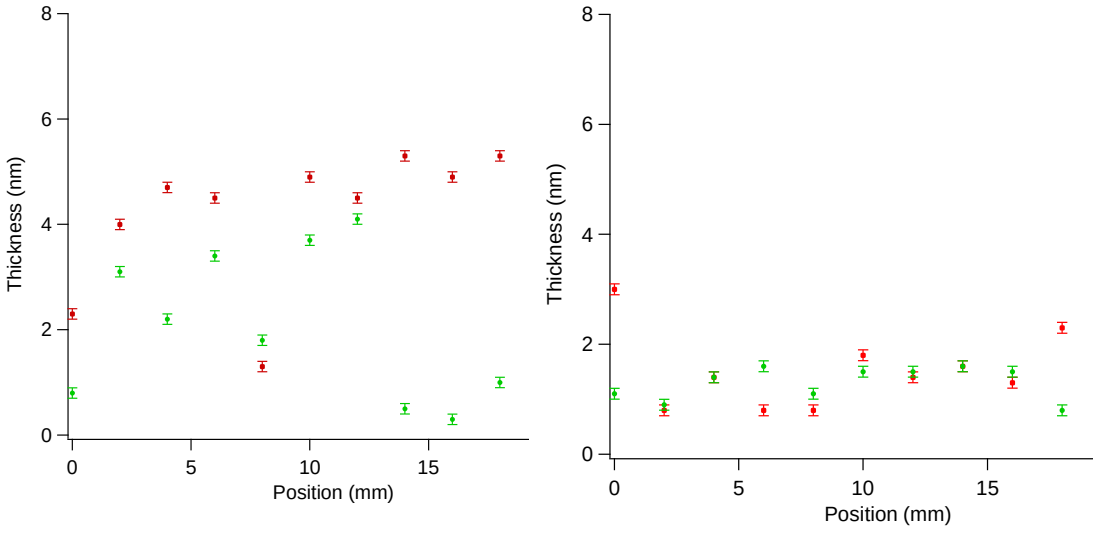

Figure 1.2.3. Thickness of the surface film measured at different positions on the Si wafer surface (highlighted in red and green). S2, left, S4, right

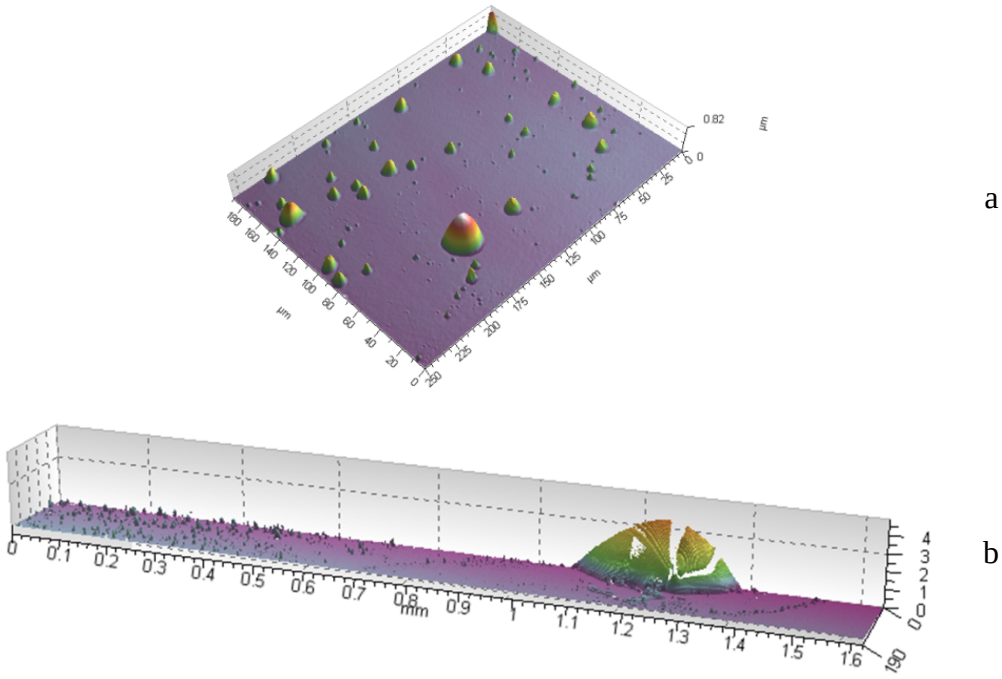

Figure 1.2.4. 200x250 μm^2 profilometric image of a S6 surface ([Si] = 1.2 M, a). Top border of the S6 surface ([Si] = 1.2 M, b). It is possible to observe a huge imperfection due to the dip-coating (?) and a lack of adherence of the S6 sol (60% OTES Figure 2b) that might justify the presence of large non-coated areas; this finding may also justify the strong decrease in the hydrophobicity observed by contact angle measurements.

No significant differences were observed in the measured contact angles when two different sampling points were taken into account for the measurements. Advancing and receding contact angles were recorded as a function of aging of hybrid-silica films. It was found that in the series S_2-S_4-S_6 there is a significant decrease in hydrophobicity. Results are showed below (mean values with standard deviations). No statistical significant differences were found as a function of aging time (Figure 1.2.5).

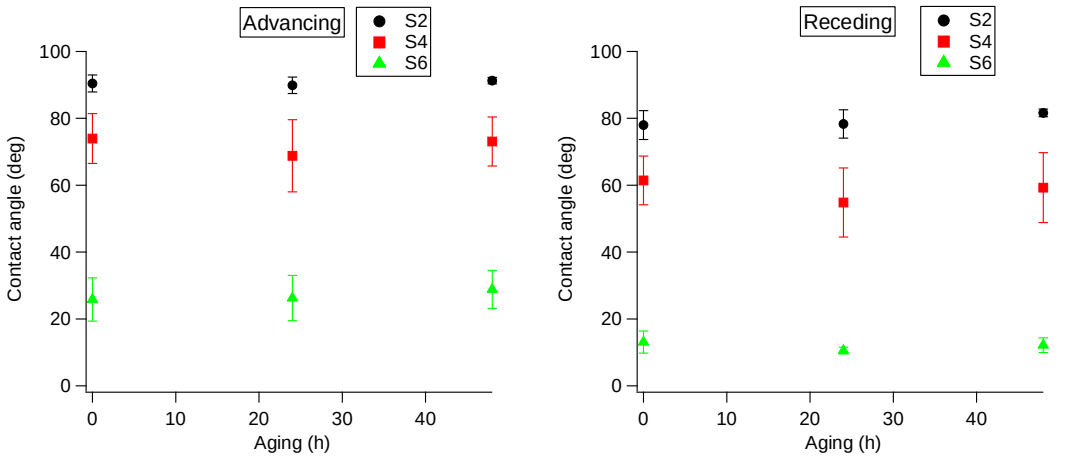

Figure 1.2.5. Contact angle measurements referred to the S2-S4-S6 films (sol obtained by R1 reaction mixture, dip-coating 2 cm min^{-1}) as a function of the aging time

So far the effects of the stirring time were considered. In the following the effects of the silane concentration on the film is presented. The same reaction mixture was diluted using a 1:10 ratio (reaction R3, same dip-coating procedure) and TM-AFM, along with ellipsometric thicknesses and contact angle measurements are shown in Figure 1.2.6.

As for 20% OTES sol, the topography is similar to that obtained by using a ten-fold more concentrated sol (Figure 1.2.6); a comparable root mean square roughness was also calculated. By contrast, in the case of 40% and 60% OTES sols, very smooth surfaces with the presence of few aggregates were obtained. RMS roughness was found to be very low for the last two films. The cross-linking, exhibited as nano-aggregates, can be induced by the presence of TEOS, a consequence of four OEt groups, which can be hydrolyzed and condensed, in acidic conditions, to a Si-O-Si bridge. As for contact angle measured after …minutes, the trend observed for the series S2-S6 was found opposite to that of 1.2M sols. Indeed, it can be observed an increase of the contact angle from 20% OTES sol to 40% with a plateau for 60% OTES sol-deposited film. It is possible to correlate the higher alkyl-containing compound fraction to a higher concentration of chains on the surface, therefore to a higher hydrophobicity. Calculated thicknesses were found to be of the same order of magnitude with respect to 1.2M sols, but with a lower dispersion, ascribable to higher homogeneity. The presence of aggregates,

taking into account a more diluted system, may be explained on the basis that the longer and the bulkier the alkoxide group, the slower the rate constant [67]. One might assume in these systems the formation of a significant amount of polyhedral oligosilsesquioxanes (POSS) containing 6, 8, 10 and/or 12 Si atoms can occur, as previously stated,[63,68] as well as several incompletely condensed silsesquioxanes (Figure 1.2.7).[69,70]

S2, Rq = 1.9 nm
T = (0.9±0.3) nm
Advancing CA = (57±7)°
Receding CA = (45±8)°
Static CA = (55±9)°

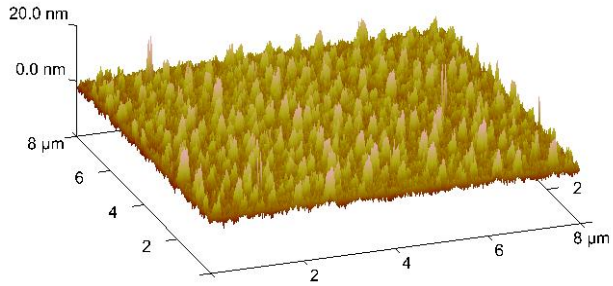

a

S4, Rq = 0.3 nm
T = (0.9±0.2) nm
Advancing CA = (89±6) °
Receding CA = (83±6)
Static CA = (87±2)°

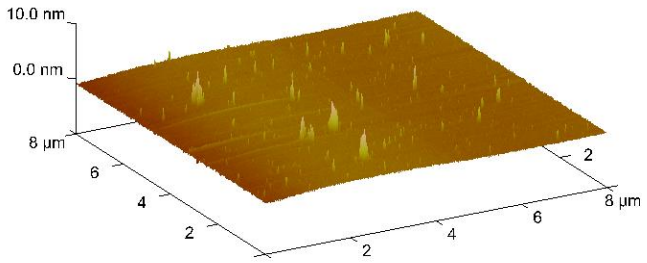

b

S6, Rq = 0.3 nm
T = (0.8±0.2) nm
Advancing CA = (93±2) °
Receding CA = (82±3) °
Static CA = (91±3)°

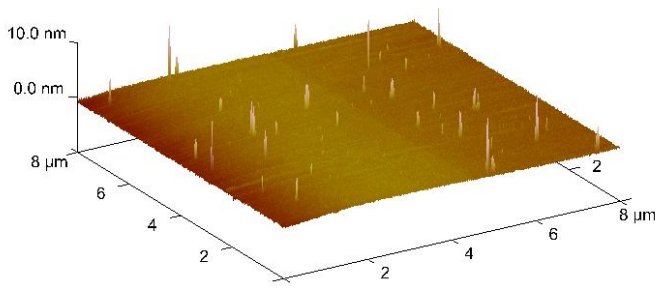

c

Figure 1.2.6. Three-dimensional TM-AFM pictures of dip-coated (rate, 2 cm min^{-1}) xerogel films obtained by 0.12 M sols in ethanol (a-c). Stirring time 12 h. Static contact angles were recorded by using water as solvent

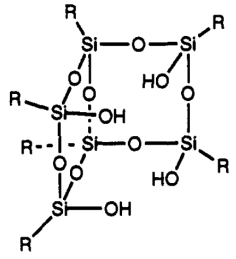

Figure 1.2.7. Example of uncompleted condensed silsesquioxanes, reprinted from Feher *et al.*[70]

The formation of a non-equilibrium mixture of products may be assumed in particular at high concentration of Si, and such products might be adsorbed on silicon oxide surfaces, increasing the hydrophobicity, as observed from contact angle data for 1.2 M sols. In the case of a more diluted sol it is reasonable to assume the formation of a less cross-linked system and that the overall degree of hydrophobicity is significantly less affected by the formation of the aforementioned non-equilibrium products. The presence of cross-condensed reaction products in organically modified silica sol-gels, by using a mixture of TEOS and an alkylsiloxane in an aqueous acidic medium, has been also investigated in the past by other Authors by high resolution ^{29}Si and ^{17}O NMR spectroscopy.[71,72] Significant amounts of both self- and cross-condensation products were formed in hybrid sol studied. These results may justify the presence of inhomogeneity found in morphology, thickness and contact angle, in particular for high concentration sols. It is likely that aggregation is not a random process, but involves self-assembly phenomena to form micelles or other extended structures similar to those observed for common oil-water-surfactants systems.[73] If these aggregates assemble and interact with the surface during film formation, monolayers will not be produced unless surface interactions are strong enough to restructure aggregates.[74] Furthermore, the hydrolysis rate may be expected to be unfavored by the concentration of the octyltriethoxysilane fraction, taken into account the electron-donor effect of the alkyl chain on the Si atom. Possible rearrangements or unlike formation of a great number of aggregates might explain the higher homogeneity found for the S4 and S6 films by 0.12 M sols, with the formation of a film similar to a monolayer of silanes.

Further investigations were carried out in order to address surface phenomena when the deposition method was changed from linear-motioned to static for one hour. From TM-AFM investigations it was found that by increasing the silane concentration of an order of magnitude an increase in surface roughness was observed, particularly evident in the case of S6-type films (Figure 1.2.8).

At a first glance the surface functionalization obtained by the use of the most diluted system did not allow to obtain significant differences in term of root mean square roughness, thickness and contact angle, even by changing the molar ratio TEOS/OTES in the mixture. Concerning the highest concentration sols, aggregates are evident as imperfections on the surface, as previously stated. In this case, chemisorption of different incompletely condensed silsesquioxanes can take place. A previous work [69] reported optimal conditions for the synthesis of these compounds, similar to our conditions in the case of the most diluted reaction mixtures. These findings may justify the substantial lack of differences found for surfaces reported in Figure 1.2.8d-e-f.

S2, Rq = 0.6 nm
T = (0.7 ± 0.3) nm
Static CA = (30±1)°

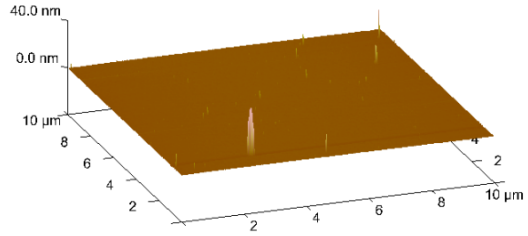

a

S4, Rq = 0.7 nm
T = (0.8 ± 0.3) nm
Static CA = (50±1)°

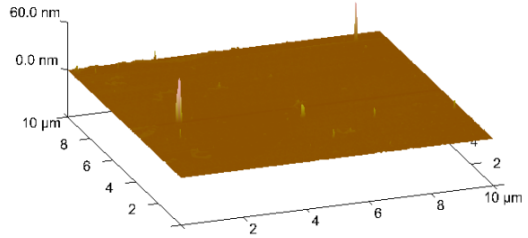

b

S6, Rq = 17.9 nm
T ≈ 3 nm
Static CA = (78±2)°

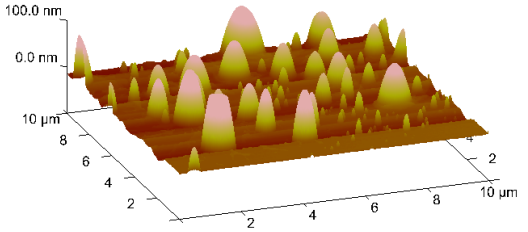

c

S2, Rq = 0.2 nm
T = (0.7 ± 0.1) nm
Static CA = (72±2)°

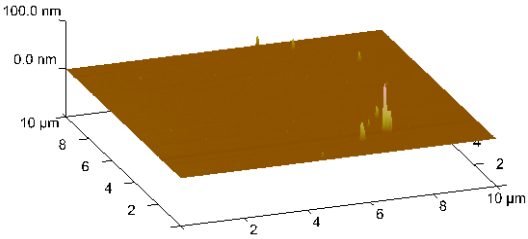

d

S4, Rq = 0.4 nm
T = (0.9 ± 0.6) nm
Static CA = (69±2)°

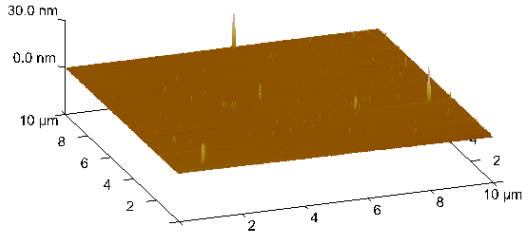

e

S6, Rq = 0.4 nm
T = (0.7 ± 0.1) nm
Static CA = (67±2)°

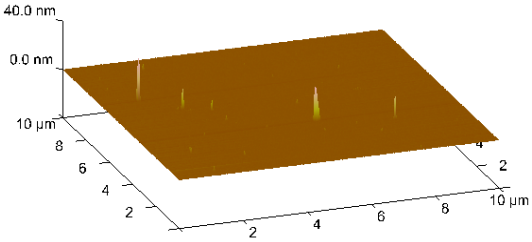

f

Figure 1.2.8. Three-dimensional TM-AFM pictures of silica xerogels by 1.2 M sols in ethanol (A-C) and by 0.12 M sols (D-F). Stirring time 12 hours. Static contact angles were recorded by using water as solvent.

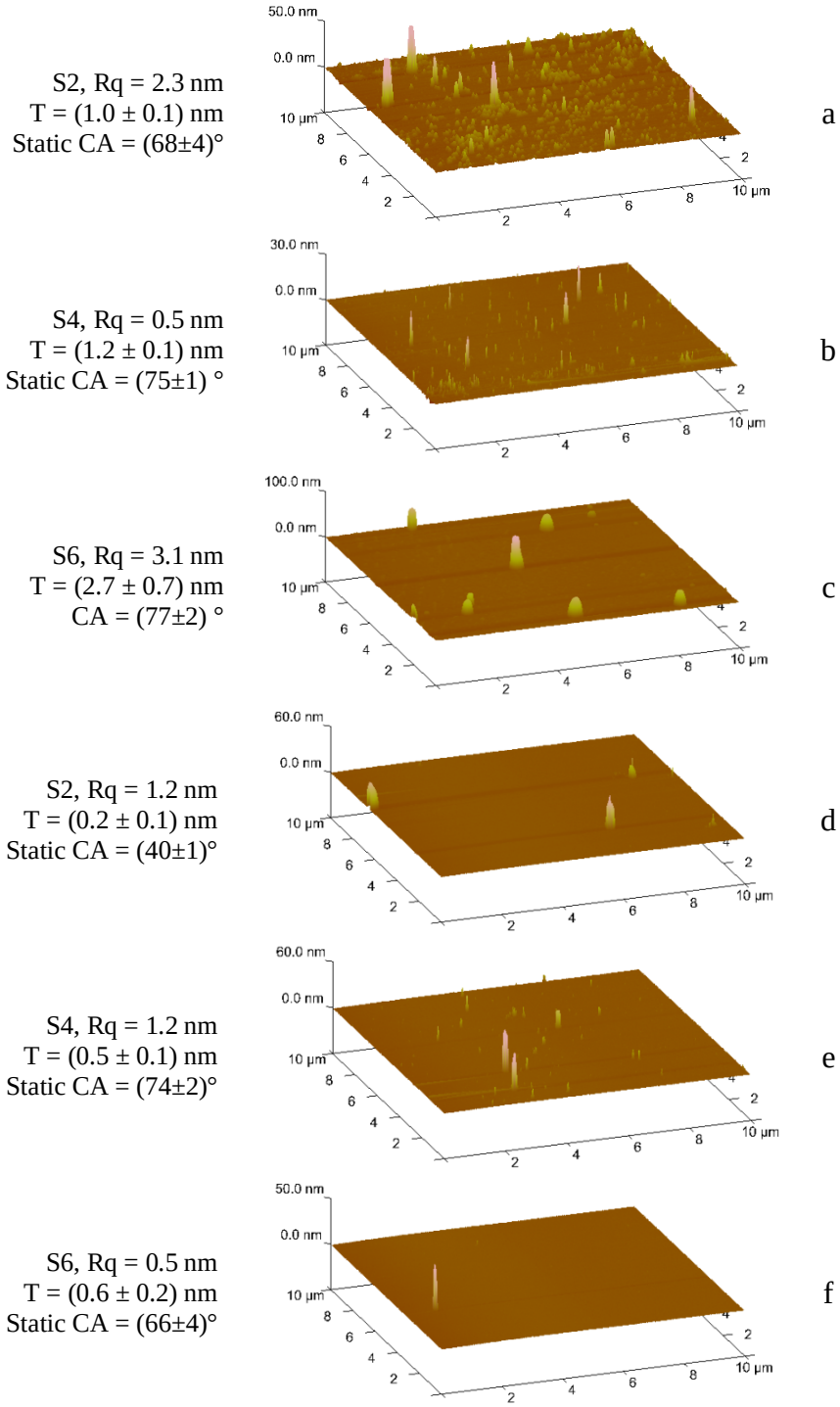

Figure 1.2.9. Three-dimensional TM-AFM pictures of films obtained by 1.2 M (a-c) and 0.12 M solutions in ethanol (d-f). Solutions were not stirred. Static contact angles were recorded by using water as solvent

Nevertheless this discussion seems to be not applicable to 1.2 M sols, where a trend correlated to OTES concentration/hydrophobicity was observed. The presence of aggregates for the surface S6 (Figure 1.2.8C) is assumed on the basis of the formation of POSS, as discussed above.

The final group of reactions, carried out in the absence of any stirring step, allowed to obtain surfaces with a lower presence of aggregates, in particular for high concentration solutions. Only for the surface S2, in Figure 1.2.9A, a higher cross-linking was observed, reasonably due to a high amount of TEOS. In the other cases the synthesis of smooth surfaces, significantly more hydrophobic than SiO_2, may be explained as a consequence of the chemisorption of silanes as such or with a low degree of polycondensation.

Conclusions

In this work a study of the effect of different factors on the synthesis of xerogel films with different physico-chemical behavior was carried out. To address the surface chemical phenomena occurring, the relative molar ratio between TEOS and OTES, the concentration of the mixtures, the deposition method, as well as the time were taken into account and results were discussed on the basis of surface morphology, thickness and contact angle. All the variables studied were demonstrated to have a considerable effect on surface homogeneity and hydrophobicity degree. The overall morphological and chemical homogeneity was due to:

- the amount of water, which strongly condition hydrolysis and condensation reaction, turning out to cross-linking and possible formation of POSS that might be assumed for high concentration of silanes;
- OTES/TEOS ratio, nevertheless found to affect the surface chemistry only in some cases and with opposite trends, as a function of other experimental variables;
- stirring time, contributing to the formation of aggregates in the liquid phase, in particular at high concentrations, in the presence of water. The presence of numerous sites for hydrolysis and condensation, favored by the time, allowed several Si-O-Si to be formed, affecting the effective adherence of particles on the surface.

The overall reproducibility was found to be poor, thus a few remarks were done as to move to more reliable way of controlling surface properties. For the subsequent investigations it was decided to:

- reduce the concentration of silanes, in order to limit silane-silane in-solution reactions, and the possible formation of soluble (and non-soluble) aggregates. An effective surface tailoring is expected to be achieved by the minimum amount of reactant to saturate the active sites on the surface. This depends upon the reactivity of the silane;

- use an one-silane solution in order to have a simpler system, taking advantage from self-assembling phenomena taking place among alkyl chains in alkoxysilanes for the synthesis of more reproducible films.

1.3

Synthesis and characterization of thin films on SiO_2 flat surfaces by adsorption of alkylsiloxanes in non-polar solvents

Introduction

So far one of the most successful approaches for the modification of solid substrates has been the chemical grafting of hydrocarbon chains on hydrated surfaces via a alkylchlorosilane (-$SiCl_3$) or alkylalkoxysilane (-$SiOR_3$) head group by the formation of self-assembled monolayer structures.[26,75,76] Nevertheless, despite extensive efforts, the silanization reaction could still be affected by scarce reproducibility in the macroscopic properties (i.e. wettability and contact angle hysteresis) of the deposited film, when experimental variables such as the nature of the substrate, [77,78] temperature,[33,77,79] concentration,[78,80] solvent type[81] and water content[82,83] are not under strict control. By doing this, it can be possible to obtain a reproducible structure of alkylsilane monolayers, because solution agglomeration on the deposition, leading to cross-polymerization, is accurately minimized[74]. A silanization reaction evolves through a thin adsorbed water layer on the "bare" silica surface.[33] In detail, in the presence of initial water layer on the substrate, the organic molecules contained in the reactive solution can gradually adsorb onto it (Figure 1.3). Following physisorption, the alkoxysilane head groups hydrolyse and form trisilanols. In addition, the presence of a thin film of fluid permits in-plane lateral mobility of the long-chain silanes by Brownian motions. This leads to important in-plane reorganizations in a analogous manner to Langmuir monolayers of short-chain surfactants submitted to lateral compression. At later times, covalent siloxane bonds can take place at the head group-substrate interface. The layer becomes grafted to the solid surface. Intermolecular cross-linking by the trisilanol head group can also occur, provided the distance and orientation between the groups are favourable. The end result is a 2D network of polysiloxane. These last steps will obviously be facilitated by a moderate baking of the substrate, which will help to remove the water layer.[33]

In this work the capability of obtaining a reproducible structure of alkyl-silane was explored with the aim of tailoring the surface free-energy by depositing a mixture of TEOS and OTES using toluene as solvent. This solvent is known as being capable of extracting significant amount of water from the substrate surface, yielding in dense silane films.[37] In addition, as a non-polar solvent, toluene allows the control of the mechanism of layer formation, in term of limiting island growth, typical phenomena observed for high water content.[82]

The experiments provided here were carried out using three different trialcoxysilanes (-$SiOR_3$), i.e. 3-mercaptopropyltriethoxysilane, octyltriethoxysilane, 1H, 1H, 2H, 2H- perfluorooctyltriethoxysilane as well as tetraethoxysilane. They were chosen on the basis of the results on chemical grafting of hydrocarbon chains on hydrated surfaces.[33] Surface characterizations were then carried out by means of TM-AFM, ellipsometry and contact angle and X-ray photoelectron spectroscopy (XPS) in small-area mode.

Experimental

Materials

Tetraethyl orthosilicate (TEOS), octyltriethoxysilane (OTES) and toluene were purchased from Acros (Acros Organics, Geel, Belgium). Hydrochloric acid was purchased from Merck (Darmstadt, Germany). Ethanol was from Scharlau (analytical grade, Spain). 3-Mercaptopropyl-triethoxysilane (MTS) was from Alfa Aesar (Ward Hill, MA, USA), octyltriethoxysilane (OTES) was from Acros (Acros Organics, Geel, Belgium) and 1H,1H,2H,2H-perfluorooctyltriethoxysilane (FOTES) was purchased from ABCR-chemicals (Karlsruhe, Germany). Deionized water was purified to 18.2 MΩ·cm using a Milli-Q water purification system (Milli-Q element A10 System, Millipore, San Francisco, CA, USA).

Silanization

Single-side-polished silicon wafers (Si(100), Si-Mat Silicon Materials, Germany) of dimensions 10 x 10 mm^2 were used as supports for each film synthesis. All wafers were cleaned by ultrasonication, first for 10 min in toluene (HPLC grade), then twice 10 minutes in ethanol to remove glue residues from the cutting and then blown dry in a stream of nitrogen. Subsequently the silicon wafers were cleaned for 2 minutes in oxygen plasma (Harrick Plasma, USA) at the pressure of 0.03 mbar. Wafers were dipped into silanes solutions (toluene) for 1 hour.

The first set of functionalized surfaces (B1) were from silanes solutions at the concentration 100 mM in toluene and reacting various molar percentage (20% (S2T), 40% (S4T) and 60% (S6T)) of OTES (MW 276.49, density 0.88 g mL^{-1}) and TEOS (MW 208.33, density 0.934 g mL^{-1}) in the starting solutions. Solutions were homogenized before use. Each silanized surface was then rinsed with water, then with toluene in an ultrasonic bath. Samples were finally annealed at 120 °C for 60 minutes.

The second set of functionalized surfaces (B2) were obtained by dipping each support for 1 hour into silanes solutions (toluene) at the concentration 100 mM for MTS and OTES and in the range 1-10 mM for FOTES respectively. Each silanized surface, i.e. S-FOTES, S-OTES and S-MTS, was then rinsed with water, annealed at the pressure 0.02 mbar, at 100 °C, for 60 minutes and finally rinsed with toluene.

Methods for characterizing hybrid-silica films

Contact-angle measurements

The equilibrium contact angle (CA, static) of a sessile drop (5 μL) was measured with a contact-angle goniometer (Rame´ Hart model 100, Rame´ Hart, Inc., Mountain Lakes, NJ) for each surface treatment. The average contact angle was determined by measurement of 5 drops. The contact angles were measured using water.

Ellipsometry measurements

The thickness of the hybrid-silica xerogel films was determined by a variable-angle spectroscopic ellipsometer (VASE, M-2000F, LOT Oriel GmbH, Darmstadt, Germany) at the incidence angle of 70° under the assumption that the film has a refractive index of 1.45. Measurements were fitted with the WVASE32 analysis software using a three-layer model for an organic layer on a SiO_2/Si substrate. Five different sampling points were used for the measurements at the relative linear distance of 1 mm from each other. The uncertainty in the measurements was estimated to be in the order of 0.1 nm, on the basis of the imperfections of silica wafers.

Atomic force microscopy investigations

Morphologies of hybrid-silica films were investigated by a DI Dimension controller (Digital Instrument, Santa Barbara, CA) in tapping mode at room temperature with a silicon nitride cantilever (Olympus, Japan), which has a resonant frequency of 265 kHz and a spring constant of 25.5 N m^{-1}.

X-ray Photoelectron Spectroscopy

The surface chemistry of silica films on Si/SiO_2 supports were investigated by means of X-ray photoelectron spectroscopy (XPS), using a Theta Probe (Thermo Fisher Scientific, East Grinstead, U.K.). A monochromatic Al Kα source with a beam diameter varying between 15 and 400 μm was used. The electrons emitted from the sample surface are collected with a radian lens having an acceptance angle of 60° (ranging from 23° to 83° emission angle) and, after passing the hemispherical analyzer, are detected by a two-dimensional detector. The average emission angle is 53°. The system is also equipped with an argon ion gun and a combined low-energy electron/ion flood gun for charge compensation. Angle-resolved XPS (ARXPS) analyses were carried out at 16 emission angles using the monochromatic Al Kα source with a beam diameter of 300 μm and a power of 70 W in the constant-analyzer-energy (CAE) mode. The pass energy and the step size were, respectively, 100 and 0.1 eV (full width at half-maximum (fwhm) of the peak height for Ag $3d_{5/2}$ = 0.84 eV). Survey spectra were acquired with pass energy of 300 eV and a step size of 1 eV. The residual pressure in the analysis chamber was always below 5×10^{-7} Pa. The spectrometers were calibrated according to ISO 15472:2001 with an accuracy of ±0.1 eV. The high-resolution

spectra were processed using CasaXPS software (v2.3.15, Casa Software Ltd., Wilmslow, Cheshire, U.K.). A linear background subtraction was applied before peak fitting using a linear least-squares algorithm. Minor charging was corrected by referencing to aliphatic carbon at 285.0 eV. The quantitative evaluation of XPS data was performed on the basis of the integrated intensity (i.e., the peak area in cps·eV obtained from the original spectra after background subtraction and curve synthesis) using a first-principles model and applying the equations of Powell.[84] The apparent atomic concentration was calculated as

$$X_j = \frac{\frac{I_{ij}}{S_{ij}}}{\sum \frac{I_{ij}}{S_{ij}}} \qquad (1.3.1)$$

where I_{ij} and S_{ij} are the area and the sensitivity factor of the peak i of the element j, respectively. The sensitivity factors were calculated from the Scofield photoionization cross-section,[85] the angular asymmetry factor,[86] the spectrometer transmission function, and the inelastic mean free path (IMFP) corrected for the emission angle, assuming the sample to be homogeneous. The inelastic mean free path, that is, the mean distance traveled by electrons with a given kinetic energy (KE) between inelastic collisions in a material M, was calculated using the equation proposed by Seah and Dench[87]

$$\Lambda_{i,M} = \left(\frac{A}{KE^2} + B\sqrt{KE} \right) \cos\theta \qquad \text{(nm)} \qquad (1.3.2)$$

where the values of A and B were, respectively, 31 and 0.087 in the case of the XPS analysis. According to Seah et al.[87], these values are valid for organic compounds. Although the formulas given by Seah and Dench[87], which were used in the present work, were not found to adequately represent the shape of the IMFP *versus* energy curves and the IMFP dependence on material parameters (such as number of valence electrons, density, atomic/molecular mass, band-gap energy)[88,89], they satisfactorily provide a first estimation of the IMFP.

Results and discussion

Roughness and morphology of the functionalized surfaces from the batch B1 were evaluated using TM-AFM. The rms roughness of cleaned silicon (100) wafers was between 0.1 and 0.2 nm and increased up to 2.9 nm (Figure 1.3.1) by dipping into TEOS and OTES solutions. The difference in roughness might suggest that multilayer structures were formed rather than monolayers, and a rougher surface was observed by decreasing OTES/TEOS ratio. The presence of such aggregates (figure 1.3.1) might be ascribed to the presence of water (about 10 mM in toluene) and to the presence of four -OEt groups, as cross-linking points, available on TEOS molecule.

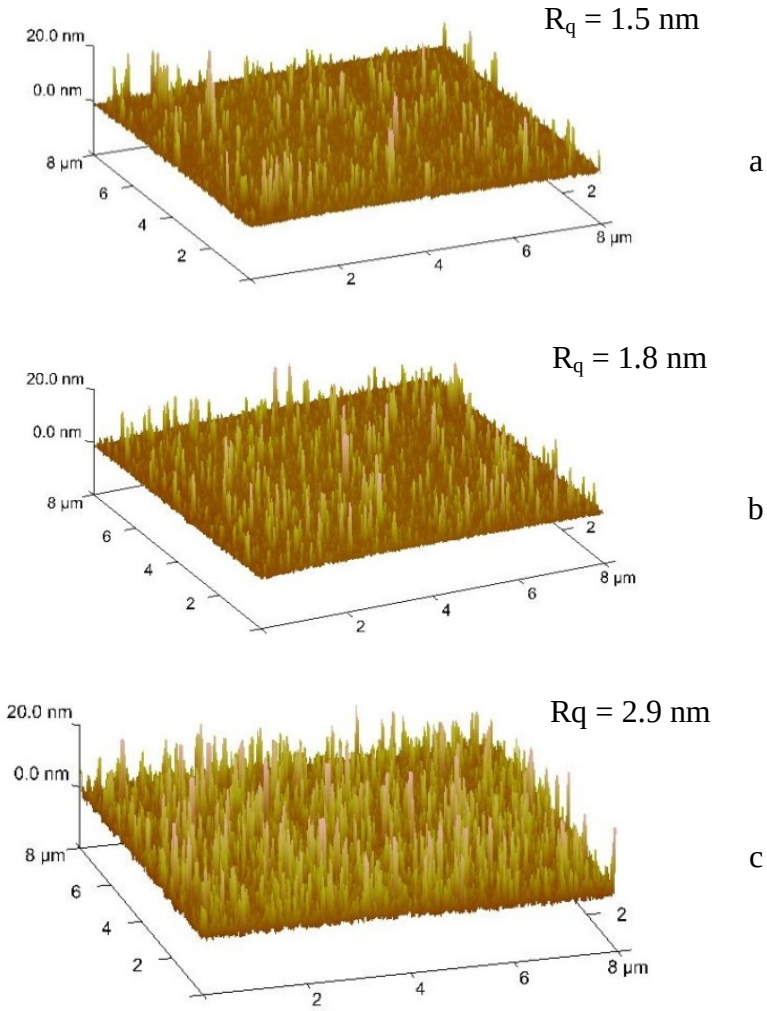

Figure 1.3.1. Three-dimensional TM-AFM pictures of S2T (20% OTES, a), S4T (40% OTES, b) and S6T (60% OTES, c)

Table 1.3.1. Film thickness and contact angle of films obtained by deposition of toluene solutions of TEOS/OTES (80/20 for S2T, 60/40 for S4T and 40/60 for S6T) on Si/SiO_2 wafers

Sample	Thickness (nm)	Contact angle (°, water)
S2T	1.5±0.1	44±1
S4T	1.8±0.1	51±1
S6T	2.5±0.1	52±1

The ellipsometric thicknesses (Table 1.3.1) of S2T, S4T and S6T were respectively 1.5, 1.8 and 2.5 nm.

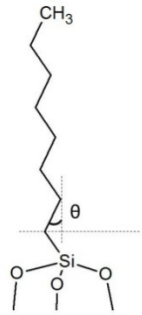

Figure 1.3.2. Model of a molecule of octyltriethoxysilane deposited on a SiO_2 surface for the calculation of the estimated thickness

To confirm the formation of multilayered systems, the expected film thickness was calculated assuming the formation of a monolayer, on the basis of bond lengths, taking 154 pm C-C, 185 pm Si-C, 109 pm C-H and taking the angle θ = 36°. It gives

$$L = \cos\theta \cdot (185 + 7 \cdot 154 + 109) = 1110 \text{ pm}$$

From this value it can be assumed that the cross-linking increases in the series S2T-S4T-S6T, as can be seen from the increase in thickness and rms roughness. Nevertheless, measured contact angles were found to be up to about 40° less than those obtained in our previous experiments, by using water and ethanol as solvents (see Chapter 1.2). In addition, small differences in the measured contact angles were ascribed to a possible oxidation process during the annealing step, which was carried out in presence of air. Another undesired result was the small difference found by varying the relative concentration of the two silanes, which was a similar result to that obtained by mixing the same reacting mixture in the presence of water, using ethanol as solvent without any stirring step (see Chapter 1.2)

On the basis of these findings, it was decided to move to a one-silane solution, the most studied system in the literature, which could be easier to control in term of surface free energy and morphology. Silanes were chosen as triethoxy-alkyl-substituted with different moieties to widen the range of polarity, by keeping the surfaces as smooth as possible, a result that was not reached up to this point. MTS, OTES and FOTES were chosen as silanes used for thin film synthesis from the literature,[90-92] to achieve a surface free energy in a wider range than previously reported in this work (estimated 5-40 mJ m^{-2}).

The annealing step was carried out both in air and in a vacuum environment to verify the possibility of surface oxidations. A discussion of surface oxidations due to the annealing conditions is further reported, in order to highlight the effect of the two different thermal treatments and of the absence of any thermal treatment. The first silane taken into account was OTES. Si/SiO_2 wafers were dipped in 100 mM solutions in toluene (see Experimental) and an annealing step at 70 °C in an air environment was carried out. Contact angle using water as solvent was found to be 83±1° and a partial oxidation on the surface is thought to take place, also taking

into account the work of Can *et al.* performed on OTES Langmuir-Blodgett films, where a contact angle of 93° was reported.[92]

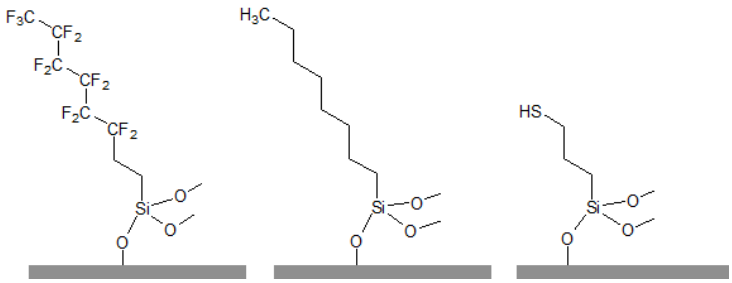

Figure 1.3.3. Model FOTES (left), OTES (middle) and MTS (right) molecules deposited on a SiO_2 surface

In terms of surface oxidation, a similar result was found when MTS was used as silane. Contact angle by using water was found to be 55±1°, significantly lower than reported in previous works.[90,93] As a consequence, an annealing step under vacuum and no annealing steps were carried out for each film synthesis.

To perform MTS and OTES surface functionalization 100 mM solutions were used, whereas 1-100 mM range was investigated for FOTES in terms of surface homogeneity. AFM investigations were carried to gain insights into morphology. Results are reported in Figure 1.3.4.

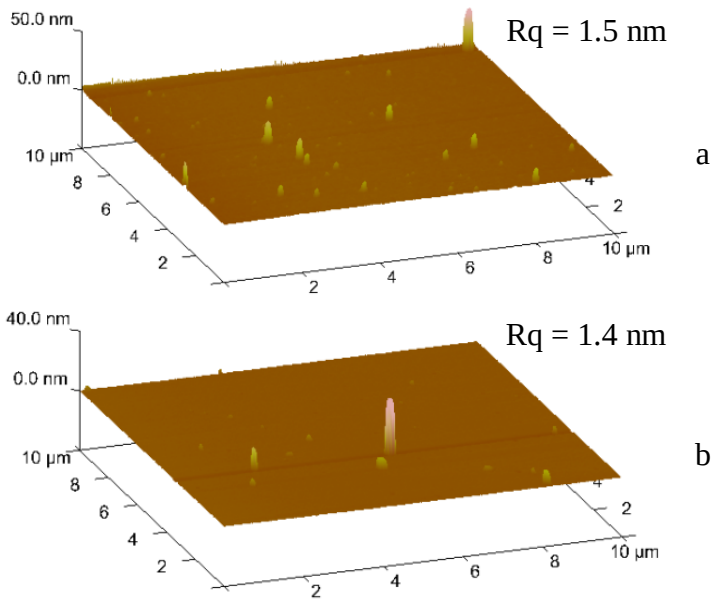

Figure 1.3.4. Three dimensional TM-AFM pictures of MTS-coated (a) and OTES-coated (b) Si/SiO_2 wafers

Contact angles, by using water as solvent, were found to be 73±1 and 90±1 for S-MTS and S-OTES respectively, consistent with literature data.[92-94] Thickness of S-MTS and S-OTES was 1.2±0.1 nm and 0.9±0.1 nm, respectively. These values were compared to the thickness of a monolayer adsorbed on the surface (i.e. 0.65 nm MTS, 1.11 nm OTES) to investigate the possible formation of multilayered

systems. In both cases a few aggregates, as a consequence of in-solution aggregation, were observed. In addition, a full coverage of silanes was likely to be gained, but alkyl chains of silanes should to be tilted with respect to normal direction from the surface. The tilting angle can be calculated by

$$\alpha = \cos^{-1}\left(\frac{\textit{experimental length}}{\textit{theoretical length}}\right)$$

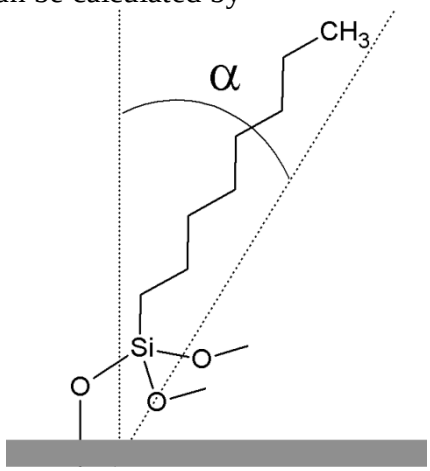

Figure 1.3.5. Model of a molecule of octyltriethoxysilane deposited on a SiO_2 surface for the calculation of the estimated tilting angle

giving 36° for OTES chains and possibly a bilayer structure for MTS. It may be reasonable to assume that MTS and OTES layers, having thiol and methyl groups at the top of the surface, showed a partial oxidation of the alkyl chains. As regards FOTES, the functionalization of the surface by the synthesis of a monolayer started from a 100 mM solution in toluene, as previously chosen for other silanes. However, it was observed that the solution turned cloudy within one hour, reasonably due to in-solution cross-polymerization among silane molecules. The fact that solutions become cloudy with time shows that such aggregation does indeed occur.[74] If these aggregates assemble and interact with the surface during film formation, monolayers will not be produced unless surface interactions are strong enough to restructure the aggregates. A cloudy liquid phase is an inadequate starting point for an optimal self-assembled monolayer, because cross-polymerization was shown to be incompatible for a fully covered monolayer and consequently a homogeneous surface.[95] The aliphatic tails will have to be splayed, and this will limit the amount of coverage. The splayed chains prevent any further cross-linking. Furthermore, they prevent any chains from being nearby. The resulting monolayer coverage will be patchy. As the degree of coverage increases (beyond some “overlap” value), the amount of cross-linking must decrease in order to satisfy the packing constraints. Thus, as to obtain the highest homogeneity, dilution factors between 1:10 to 1:100 were taken into account for the further surface functionalization. By diluting the silane, a lower degree of in-solution cross-linking was expected. Insights about homogeneity of the coverage could be inferred from static contact angle measurements and ellipsometric thickness (Table 1.3.2), for three independent films for each concentration of silane. In addition,

TM-AFM pictures of 10 μm×10 μm of the investigated surfaces are provided in Figure 1.3.6 (one representative for each concentration level).

From these results it was reasonable to assume that 5 mM is the minimal concentration from which it is possible to obtain almost a full coverage, according to contact angle values reported in literature,[96] also because contact angles in excess of 115° are not indicative of continued packing of fluoroalkylsilane molecules into the monolayer, but are associated with a roughening of the surface.[74] Below 5 mM of FOTES in toluene, it may be inferred that a full coverage cannot be obtained. Further comments can be addressed by comparing each experimental thickness and the expected, i.e. 1.13 nm (C-F, 134 pm), as previously done for MTS and OTES molecules. As concerns the surface functionalized by using the solution with the lowest FOTES concentration, as can be seen from TM-AFM pictures a patchy surface was obtained and fluoroalkyl chains so one might assume that either the chains are tilted (from VASE measurements, averagely about 25°) or the coverage is not complete (full). On the other hand, by increasing FOTES concentration thickness is significantly increased far above the expected value for a monolayer on the surface and the presence of abundant in-solution cross-linking lead to a multilayered system, with a higher rms roughness. These results showed that high reactivity of fluorinated silanes can influence surface roughness, even in presence of impurity levels of water (estimated as 0.02% v/v in toluene).

Table 1.3.2. Film thickness and contact angle of films obtained by deposition of toluene solutions of FOTES on Si/SiO_2 wafers

Silane concentration (mM)	Thickness (nm)	Static contact angle (°, water)
1	0.7±0.1	95±1
1	0.7±0.1	95±1
1	1.0±0.1	94±1
5	1.5±0.3	112±1
5	1.2±0.1	112±1
5	1.3±0.2	113±1
10	2.9±0.2	113±1
10	2.5±0.2	114±1
10	3.2±0.3	113±1

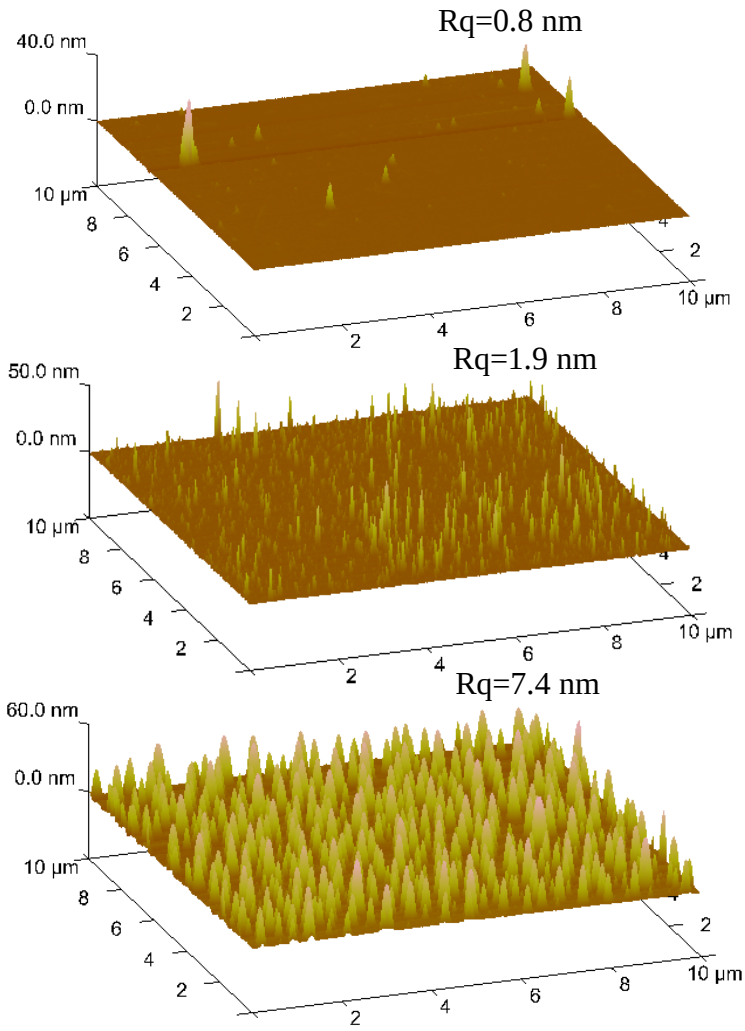

Figure 1.3.6. Three dimensional TM-AFM pictures of FOTES-coated Si/SiO_2 wafers from 1 mM (a), 5 mM (b) and 10 mM (c) silane solutions in toluene

At this point, since surface oxidations were speculated in the annealing step of MTS and OTES monolayers, all the surface functionalizations were ended up by a vacuum annealing (pressure approximately 0.2 mbar). The characterization of each surface was performed using the same techniques described so far. Table 1.3.3 reports thickness and contact angles (water) for each functionalized SiO_2 surface.

Table 1.3.3. Film thickness and contact angle of films obtained by deposition of toluene solutions of FOTES on Si/SiO_2 wafers

Sample	Thickness (nm)	Contact angle (°, water)
s-MTS	1.2±0.1	73±1
s-MTS	1.3±0.2	73±1
s-MTS	1.1±0.3	73±1
s-OTES	1.4±0.1	88±1
s-OTES	0.9±0.1	90±1
s-OTES	1.1±0.1	90±1
s-FOTES	1.4±0.3	113±1
s-FOTES	1.2±0.1	113±1
s-FOTES	1.9±0.3	113±1

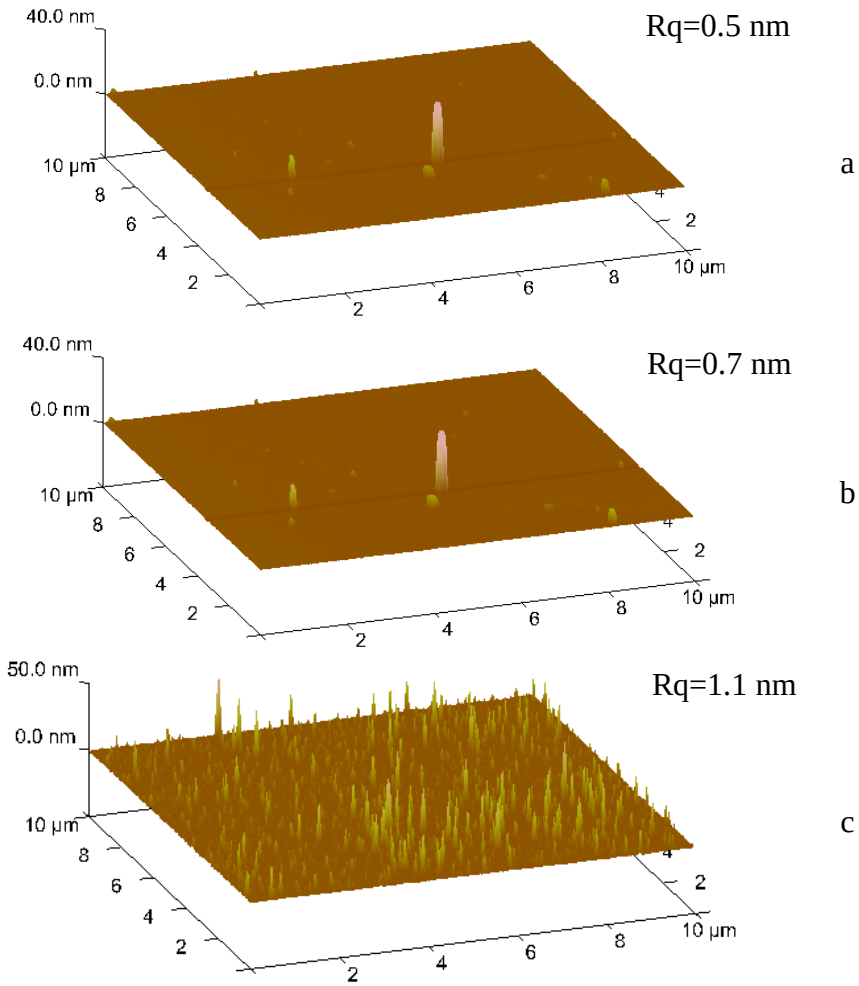

Figure 1.3.7. Three-dimensional TM-AFM pictures of silane-coated Si/SiO_2 wafers by MTS (a), OTES (b) and FOTES (c) solutions in toluene. A vacuum annealing step at 100 °C was carried out

TM-AFM investigations were carried out and the observed topography confirmed the synthesis of smooth surfaces (Figure 1.3.7).

To complete surface characterization, XPS investigations were performed for each sample. XPS spectra of clean SiO_2, s-MTS, s-OTES and s-FOTES were acquired. As far as functionalized glasses it concerns, further peaks found in the survey spectra of each surface showed signals ascribable to silicon oxide, such as from Si and O. Further signals were attributed to the presence of adsorbed silanes onto silica surfaces, namely S 2s and S 2p for g-MTS, and F 1s for g-FOTES (Figure 1.3.8).

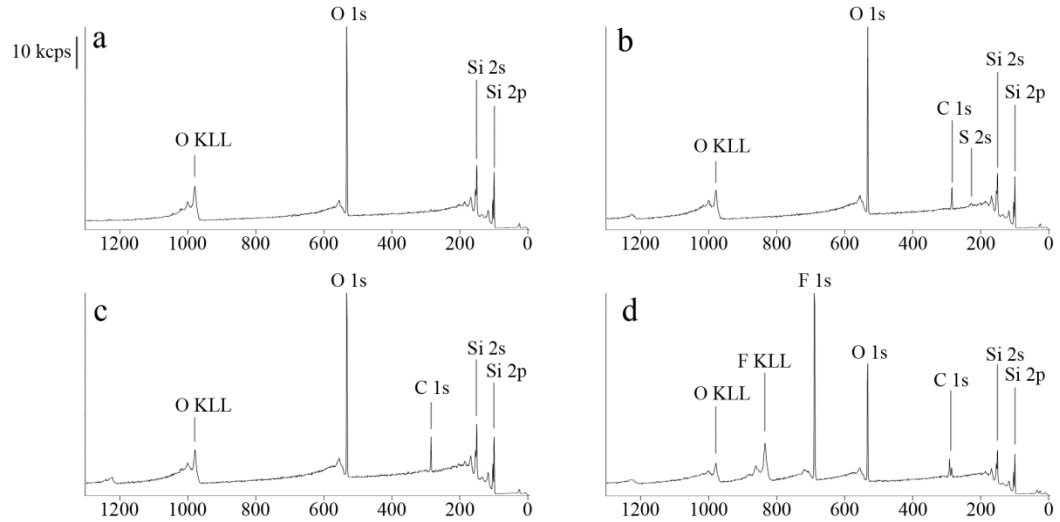

Figure 1.3.8. Survey XP-spectra of SiO_2 (a), s-MTS (b), s-OTES (c) and s-FOTES (d)

Starting from s-MTS, three major peaks are identified in the C 1s spectrum (Figure 1.3.9a). The peak centered at 285.0 eV was ascribed to C-C and C-Si bonds,[90,94,97] whereas carbon atoms bonded to sulfur and oxygen appear at 286.3 eV.[98,99] A third minor peak, found at about 288 eV, might be due to an oxygen-containing compound adsorbed on the sample surface. A further confirmation of the effectiveness of the functionalization was from Si 2p, where the high-resolution spectrum signal was found to contain contributions at 103.2 and 103.6 eV (Figure 1.3.9d) attributable to Si-O of silicon oxide[100] and Si-C of s-MTS respectively.

The high-resolution spectrum of S2s shows a contribution at 227.8 eV due to the presence of well-ordered MTS layers having thiol groups at the top of the surface. [101] Spectrum of S 2p shows two contributions at 164 and at about 168 eV, assigned to the presence of -SH groups from adsorbed MTS and to a plasmon resonance attributable to elemental silicon [97,102,103] (data not shown). Concerning s-OTES, similarly to that observed for s-MTS, C 1s showed three major contributions at 285 eV, 286.5 eV, 288 eV (Figure 1.3.9b) and two components for the Si 2p signal at 103.1 and 103.7 eV ascribed to SiO_2 and Si-C (Figure 1.3.9e). In the case of s-FOTES, C 1s signal was a convolution of five components at 285.2 eV, originating from C-C and C-Si,[96,104] and at 286.5, 291.4, 293.8 and 288 eV due

to C-O,[98] CF_2 and CF_3 groups,[96,98,104] and a contamination, respectively (Figure 1.3.9c). Two components for the Si 2p signal at 103.1 and 103.2 eV were ascribed to silicon oxide and Si-C, as showed in Figure 1.3.9f. All Si 2p high resolution spectra showed the contribution of elemental silicon at 99.3 eV.

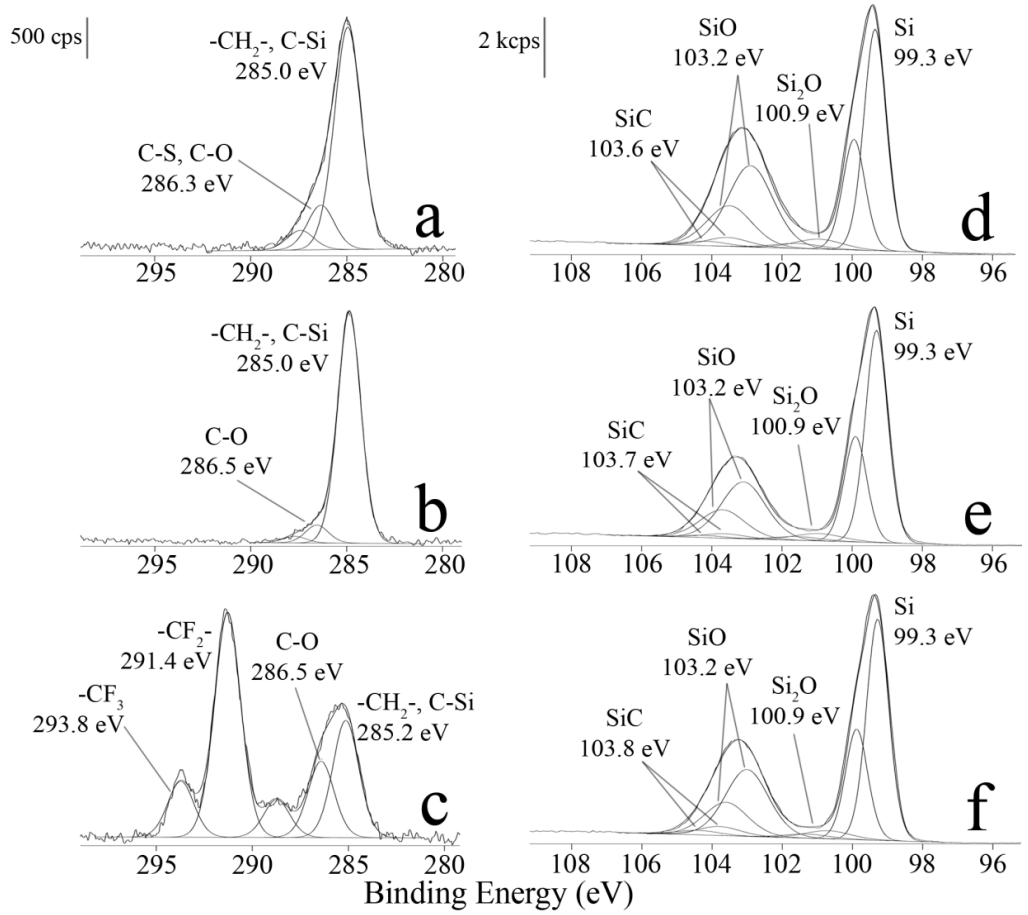

Figure 1.3.9. Curve-fitting of high-resolution C 1s spectra of samples s-MTS (a), s-OTES (b), s-FOTES (c) and Si 2p spectra of samples s-MTS (d), s-OTES (e) and s-FOTES (f)

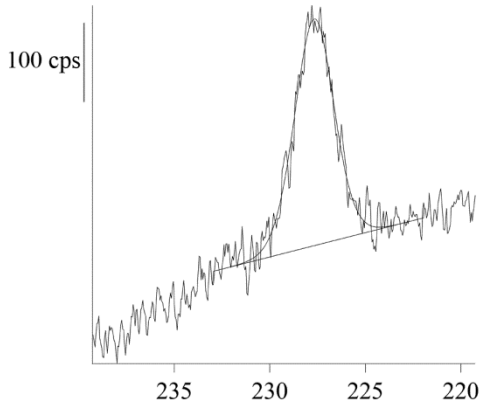

Figure 1.3.10. Curve-fitting of high resolution S 2s spectrum of s-MTS

High-resolution O 1s spectra of s-MTS, s-OTES and s-FOTES, shown in Figure 1.3.11, were composed by a convolution of two contributions due to the presence of silicon oxide and possibly oxygen atoms from adsorbed silanes at 532.8 eV and possibly unreacted EtO groups at 533.6 eV. Further confirmations on effectiveness of the functionalization were provided by relative ratios among C 1s, O 1s (533.6 eV), Si 2p signals. Regarding s-MTS, the ratio of C 1s at 285 eV over C 1s at 286.3 eV is about 6, consistent with MTS condensing on the glass surface, according to previously published results referred to solution-deposited mercapto-silanes.[94] This result indicates that ethoxy groups have been lost during adsorption, even though some ethoxy groups within the film, although only to a minor extent. C1s/O1s ratio was found to be 6.4, thus consistent with the hypothesis of a multilayered adsorption of silanes, involving ethanesulfonic acid or ethylmercaptan elimination as the multilayer mercaptan grows.[97] In case of s-OTES, the ratio C 1s /O 1s was found to be 7.7, consistent with a monolayer of OTES molecules bound to the surface. Also in the case of s-FOTES films, the effectiveness of the coating was confirmed by the elemental analysis. The atomic ratio of carbon at 294.1 eV to that at 291.5 eV was found to be in perfect agreement with the expected value $(CF_3)/(CF_2)_5$=0.2. Furthermore, for the C 1s peak originating from CH_2 carbons found at 285.2 eV in this spectrum, the observed peak area intensity ratio of CH_2 carbons to CF_3 carbons is 3.35, which is larger than the carbon content ratio of $(CH_2)_2/(CF_3)$=2 in the FOTES molecules, in consequence of X-ray damage, according to data previously reported in the literature.[105] C 1s/O 1s ratio was found to be 10.3 consistent with a partial loss of OEt groups during condensation.

ARXPS investigations were carried out to estimate films thickness, by monitoring the attenuation of Si 2p signal at 99.3 and 103.1 eV as a function of the emission angle (EA). The thickness of carbons (d) for each functionalized surface is given by the equation $I = I_0 \exp(-d/\lambda\cos\theta)$, where I_0 is the intensity of the emission from the bulk, θ is the emission angle (with respect to sample normal), λ is the inelastic mean free path (referred to the overlayer) and d is the film thickness. From the data reported in Table 1.3.3, it was possible to discuss the experimental thickness with those fitted by ellipsometric analysis (averaged over 5 positions) and a theoretic value, under the assumption that a monolayer of silanes had been bound on the surface, with alkyl chains standing perpendicular to the adsorption plane. From ellipsometry it might be reasonable to assume that a monolayer of silanes was formed both by OTES and by FOTES deposited on the surfaces, possibly slightly tilted with respect to the plane normal to the surface. On the contrary s-MTS seems to be composed by multilayered structure of MTS molecules, which is supported by atomic relative ratios obtained in aforementioned XPS experiments. An apparent underestimation of thickness might be justified by a significantly larger deviation (up to 30–40%, attributable to the uncertainty of λ) observed by Semak *et al.*, when ARXPS was compared to other techniques for thickness determinations.[106] It has to be highlighted that thickness determination is strictly related to the sampling point, whereas the value obtained by averaging those

obtained by ellipsometry is a less reliable approach, because the homogeneity of the surface cannot be demonstrated by data shown in this chapter.

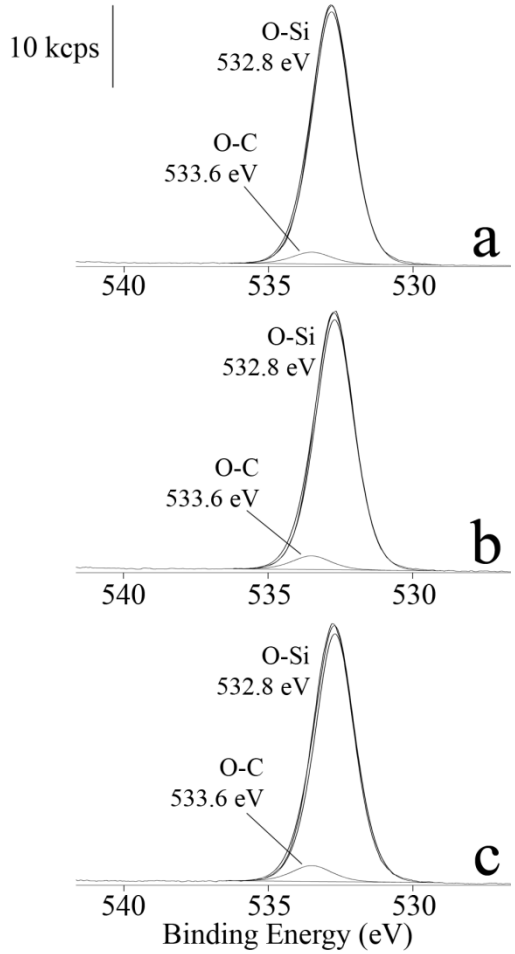

Figure 1.3.11. Curve-fitting of high resolution O 1s XP-spectra of s-MTS (a), s-OTES (b) and s-FOTES (c)

Table 1.3.3. Thickness values for the three functionalized Si wafers calculated by Si 2p signal attenuation (103.2 eV) as a function of the photoemission angle. Thickness fitted from ellipsometric data are referred to the sample before introduction into the XPS chamber.

	Thickness (nm)		
	ARXPS[a]	Ellipsometry[b]	Expected
s-MTS	0.7±0.1	1.2±0.1	0.65
s-OTES	0.7±0.1	0.9±0.1	1.11
s-FOTES	0.8±0.1	1.2±0.1	1.13

[a] Referred to a well-defined XPS sampling point
[b] Averaged among 5 five positions

It is therefore reasonable to assume that an inhomogeneous multilayered system may be assumed for s-MTS, yet on a nm scale. Nevertheless a good interpretation of the composition of the surface was given for all samples taken into

account and further insights and applications of these thin films will be later presented in this Ph.D. work.

Conclusions

In conclusion, the present work suggested that it was possible to tailor surface free-energy by functionalizing Si wafer (100) covered by the natural SiO_2 layer formed in contact with the ambient, with different alkylsiloxanes. It was demonstrated that, on the basis of instrumental characterizations, they are likely to bind the surface by a self-assembly process. Contact angle measurements were found to be reproducible, as well as thickness and morphology, proving the capability of modifying surfaces without increasing surface roughness beyond a nm scale limit. In the next chapter, it will be further described how to extent the proposed functionalization reactions to amorphous SiO_2 surface, i.e. glass, used for further mass spectrometric applications.

1.4

Synthesis and characterization of tailored surfaces as supports for surface effects investigations in desorption electrospray ionization-mass spectrometry

Introduction

So far a great number of papers have highlighted DESI-MS as a high-throughput technique in a variety of application fields.[4,17] Several papers have been published elucidating the ionization mechanisms leading to the formation of isolated gas-phase ions, supporting the hypothesis of a two-step droplet-pick-up model followed by ESI-like desolvation and gas-phase ion formation by action of the electrical field[13,107-109]. In this context, the role of surface and pneumatic effects on ion-formation yield has recently been investigated, by investigating surface charge,[15,56] hydrodynamical and pneumatic forces[110-113] and interactions between analytes and the surface.[68] In this study surface chemistry effects on DESI-MS response were thoroughly investigated and correlated to the ion formation yield. It is known that the electrical properties of the substrate strongly influence the mass spectrometric response in terms of magnitude of the steady state current and different capacitor time constants of the equivalent RC circuits.[56] Therefore, in order to address only chemical contributions from the surface on the ion formation the electrical contribution of the substrate, i.e. electrical resistivity, was set to be constant by using the same material as support for the functionalization reactions.

So far one of the most successful approaches for the modification of solid substrates has been the chemical grafting of hydrocarbon chains on hydrated surfaces via an alkylchlorosilane ($-SiCl_3$) or alkylalkoxysilane ($-SiOR_3$) head group by the formation of self-assembled monolayer structures.[26,75,76] However, despite extensive efforts, the silanization reaction could still be affected by scarce reproducibility in the macroscopic properties (i.e. wettability and contact angle hysteresis) of the deposited film, when experimental variables such as the nature of the substrate,[77,78] temperature,[33,77,79] concentration,[78,80] solvent type[81] and water content[82,83] are not under strict control. By controlling these parameters it can be possible to obtain a structure of alkylsilane monolayers with good reproducibility, because solution agglomeration on the deposition, leading to cross-polymerization, is accurately minimized.[74]

Taking into account the aforementioned knowledge about surface functionalizations and starting from our previously published results,[68] the aim of this work was to address further questions regarding the surface effects in DESI

mechanism. For this purpose, in order to obtain surfaces in a wide range of surface free energy we set up an experimental strategy based on the synthesis and the characterization of differently functionalized glasses, namely by means of three different silanes (Figure 1.4.1), i.e. mercaptopropyl-triethoxysilane (MTS), octyl-triethoxysilane (OTES) and 1H,1H,2H,2H-perfluorooctyl-triethoxysilane (FOTES), and glass as such, used as a hydrophilic surface. Surface characterizations were carried out by means of tapping-mode atomic force microscopy (TM-AFM), contact angle measurements and X-ray photoelectron spectroscopy (XPS).

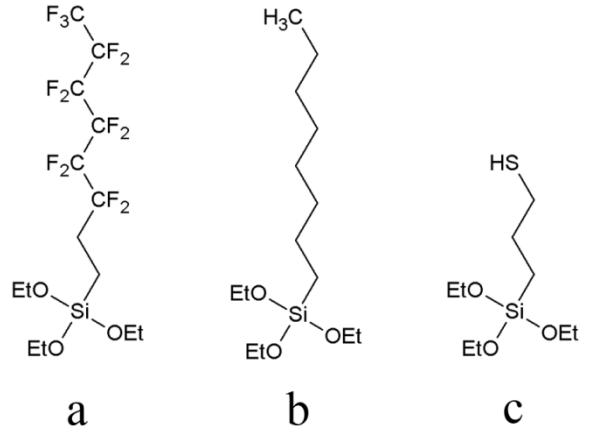

Figure 1.4.1. Chemical formulas of silanes adsorbed onto glass slides, i.e. (a) FOTES, (b) OTES and (c) MTS

Finally, these four supports were used for pneumatically-assisted DESI-MS experiments for the analysis of mixtures of small molecules with widely known acid-base behavior and deposited on all substrates. In particular, melamine (organic base, MW 126), lincomycin (lincosamide antibiotic, MW 406) and tetracycline (polyketide antibiotic, MW 444) (Figure 1.4.2) were considered. Functionalized surfaces allowed the demonstration on how surface chemistry plays a role in different spectrometric conditions.

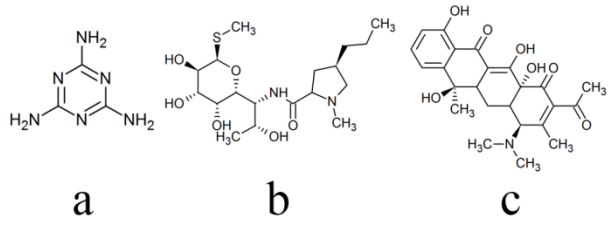

Figure 1.4.2. Chemical formulas of the compounds used for DESI-MS, i.e. melamine (a), lincomycin (b) and tetracycline (c)

Experimental

Materials

Microscope glass slides (76 mm x 25 mm x 1 mm) were provided by Thermo Scientific (Wohlen, Switzerland). 3-mercaptopropyl-triethoxysilane (MTS) was from Alfa Aesar (Ward Hill, MA, USA), octyltriethoxysilane (OTES) was from Acros (Acros Organics, Geel, Belgium) and 1H,1H,2H,2H,perfluorooctyl-triethoxysilane (FOTES) was purchased from ABCR-chemicals (Karlsruhe, Germany). Methanol, toluene, hydrogen peroxide and sulphuric acid were from Sigma-Aldrich (St. Louis, MO, USA). Ethanol was from Scharlau (analytical grade, Spain). Deionized (DI) water was purified to 18.2 MΩ·cm using a Milli-Q water purification system (Milli-Q element A10 System, Millipore, San Francisco, CA, USA).

Silanization

Microscope glass slides were used as supports for each film synthesis. All materials were cleaned by ultrasonication, first for 10 minutes in toluene, then twice 10 minutes in ethanol and then blown dry in a stream of nitrogen. Subsequently, the supports were cleaned for 2 minutes in oxygen plasma (Harrick Plasma, USA) at the pressure of 0.03 mbar. All microscope slides were then dipped for 1 hour into silane solutions (toluene). One hundred mM solutions in toluene for MTS and OTES, 5 mM for FOTES were used respectively. Each silanized surface was rinsed with water, then with toluene. Samples were annealed at 100 °C at the pressure 0.2 mbar for 60 minutes.

Surface characterization

Contact-angle goniometry and surface free energy calculations

The equilibrium contact angle of a sessile drop (5 μL) was measured with a contact-angle goniometer (Rame´ Hart model 100, Rame´ Hart, Inc., Mountain Lakes, NJ) for each surface treatment. The average contact angle was determined by measurement of 10 drops. The Owens-Wendt-Kaelble (OWK)[114] method was used to calculate surface energies.

In OWK method, the polar (γ_S^p) and dispersion (γ_S^d) components of the surface energies of functionalized slides were determined by Equations 1.4.1 and 1.4.2.

$$\gamma_L(1+\cos\theta) = 2\left(\sqrt{\gamma_S^d \gamma_L^d} + \sqrt{\gamma_S^p \gamma_L^p}\right) \quad (1.4.1)$$

$$\gamma_S = \gamma_S^p + \gamma_S^d \quad (1.4.2)$$

The parameters γ_L, γ_L^d, and γ_L^p refer to the total surface tension and dispersion and polar components of the probe liquid, respectively. The surface

energy (γ_S) of a modified surface is the sum of polar (γ_S^p) and dispersion (γ_S^d) components of the solid.

The contact angles were measured using two liquids, that is, water and diiodomethane (DM). The corresponding surface tensions (γ_L) are 72.8 and 50.8 mN/m, respectively. Polar and dispersion components to the surface tension were from Yu and Dekker.[115]

Tapping mode-atomic force microscopy

Morphologies of hybrid-silica films were investigated by a DI Dimension controller (Digital Instrument, Santa Barbara, CA) in tapping-mode at room temperature with a silicon nitride cantilever (Olympus, Japan), which has a resonant frequency of 265 kHz and a spring constant of 25.5 N m^{-1}. Ten µm x 10 µm pictures were acquired, root mean squared roughness (R_q) was calculated for each surface and then averaged among 3 independent investigations.

X-ray photoelectron spectroscopy

The surface chemistry of silica films on glass supports were investigated by means of XPS using a Theta Probe (Thermo Fisher Scientific, East Grinstead, U.K.). A monochromatic Al Kα source with a beam diameter varying between 15 and 400 µm was used. The electrons emitted from the sample surface are collected with a radian lens having an acceptance angle of 60° (ranging from 23° to 83° emission angle) and, after passing the hemispherical analyzer, are detected by a two-dimensional detector. The average emission angle is 53°. The system is also equipped with an argon ion gun and a combined low-energy electron/ion flood gun for charge compensation. Angle-resolved XPS (ARXPS) analyses were carried out at 16 emission angles using the monochromatic Al K_α source with a beam diameter of 300 µm and a power of 70 W in the constant-analyzer-energy (CAE) mode. The pass energy and the step size were 100 and 0.1 eV (full width at half-maximum (fwhm) of the peak height for Ag $3d_{5/2}$ = 0.84 eV), respectively. Survey spectra were acquired with a pass energy of 300 eV and a step size of 1 eV. A low-energy electron/ion flood gun for charge compensation was used with electron energy –1.6V at $7 \cdot 10^{-7}$ mbar. The spectrometer was calibrated according to ISO 15472:2001 with an accuracy of ± 0.1 eV. The high-resolution spectra were processed using CasaXPS software (Casa Software Ltd., Wilmslow, Cheshire, U.K.). A linear background subtraction was applied before peak fitting using a linear least-squares algorithm. Minor charging was corrected by referencing to aliphatic carbon at 285.0 eV. Peak fitting was performed with a linear type background and 30% Lorentzian/70% Gaussian components. Data processing was carried out by imposing shifts between $2p_{3/2}$ and $2p_{1/2}$ signals, concerning Si 2p and S 2p equal to 0.7 eV and 1.3 eV respectively.

The quantitative evaluation of XPS data was performed on the basis of the integrated intensity (i.e., the peak area in cps·eV obtained from the original spectra

after background subtraction and curve synthesis) using a first-principles model and applying the equations of Powell.[84] The sensitivity factors were calculated from the Scofield's photoionization cross-section,[85] the angular asymmetry factor,[86] the spectrometer transmission function, and the inelastic mean free path (IMFP) corrected for the emission angle, assuming the sample to be homogeneous. The inelastic mean free path, that is, the mean distance traveled by electrons with a given kinetic energy (KE) between inelastic collisions in a material M, was calculated using the equation proposed by Seah and Dench.[87]

Desorption electrospray-mass spectrometry

A linear ion trap LTQ Orbitrap XL™ mass spectrometer (Thermo Fisher Scientific, San Josè, CA, USA) equipped with a DESI ion source (Prosolia Inc., Indianapolis, IN, USA) was used. The source parameters were set as follows: solvent flow-rate, 2 µL min^{-1}; nitrogen pressure, 150 psi; capillary voltage, 20 V; tube lens voltage, 40V; injection time, 100 ms; tip-to-surface distance, 2 mm; tip-to-inlet distance, 4 mm; incidence angle, 54°. The capillary temperature was 250°C. Methanol (MeOH) and acetonitrile (ACN) were used as spray solvents. The sprayer potential was varied in the range 1-3 kV.

Results and discussion

TM-AFM. TM-AFM investigations were carried out to observe surface morphology. At first, TM-AFM picture were acquired for plasma-cleaned glass slides to select the smoothest side of the slide, in order to obtain the smoothest surfaces possible. According to data reported in the literature, that is, 0.3-3 nm,[116] root mean square roughness (R_q) was found to be within this range, i.e. 0.9 nm. R_q was also calculated for the silane-coupled glasses, i.e. g-MTS, g-OTES and g-FOTES, but a significant increase in surface roughness was not observed (Figure 1.4.3). The presence of imperfections on a nano-scale was observed and ascribed to inhomogeneity of the starting glass surfaces and possibly aggregates from in-solution reactions among silanes. Taking into account the well-known reactivity of silanes with water, in particular using fluorinated compounds, to avoid self-polymerization of silanes particular conditions of hygrometry were conditioned by the use of dry toluene as solvent.[33] Toluene was also used for the surface functionalization for its capability of extracting significant amounts of water from the substrate surface yielding dense alkylsiloxanes films.[37] The presence of self-assembled monolayers (SAMs) on glass surfaces might be supported by a non-significant changes of the surface roughness of the cleaned slide,[116] but it will be further discussed with XPS results. Finally it is to be noted that the use of smooth surfaces, expressed in term of comparable R_q values, for subsequent DESI-MS experiments, allowed drawing conclusions on how surface chemistry affects ion

formation yield, without any contribution from morphological changes, further discussed with mass spectrometric data.

Table 1.4.1. Contact angles and surface free energy values of cleaned glass and functionalized slides with the three different silanes

Surface	Contact angle (°)		Surface free energy (mJ m^{-2})
	Water	Diiodomethane	
Glass	12±1	42±1	71.1±0.6
g-MTS	72±1	46±1	39.7±0.4
g-OTES	91±1	64±1	27.3±0.4
g-FOTES	106±2	88±2	14.5±0.5

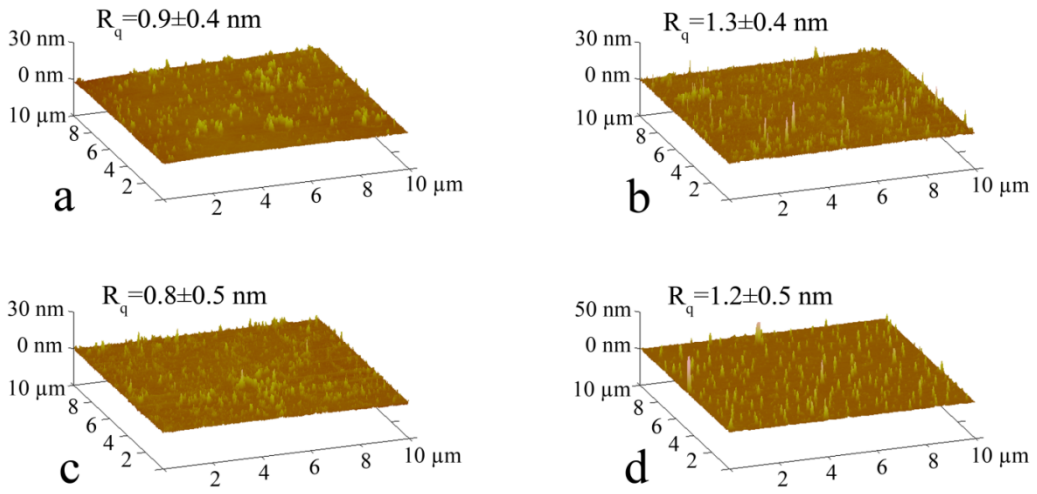

Figure 1.4.3. Three-dimensional TM-AFM pictures of a clean non-coated glass slide (a), g-MTS (b), g-OTES (c) and g-FOTES (d). Results are expressed as mean value (n=3) with standard deviation.

Contact angle and surface free-energy calculations. Contact angle were reported in Table 1.4.1, as well as the surface free-energy, determined according to the OWK method, using a polar–nonpolar pair of liquids, that is, water–diiodomethane. As expected, the highest surface free energy was found for g-FOTES and it decreased in the series g-OTES, g-MTS, glass, the last one chosen as hydrophilic surface. Maximum density of silane coverage was reasonably reached by using each silane, according to previously published results.[90,92,94,96,104,117] These results prove successful chemical modifications of glass surface. Further confirmations concerning SAMs structures and homogeneity of the coverage were by XPS.

XPS. XPS spectra of clean glass, g-MTS, g-OTES and g-FOTES were acquired. Concerning functionalized glasses, further peaks found in the survey spectra of each surface showed signals ascribable to glass, such as from Si and O as well as from Na, K and Ca, naturally abundant as counter-ions within the silicate

glass network. Further signals were attributed to the presence of adsorbed silanes onto glass slides, namely S 2s and S 2p for g-MTS, and F 1s for g-FOTES (Figure 1.4.4).

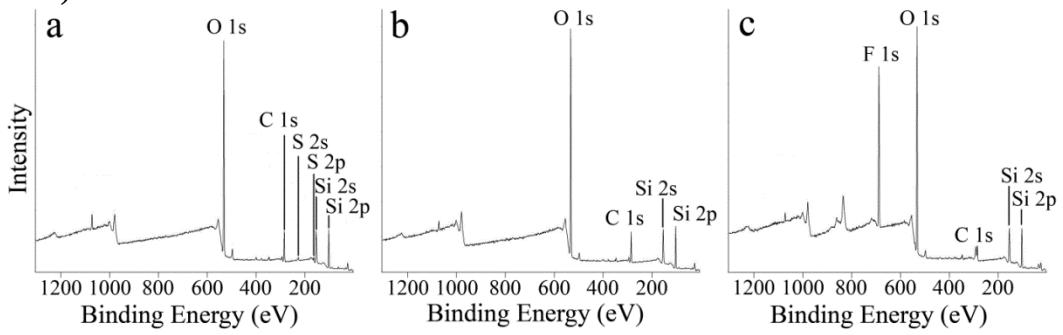

Figure 1.4.4. Survey XP-spectra of g-MTS (a), g-OTES (b) and g-FOTES (c)

Starting from glass surface functionalized with MTS (g-MTS), three major peaks are identified in the C 1s spectrum (Figure 1.4.5a). The peak centered at 285.0 eV was ascribed to C-C and C-Si bonds,[90,94,97] whereas carbon atoms bonded to sulfur and oxygen appear at 286.3 eV.[98,99] A third minor peak, found at about 288 eV, might be due to an oxygen-containing compound adsorbed on the sample surface. A further confirmation of the effectiveness of the functionalization was from Si 2p, where the high-resolution spectrum signal was found to contain contributions at 103.1 and 103.7 eV (Figure 1.4.5d) assigned to SiO of glass[100] and Si-C of g-MTS respectively. The high-resolution spectrum of S 2p was fitted with two doublets whose maxima of their $2p_{3/2}$ components were at 164 and at about 168 eV, assigned to the presence of well-ordered MTS layers having thiol groups at the top of the surface[101] and to a minor contribution from oxidized sulfur[97,102,103] (Figure 1.4.6). As far as g-OTES is concerned, similarly to what observed for g-MTS, C 1s showed three major contributions at 285 eV, 286.5 eV, 288 eV (Figure 1.4.5b) and two components for the Si 2p signal at 103.1 and 103.8 eV ascribed to glass and Si-C (Figure 1.4.5e). In the case of g-FOTES, C 1s signal was a convolution of five components at 285.2 eV, originating from C-C and C-Si,[96,104] and at 286.5, 291.5, 294 and 288 eV due to C-O,[98] CF_2 and CF_3 groups,[96,98,104] and some contamination, respectively (Figure 1.4.5c). Two components for the Si 2p signal at 103.1 and 104.1 eV were ascribed to Si-O from the glass substrate and Si-C, as showed in Figure 1.4.5f.

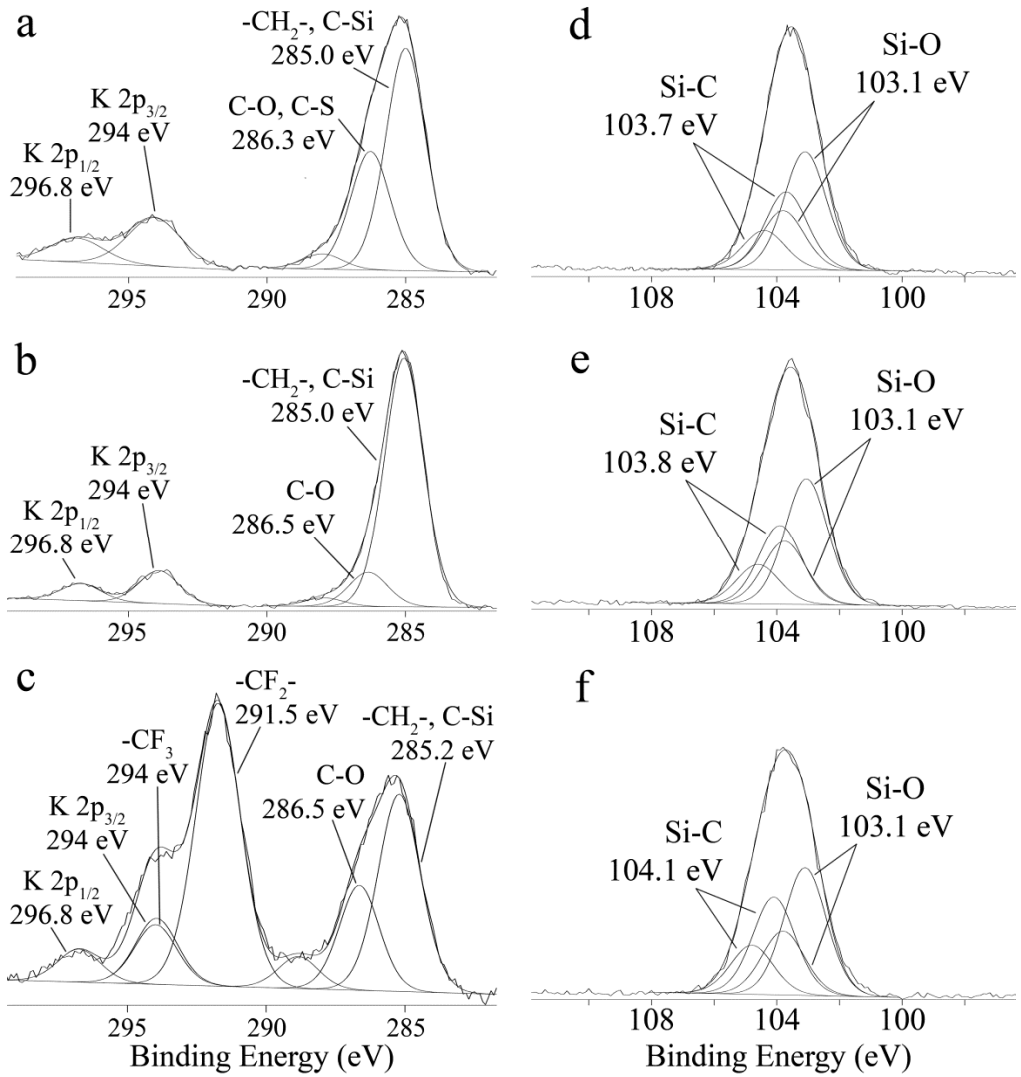

Figure 1.4.5. Curve-fitting of high resolution C 1s spectra of samples g-MTS (a), g-OTES (b), g-FOTES (c) and Si 2p spectra of samples g-MTS (d), g-OTES (e) and g-FOTES (f)

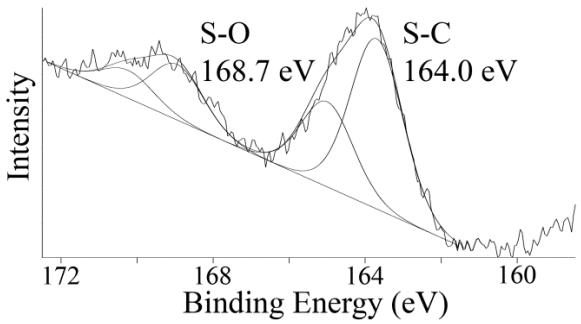

Figure 1.4.6. Curve-fitting of high-resolution S 2p XP-spectrum of glass surfaces functionalized with MTS.

O 1s high-resolution spectra of g-MTS, g-OTES and g-FOTES, shown in Figure 1.4.7, were composed by a convolution of three contributions due to the presence of glass and possibly signals ascribable to the adsorption of silanes at 532.8 eV and possibly unreacted EtO groups. In addition, contribution from Na, K and Ca metasilicates shows a contribution at about 531 eV[118] and a contribution from unreacted alkoxy groups in the uppermost layers at above 533 eV.

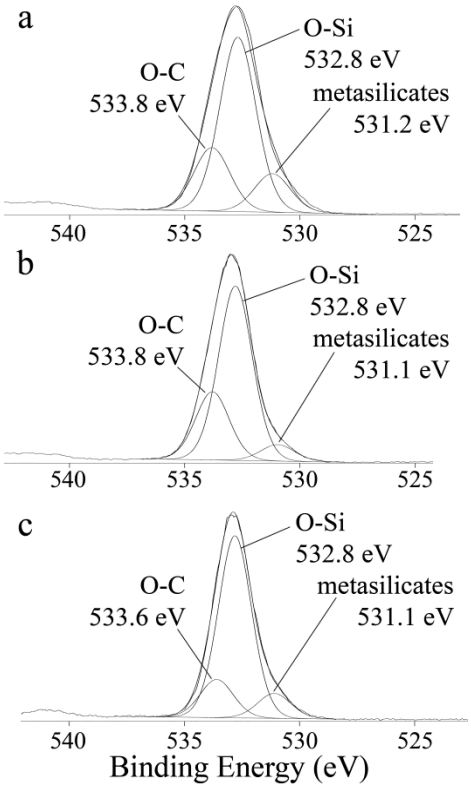

Figure 1.4.7. Curve-fitting of high resolution O 1s XP-spectra of g-MTS (a), g-OTES (b) and g-FOTES (c)

ARXPS investigations were carried out to estimate films thickness, by monitoring the attenuation of Si 2p signal at 103.1 eV as a function of the emission angle (EA). The thickness of carbons (d) for each functionalized glass is given by the equation $I = I_0 \exp(-d/\lambda\cos\theta)$, where I_0 is the intensity of the emission from the bulk, θ is the emission angle (with respect to sample normal), λ is the inelastic mean free path (referred to the overlayer) and d is the film thickness.

Table 1.4.2. Thickness values for the three functionalized glasses calculated by Si 2p signal attenuation (103.1 eV) as a function of the photoemission angle and relative comparison with expected values upon the hypothesis of the formation of a monolayer on glass surfaces

	Thickness (nm)	
	ARXPS	Expected
g-MTS	1.3±0.1	0.65
g-OTES	1.3±0.1	1.11
g-FOTES	1.2±0.1	1.13

From these calculations it was possible to compare the experimental thickness with the expected one, assuming that a monolayer of silanes had been bound on the surface, with alkyl chains standing perpendicular to the adsorption plane. According to data reported in Table 1.4.2, it might be reasonable to assume that a monolayer of silanes was reached by depositing OTES and FOTES from dry toluene solutions, whereas by MTS the formation of a multilayered system might be assumed. Further insights into surface chemistry were gained by calculating relative ratios among elements characteristic of each coating. Concerning g-MTS, the ratio of C 1s at 285 eV over C 1s at 286.3 eV is 1.8, consistent with MTS condensing intact on the glass surface, according to previously published results referred to solution-deposited mercapto-silanes.[94] This indicates that ethoxy groups have been lost during adsorption, even though some ethoxy groups remain within the film, although only to a minor extent. C 1s/O 1s (533.8 eV) ratio was found to be 5.9 consistent with previous hypotheses. In addition, the ratio C 1s over S 2p was found to be 5.0, consistent with the hypothesis of a multilayered adsorption of silanes, involving ethanesulfonic acid or ethylmercaptan elimination as the multilayer mercaptan grows.[97] These findings support what observed by ARXPS, according to which a thickness doubled than expected with a monolayer of MTS molecules. In the case of g-OTES, the ratio C 1s over O 1s was found to be 9. Regarding g-FOTES, the effectiveness of coating was confirmed by the elemental analysis. The atomic ratio of carbon at 294.1 eV to that at 291.5 eV was in perfect agreement with the expected value $(CF_3)/(CF_2)_5$=0.2. Furthermore for the C 1s peak originating from CH_2 carbons found at 285.2 eV in this spectrum, the observed peak area intensity ratio of CH_2 carbons to CF_3 carbons is 3.35, which is larger than the carbon content ratio of $(CH_2)_2/(CF_3)$=2 in the FOTES molecules, in consequence of X-ray damage, according to data previously reported in the literature.[105] C 1s/O 1s ratio was found to be 6.3 consistent with a partial loss of OEt groups during condensation.

DESI-MS. The three functionalized glasses, as well as clean glass, were used as supports to address surface effects on MS response when molecules with different acid-base behavior were used as analytes. Melamine was chosen as organic base (pKa=8.95), tetracycline as acid (pKa=3.3) and lincomycin with intermediate pKa (7.6). The idea of taking into account surface free energy to gain insights into DESI process was from Volný et al.[56]: in that work this physical quantity, calculated for different supports ranging from glass to polymethylmetacrylate (PMMA) and polytetrafluoroethylene (PTFE), was reported to influence DESI current. In addition, in the study of Volný capacitor time constants of the equivalent RC circuits for different DESI surfaces were calculated and the highest value turned to gain the best analytical response. However, in those experiments, both the electrical and the surface chemical properties of each material contributed to the analytical response, although electrical resistivity for the three different materials are reported to be significantly different, i.e. 10^{11} to 10^{14}

Ωm for glass[119], about·10^9 Ωm for PMMA[120] and estimated above 10^{20} Ωm for PTFE (DuPont). Therefore, to successfully address surface free energy effects to DESI efficiency we applied a functionalization approach by a self-assembly method allowing to obtain surfaces within a wide range of polarity and, at the same time, to have a constant electrical contribution from the support. In addition, by having comparable roughness, found to be in the same order of magnitude as shown by TM-AFM investigations, it was possible to avoid contributions to the ionization induced by changes in surface morphology and to address DESI current variations only to chemical surface modifications. MS experiments were carried out by setting different potential on the sprayer, in order to work on one hand under electrospray and on the other hand in pneumatically-assisted ionization conditions. It was possible to calculate the potential for the onset of the electrospray flow by the approximated formula proposed by Smith (Equation 1.4.3).[121]

$$V_{on} \approx \left(\frac{r_c \gamma \cos\theta}{2\varepsilon_o} \right)^{1/2} \ln\left(\frac{4d}{r_c} \right) \quad (1.4.3)$$

By substituting the values ε_o = 8.8 × 10-12 J^{-1} C^2, θ = 49.3° [122], r_c = 50 μm, d = 3 mm and taking into account methanol (surface tension, 0.0226 N m^{-1}) and acetonitrile (surface tension, 0.0293 N m^{-1}) as spray solvents, the equation leads to an onset potential equal to 1.2 kV and 1.3 kV respectively. Therefore 1 kV and 3 kV were chosen as potential. In both conditions it is possible to get protonated molecular ions of each analyte. Desorption/ionization experiments were carried out by spraying solvent onto each support and extracted ion currents for each analyte were compared with a three-way ANOVA with interactions (α=0.05), considering surface free energy, spray solvent and sprayer potential as factors. In all cases, log10 data transformation was applied to ensure variance homogeneity among samples. For all analytes a significant decrease in ion current *versus* increasing surface free energy was observed (Figure 1.4.8a-c), namely by moving from a hydrophobic to a hydrophilic surface by ionization both in desorption electrospray and pneumatically conditions. This is the same result gained by previous studies,[56] except that results obtained in this case were by desorbing analytes from a support with constant electrical resistivity, i.e. same bulk electrical properties. As a consequence, it is reasonable to assume that the significant differences in ion current are due to wettability effects, that is a confinement of the solution layer on a hydrophobic surface leads to a more efficient microextraction step at the solid interface. All the second order interactions were found to be significant, as well as the third order interaction of the factors. Particular attention was devoted to the interaction between surface free energy and sprayer potential for all analytes, namely the effect of the wettability was found to be different when ions are created either by ESI or only by pneumatically-assisted conditions (Figure 1.4.8d-f). These results might be read by taking into account that, as consequence that a Taylor cone is formed at the capillary tip, by working at a high positive potential (in this case 3 kV), an accumulation of positive charges takes place, leading to a more efficient

ionization process with a consequent apparent leveling effect of the response as a function of surface free energy. Finally, it might be assumed that surface-activated chemical ionization, induced by SH residues by g-MTS, appears to give a minor contribution to the ionization.

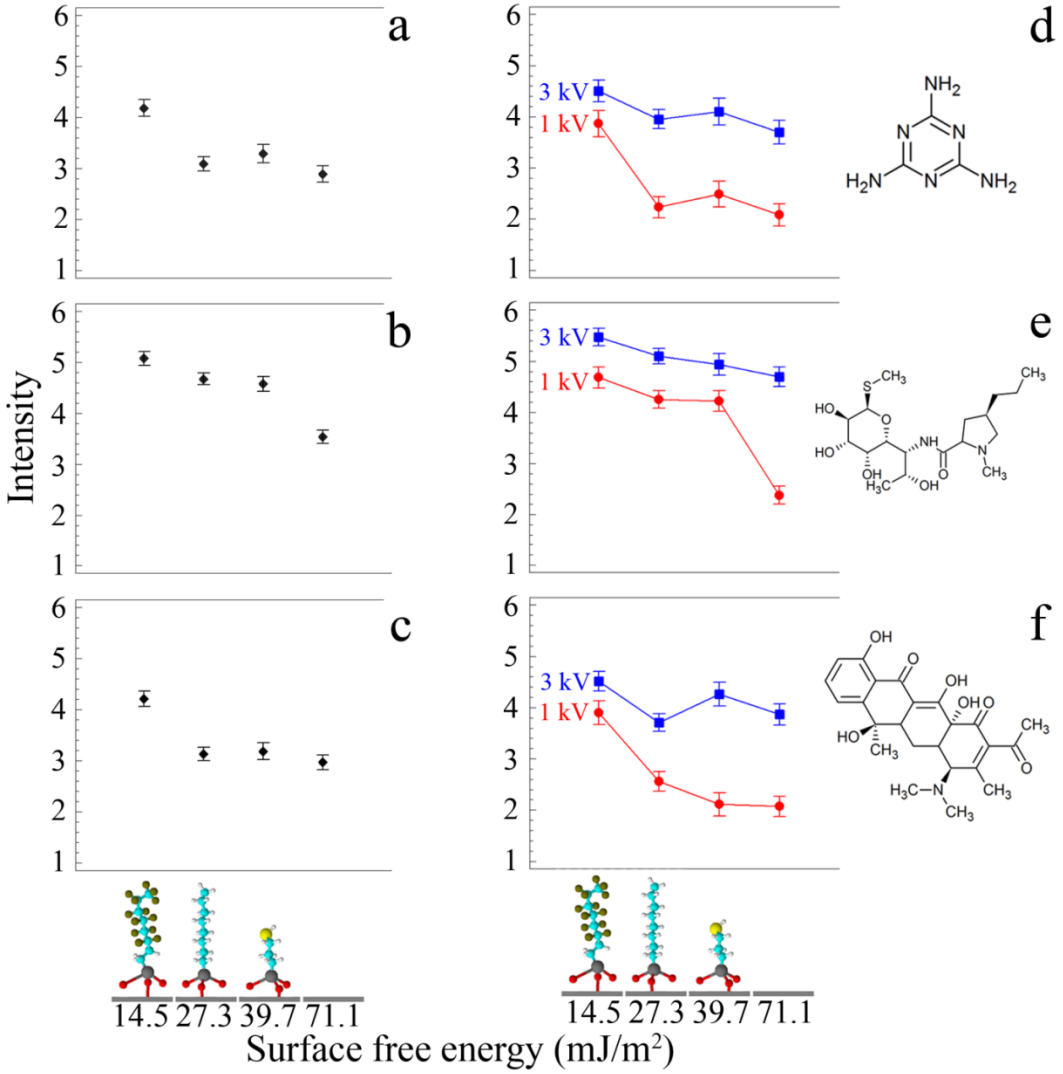

Figure 1.4.8. Three-way ANOVA plots of extracted ion current signals (n=9) of melamine (a), lincomycin (b) and tetracycline (c) and interaction plots of extracted ion current signals (n=9) of melamine (d), lincomycin (e) and tetracycline (f) as a function of surface free energy. At the bottom, associated to surface free energies, models of g-FOTES (left), g-OTES, g-MTS and glass (right) are reported.

In this section mass spectra of a mixture of melamine, lincomycin and tetracycline (100 pmol) obtained by setting the sprayer potential at 3 kV and 1 kV are reported (Figure 1.4.9a-b). As expected, it was observed that even in the absence of any electrical field, able to activate the onset of an electrospray flow, protonated molecular ions of each analyte were detected.[107,112] Differences in

relative ion abundance were not observed, but a significant drop in total ion current, according to the setting of a lower sprayer potential was obtained.

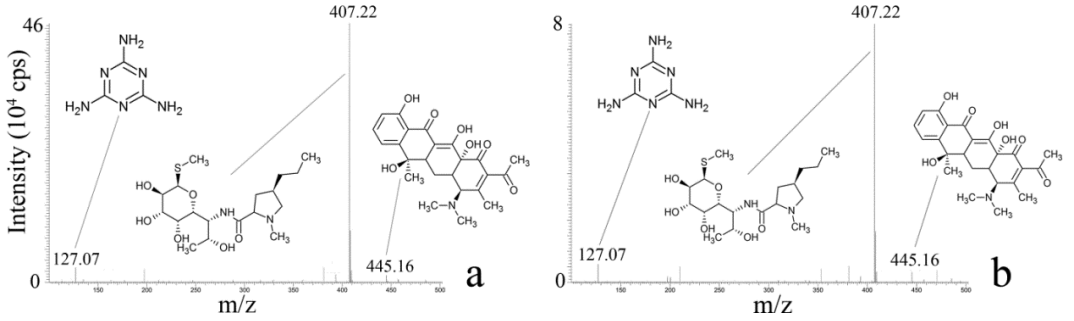

Figure 1.4.9. Desorption electrospray ionization (sprayer voltage, 3kV, a) and desorption spray ionization (sprayer voltage, 1 kV, b) mass spectra of 100 pmol of melamine, lincomycin and tetracycline (on g-FOTES as an illustrative example).

Conclusions

In conclusion, the results present work substantiate that tailoring the surfaces allows the change of the performances of a DESI-MS experiment. Furthermore, the role of surface free-energy when a DESI-MS experiment is carried out was clarified. Surface wettability was successfully tuned by adsorbing different silanes onto common glass surfaces and it was demonstrated by contasct angle goniometry, AFM as well as XPS investigations that, on the basis of instrumental characterizations, surfaces are functionalized by molecules arranged by self-assembling. It was demonstrated how analytical response dropped by using hydrophilic surfaces rather than hydrophobic both in ESI and in pneumatic ionization conditions as a consequence of differences in efficiency of the microextraction step at the solid interface.

1.5

Investigation on pneumatic aspects in desorption electrospray and electrospray ionization

Introduction

Desorption Electrospray Ionization belongs to the family of ambient ionization techniques, depending on a solvent spray in a manner similar to ESI. Experiments are typically performed by directing charged droplets produced from a pneumatically-assisted electrospray onto a sample deposited on a solid support at atmospheric conditions. In the DESI source, solvent droplets formed by electro-hydrodynamic process desorb the analyte molecules from the surface before ionization occurs, resulting in a final process that shares only some properties with the parent ESI mechanism. For DESI a number of mechanisms have been proposed, supporting the hypothesis of a two-step droplet-pick-up model followed by ESI-like desolvation and gas-phase ion formation by action of the electrical field.[17,108] Inside a DESI source, droplet dynamics, analyte pick-up and ionization are dependent by various key parameters, such as ESI parameters, source geometry and substrate effects.[56] As emphasized by Takats *et al.*,[17] the intensity of the signals in DESI mass spectrometry does not drop to zero in absence of the electrospray voltage. According to this phenomenon, Eberlin and co-workers[123] reported that the DESI source can operate also in the sonic spray ionization conditions, even if at a lower sensitivity.[124]

Recently, emphasis has been put on the critical questions about droplet dynamics with the aim of characterizing these ionization processes and underlying principles. Ion formation mechanisms were investigated by fluid dynamics experiments and simulations of contribution from electrostatic forces. [107,108] In addition, surface effects were investigated by electrochemical cell capacitance measurements by investigating the most important DESI parameters that affect analyte uptake and response reproducibility.[56,125] Microscopic imaging was also carried out with or without applying high voltages on the sprayer, thus demonstrating an important role of pneumatic rather than electrostatic forces.[15,112] The effect of the electric field, which is known to play a fundamental role on the electrostatic forces in the gas-phase, was thoroughly investigated[112] by changing potentials on the sprayer and on the entrance capillary of the mass spectrometer, proving that pneumatic effects play a fundamental role in the ionization processes operating in DESI conditions. However, it has to be underlined that a non-pneumatic version of DESI (nano-desorption electrospray) has been described.[126] This system proved to be highly effective in the chiral analysis of drugs in whole human blood samples.

Taking into account these findings, the aim of this study was to address further questions regarding DESI mechanism. For this purpose, we set-up an experimental strategy based on the analysis of mixtures of small molecules exhibiting different known physico-chemical properties, deposited on PTFE surfaces. In particular, melamine (organic base, MW 126.1), lincomycin (lincosamide antibiotic, MW 406.1) and tetracycline (polyketide antibiotic, MW 444.2) (Figure 1) were considered. Experiments were carried out on commercial PTFE surfaces. Pneumatically assisted ionization and desorption/ionization (DI) experiments were carried out exploring effects of ESI parameters on the ionization of the selected compounds and investigating the physico-chemical processes involved in the ion formation mechanism.

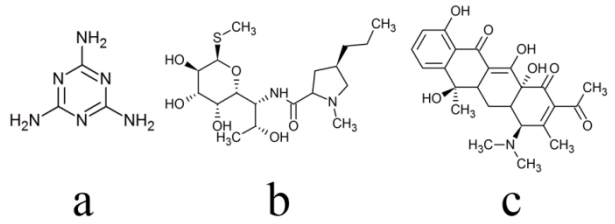

Figure 1.5.1. Chemical formulas of the compounds used for DESI-MS, i.e. melamine (a), lincomycin (b) and tetracycline (c)

Experimental

Chemical and reagents

Methanol (MeOH), formic acid (FA), hydrochloric acid, melamine, lincomycin and tetracycline were purchased from Sigma Aldrich (St. Louis, MO, USA). All commercially available chemicals were of analytical grade. Aqueous solutions were prepared in Milli-Q water (Milli-Q element A10 System, Millipore, San Francisco, CA, USA).

Instruments

Experiments were performed using a linear ion trap LTQ-Orbitrap mass spectrometer (Thermo Fisher Scientific, San Josè, CA, USA) equipped with a DESI ion source (Prosolia Inc., Indianapolis, IN, USA). ESI source parameters were set as follows: capillary voltage, 110 V; tube lens voltage, 250V; injection time, 100 ms; number of microscans, 5; tip-to-inlet distance, 10 mm. Finally, DESI source parameters were set as follows: spray voltage, 1.5 kV; tip-to-surface distance, 2 mm; tip-to-inlet distance, 3 mm; capillary temperature, 300°C; capillary voltage, 20 V; tube lens voltage, 40 V; injection time, 200 ms; incidence angle, 54°.

ESI-MS experiments

Methanol was infused in the mass spectrometer by setting the spray voltage to 1.5 kV. Solvent flow-rate was within a 10-20 μL min^{-1} range, capillary

temperature in the 200-300 °C range and sheath gas flow between 8 and 10 arbitrary units. Melamine, tetracycline and lyncomycin standard solutions were prepared in methanol at the final concentration of 10^{-5} M.

DESI-MS experiments

Melamine, tetracycline and lincomycin standard solutions were prepared in water:methanol (50:50, *v/v*) in order to deposit 1 nmol of each compound (deposition volume: 2 µl). Analyte solutions were spotted on PTFE surfaces and dried at room temperature. Pure methanol was used as spray solvent at the flow-rate of 2 µL min^{-1}.

Computational method

Molecular orbital calculations were carried out by using the G09 version of the GAUSSIAN series of programs. All the geometries were optimized in the gas phase at the B3LYP density functional level of theory using standard 6-31G(d) (6D, 7F) basis functions. Optimized geometries were tested by means of the Hessian calculation to confirm convergence criteria at the minimum and in order to exclude saddle points. Proton affinity (PA) was calculated by means of single point energy calculation on the optimized geometries and using the following equations,

$$A + H^+ \rightarrow AH^+ \qquad (1.5.1)$$

$$PA = \Delta H_f(AH^+) - \Delta H_f(A) - \Delta H_f(H^+) \qquad (1.5.2)$$

where ΔH_f is the formation enthalpy of each species calculated at 298 K and 1 atm. The gas phase basicity (GB) was calculated using the same previous equation, but substituting the formation enthalpy with the Gibbs free energy.

Results and Discussion

In order to achieve useful information about DESI mechanism, the first part of this work was focused on the study of the reactions occurring in a classic pneumatically assisted ESI source under no-electrospray conditions.

The central role played by the ESI capillary voltage on the ion signal has been hugely discussed in the literature, and it is known to strongly affect the total ion current. According to the equation derived from Smith[121] (Equation 1.5.3), a potential, V_{on}, is required for the onset of electrospray, which depends on the surface tension of the solvent, γ, the permittivity of the vacuum, ε_o, the distance from the tip of needle to the orifice of the mass spectrometer, d, the radius of the capillary, r_c, and the half angle of the Taylor cone, θ.

$$V_{on} \approx \left(\frac{r_c \gamma \cos\theta}{2\varepsilon_o}\right)^{1/2} \ln\left(\frac{4d}{r_c}\right) \qquad (1.5.3)$$

Substituting the values $\varepsilon_o = 8.8 \times 10^{-12}$ J^{-1} C^2, $\theta = 49.3°$ [127], $r_c = 100$ µm, $d = 1$ cm and surface tensions of methanol (0.0226 N m^{-1}), the equation leads to an onset potential equal to 2.2 kV for methanol. By scanning the V_{on} potential from 0 to 4

kV, it was found that, even in the absence of any electrical field, protonated ions of methanol were observed (Figure 1.5.2).

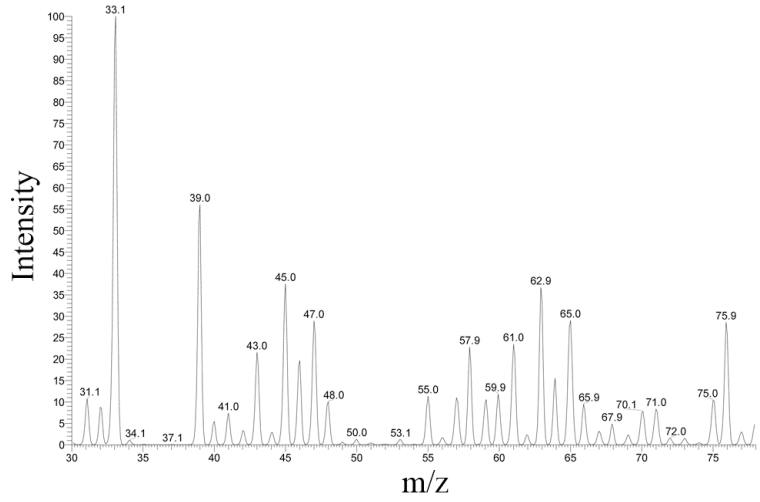

Figure 1.5.2. Full-scan pneumatically-assisted MS spectrum of MeOH (1.5 kV). Experimental conditions: flow rate, 20 µL min^{-1}, capillary temperature, 300 °C, sheath gas flow, 10 arbitrary units

Then, the sprayer potential was set at 1.5 kV to achieve better ion transmission efficiency. These conditions correspond to a potential under the onset one, as proved by the drop of ion intensity compared to electrospray ionization conditions (e.g. 3 kV). The other variables affecting ion formation efficiency in the source spray were further evaluated. Pure methanol was directly infused into the ESI source by varying temperature, sheath gas and solvent flow-rate, as described in the Experimental section. The effect of each source parameter was assessed by comparing mean values of molecular ion current with a three-way ANOVA with interactions. This investigation demonstrated a significant effect (p<0.05) for each variable and for each interaction among them. By increasing sheath gas flow, solvent flow-rate and temperature, a clear increase of ion current was observed. These behaviors can be considered due to many different factors:

i) the higher solvent flow-rate the higher amount of sample;

ii) the highest temperature could lead to a significant increase of sample concentration for the increased sample evaporation;

iii) the highest sheath gas flow would decrease the droplet dimension, further favouring the solvent evaporation, and would increase the droplet kinetic energy.

All of these factors contribute to an enhanced emission of ions from the sprayed droplets.

In a further stage of the work, a methanol solution of compounds with different gas phase basicity (GB) was submitted to ESI analysis in order to investigate ion formation as a function of the applied spray voltage. Chemical species with PA values higher and lower with respect to that of methanol (GB, 724.5 kJ mol^{-1}) were chosen. Attention was paid to melamine (GB, 914.2 kJ mol^{-1}

as calculated by Mukherjee *et al.*[128]) and to carbon disulfide (GB, 657.7 kJ mol^{-1}, NIST). The spray potential was varied in the 0-4 kV range with steps of 500 V and ion current of each protonated molecule was monitored. As illustrated in Figure 1.5.3, melamine/carbon disulfide ion current ratio changed with electrical field intensity and this value increased sharply when potential dropped to zero, thus suggesting that ion formation is ruled by thermodynamics and proton transfer is preferred towards the species with the highest gas phase basicity.

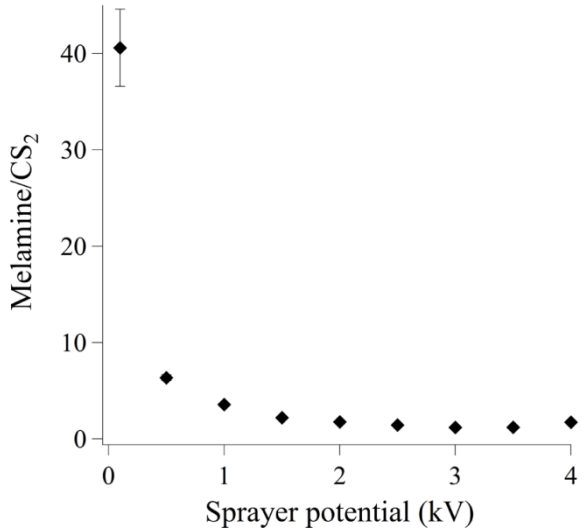

Figure 1.5.3. Melamine/carbon disulfide ion current ratio as a function of the sprayer potential

A further investigation regarded measurements carried out on substances with known acid-base properties, such as pK_a and proton affinity. In particular, melamine was chosen as organic base (pK_a, 8.95), tetracycline as acidic compound (pK_a, 3.30), and lincomycin with an intermediate pK_a value (pK_a, 7.60). Gas phase basicity of melamine was from literature data,[128] whereas a DFT level of accuracy was used to calculate PA and GB for lincomycin and tetracycline. PA and GB for melamine, lincomycin and tetracycline are reported in Table 1.5.1.

Table 1.5.1. PA and GB for lincomycin and tetracycline protonation process. Proton formation enthalpy and Gibbs free energy are 6.4 kJ/mol and -26.3 kJ/mol respectively.[129] PA and GB of melamine are from Mukherjee et al[128]

	PA (kJ/mol)	GB (kJ/mol)
Melamine	946.9	914.2
Lincomycin	1006.3	970.7
Tetracycline	956.9	925.5

A 10^{-5} M methanol solution of the mixture of the three compounds investigated was pneumatically sprayed into the mass spectrometer. Results confirmed the previous findings, since protonated ions of each molecule were observed in the mass spectra, even by setting to 0 kV the sprayer potential, with a relative intensity proportional to their PA. As expected, in this case ion current about 100 times

lower than that obtained by setting it to 1.5 kV was observed: in fact, considering that the presence of the electrical field leads to an enrichment of the ions of interest at the Taylor cone level, its absence leads to the analysis of the solution as it is.
After this preliminary investigation devoted to the evaluation of the ESI behavior in absence or in presence of the spraying capillary voltage, in the second part of the work pneumatically assisted DI experiments were performed. For this purpose, ionization of melamine, tetracycline and lincomycin deposited on the surface was investigated by using methanol as spray solvent. Equimolar quantities (1 nmol) of the three analytes were deposited on the DESI surface and sprayed with methanol. In these conditions the interaction of the sprayed solvent droplets with the thin solvent-solute layer originates by the pre-wetting due to the initial droplets. This leads to the emission from the liquid-phase sample of offspring droplets generated by the bombardment of the solution originally formed. Among the compound investigated, lincomycin shows the highest solubility in polar alcohols (>20 mg/mL in MeOH and EtOH[130]) with respect to melamine and tetracycline, reported as slightly soluble in alcohols.[131,132]

In the pneumatically-assisted DI mass spectrum recorded on PTFE surfaces, the relative abundance of analyte signals was in accordance with GB values (Figure 4b), consistent with the hypothesis that charged solvent molecules are responsible for proton transfer reactions, leading to the formation of analyte protonated molecular ion. Furthermore, pneumatically-assisted spray ionization spectrum was found to be equivalent in term of relative abundance compared to that obtained by pneumatically-assisted desorption ionization, as reported in Figure 1.5.4, thus suggesting that desorption/ionization process is mainly due to analyte solubilization and pneumatic effects, according to previous findings.[133,134] Once the mixture of analytes is solubilized into a thin layer of solution, the ionization process may be due to droplet pick-up processes in an ESI-like manner.

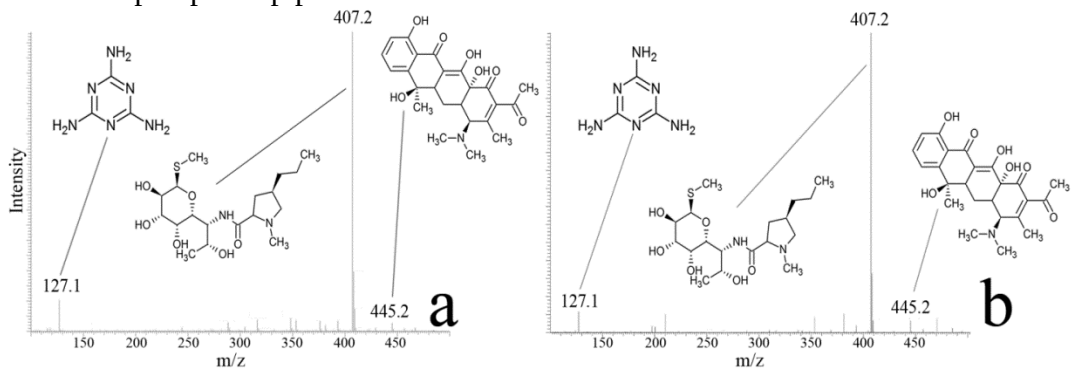

Figure 1.5.4. Pneumatically-assisted spray (a) and desorption spray ionization (b) mass spectra of a mixture of melamine (127.1 m/z), lincomycin (407.2 m/z) and tetracycline (445.2 m/z)

Nevertheless, considering the small dimension of the offspring droplets, the field-induced droplet ionization (FIDI) mechanism, recently proposed by Grimm and Beauchamp for the emission of ions from uncharged droplets in presence of electrical fields might be considered operative for the ionic species production.[16] In

fact, considering an offspring droplet velocity of 100 m s^{-1} the time required for the pathway surface-entrance capillary (~3 mm) is 0.3 ms. Considering the distance sprayer-entrance capillary of 5 mm and an applied voltage of 1.5 kV, it would lead to an electrical field of $1500/0.005 = 3 \cdot 10^5$ V/m, able to activate a symmetrical elongation of the droplet in the ~ 10^2 µs times with the consequent charged progeny jet formation characteristic of FIDI.

Conclusions

Taking into account that there is not a simple "unified" theory able to explain the mechanisms of DESI, EASI, nano-DESI and pneumatic assisted desorption, in this study we explored desorption and ionization mechanisms occurring in a DESI system by studying the effect of source potential on ionization yields. The results obtained by analyzing three substances having different acid-base properties demonstrated that pneumatic and solubility effects play a pivotal role in the ion yields of substances adsorbed on the surface.

2 Novel applications of MS in proteomics: development of analytical methods for multi-allergen determination in food by liquid chromatography-tandem mass spectrometry

In a research program dealing with the development of new analytical strategies based on mass spectrometry in proteomics, we proposed a proteomic-based approach for the determination of hidden allergens in foods using characteristic peptide markers of the allergens. Food allergy is a growing topic in the life sciences, affecting about 2% of the global population.[135] The presence of allergens could be intentional or could occur accidentally *via* cross-contamination at any stage of food production. One hundred nineteen food allergic reactions (22.4%) are considered to be due to hidden allergens.[136] The presence in foods of undeclared allergenic ingredients or hidden allergens arising from accidental contamination can cause serious reactions to sensitized individuals and clearly represents a growing food-safety issue. In the European Union (EU) food-labeling regulations have recently been revised and the labeling of several allergenic ingredients is now mandatory (Directives 2003/89/EC and 2007/68/EC).[137-139] However, little is known about the so called threshold doses, i.e. the minimum amount of an allergenic food which is able to cause an allergic reaction. For these reasons, the development of selective and sensitive analytical methods for allergen analysis at the trace level is recommended in order to improve food labeling directives and to increase consumer protection.

Taking into account that the dose eliciting allergic reactions has been estimated in the order of subunits or units of micrograms depending on the allergenic food,[140] a considerable reduction of the detection and quantification limits as well as an improvement in reliability of analytical methods available for allergen determination are of paramount importance to safeguard consumers' health.

The most commonly methods used for the detection of allergens in foods have been reviewed[141,142] and include immunoblotting, rocket immunoelectrophoresis, radio-allergosorbent test, radioimmunoinhibition assay, enzyme-linked immunosorbent assay (ELISA). Some commercially available ELISA test kits have been used for the analysis of hazelnut and peanut content in foodstuff,[143-145] however, the most current available commercial ELISA test kits are suitable for qualitative screening but fail for accurate quantitative assays.[143,145]

In the last years, increasing emphasis has been put on the development of confirmatory methods based on the use of liquid chromatography-electrospray-

tandem mass spectrometry (LC–ESI-MS/MS) techniques, for unambiguous identification and accurate quantification of proteins and peptides.[146-153]

For these reasons, in the last part of this manuscript an innovative rapid method for the simultaneous sensitive detection of five allergens in foods was developed and presented in the last two chapters.

2.1

Particle-packed column versus silica-based monolithic column for liquid chromatography–electrospray-linear ion trap-tandem mass spectrometry multi-allergen trace analysis in foods

Introduction

In the context of food allergens detection by LC our research group successfully developed and validated innovative confirmatory and screening mass spectrometry based-methods for the identification and determination of hidden peanut allergens in foods. By using a shotgun proteomic approach, peanut proteins were enzymatically degraded to peptides and two selected biomarker peptides for each allergen were then analyzed under selected reaction monitoring (SRM) mode in a triple quadrupole or a linear ion trap (LIT) mass analyzer.[154-156] In this work, our attention was paid to the evaluation of the LC–LIT-MS/MS capabilities to obtain useful and simultaneous detection and quantification of five different hidden allergens in different food samples in a single short run. Ana o 2 (cashewnut), Cor a 9 (hazelnut), Pru 1 (almond), Jug r 4 (walnut) and Ara h3/4 (peanut) proteins were investigated. These no-glycosylated seed storage proteins belong to the 11S-globulin family (Cupin superfamily) that accounts for a number of known major food allergens and are of interest to both the public and industry due to food safety concerns.

Taking into account that the chromatographic separation plays a fundamental role in the MS analysis of complex peptide mixtures, two different chromatographic columns (i.e. C18 particle-packed column and a silica-based C18 monolithic column) were compared in terms of resolution, peak shape and analysis time before MS method development. As for MS acquisition mode, the non-scanning nature of SRM analysis, usually performed on a triple quadrupole mass spectrometer allows to obtain excellent sensitivity and enables the detection of low-abundance proteins in highly complex mixtures. In the IT instruments, collision induced dissociation (CID) experiments allow to perform single-step fragmentation and to obtain product ions that are not subjected to further fragmentation. Thus, the analysis of large peptides by SRM in LIT mass spectrometers can be performed with improved detection limits owing to the formation of fewer but more intense product ions. In addition, the capability of LIT-MS of performing MS^n experiments allows to obtain increased selectivity on the target peptides in complex matrices. In this work, using one-dimensional chromatographic separation and linear ion trap MS detection, the quantitation of five allergens by SRM under MS^2 mode was

evaluated in terms of sensitivity, selectivity, accuracy, recovery, limits of detection and quantitation. Performance of the LC–ESI-LIT-MS method under MS^3 acquisition mode was also assessed. Finally, the LC–MS^2 and LC–MS^3 methods were applied to commercially available samples and the quantitative results were compared.

Experimental

Chemicals

Bicarbonate buffer (pH 8.0), acetonitrile (HPLC purity), trifluoroacetic acid (TFA), formic acid (analytical reagent grade) were purchased from Carlo Erba (Milan, Italy). Trypsin from bovine pancreas, Bradford reagent and leukine-enkefaline acetate hydrate were from Sigma-Aldrich (St. Louis, Missouri, USA). Roasted peanuts (*Arachis hypogea*), walnuts (*Juglans regia*), hazelnuts (*Corylus avellana*), almonds (*Prunus dulcis*) and cashewnut (*Anacardium occidentale*), three different commercial biscuits and five breakfast cereals samples (cornflakes, breakfast cereals based on cereal flakes and dried fruit, cereal mix with fruit and chocolate) were obtained at a local food store. All the products analyzed reported the precautionary label "may contain trace of nuts, milk and soy".

Sample treatment

Fortified samples were prepared by adding the five ground nuts at different amounts and by homogenizing the mixture before weighting and extraction. Nuts-containing food extracts were prepared by adding 10 mL of 50 mM bicarbonate buffer (pH 8.0) to 1 g of ground sample. The efficiency of the protein extraction procedure was initially evaluated by varying the extraction time (2 h, 4 h and 6 h), extraction temperature (37°C, 60°C) and by quantifying the total protein content using a Bradford assay. The best results were obtained by performing a 6 h extraction at 60°C.

Proteins were extracted by shaking for 6 h at 60°C, then the extract was centrifuged (4000 g, 20 min) and filtered on 0.2 μm nylon filter before tryptic digestion. Enzymatic digestion was performed by adding a trypsin solution (12.5 μL, 200 μg mL^{-1}) to 100 μL of protein extract in order to obtain a protein:trypsin ratio 50:1 and carried out at 50°C overnight. The digestion reaction was quenched with 2 μL TFA.

Liquid chromatography–ion trap mass spectrometry

LC separation was carried out on a C18 Kinetex (100 mm×2.1 mm, 2.7 μm particles) (Phenomenex, CA, USA) column thermostated at 25°C using a gradient solvent elution system [(A) aqueous formic acid 0.1% solution (v/v)/(B) 0.08% (v/v) formic acid in acetonitrile]. Gradient elution was as follows: solvent B was set at 5% for 3 min, then delivered by a linear gradient from 5% to 20% in 6 and to 60% in 1 min. Solvent B was maintained at 60% for 1 min before column

reequilibration (5 min). The flow-rate was 250 μL min^{-1}. The same gradient was used to elute peptides on a C18 Chromolith Performance column (100 mm×2mm) (Merck KGaA, Darmstadt, Germany) at a flow-rate of 350 μL min^{-1}. The mobile phase was delivered by the Surveyor chromatographic system (ThermoElectron Corporation, San Josè, CA, USA) equipped with a 200-vial capacity sample tray. Injection volume was 10 μL.

A LTQ XL linear ion trap instrument (ThermoElectron Corporation) equipped with a pneumatically assisted ESI interface was used. The system was controlled by the Xcalibur software.

The sheath gas (nitrogen, 99.999% purity) and the auxiliary gas (nitrogen, 99.998% purity) were delivered at flow-rates of 45 and 5 arbitrary unit, respectively.

Optimized conditions of the interface were as follows: ESI voltage 3.5 kV, capillary voltage 20 V, capillary temperature 270°C. MS^2 and MS^3 experiments were performed under both product-ion and SRM conditions with a collision gas (He) pressure of 2.1×10^{-3} mbar in the collision cell. In the product-ion scan mode the 200–1600 *m*/*z* range was monitored. The SRM transitions monitored were reported in Table 2.1.1. For quantitative purposes, the most intense SRM transition was monitored for each allergen source, whereas the other transitions reported in Table 2.1.1 were monitored for confirmatory purposes.

Table 2.1.1. Allergen source, target peptides and SRM transitions monitored in MS^2 and MS^3 mode.

Allergen (*source*, UNIPROT ID)	**Peptide**	**SRM transitions (*m*/*z*) (CE 30 eV)**	
		MS^2	**MS^3**
Ana o 2 (*Anacardium occidentale*, Q8GZP6)	VFDGEVR	412/575[a]	575/460[a]
		412/460	
	ADIYTPEVGR	561/552	552/459
		561/658	
Cor a 9 (*Corylus avellana*, Q8W1C2)	ADIYTEQVGR	577/689	689/646[a]
		577/567	
	QEWER	374/365[a]	365/490
		374/490	
Pru 1 (*Prunus dulcis*, Q43607)	QQGQQEQQQER	694/685	685/677[a]
		694/677	
	QQEQLQQER	594/585[a]	585/576
		594/576	
Ara h3/4 (*Arachis hypogea*, Q8LKN1)	SPDIYNPQAGSLK	695/977[a]	977/700[a]
		695/815	
	YQQQSR	406/518	518/500
		406/397	
Jug r 4 (*Juglans regia*, Q2TPW5)	LDALEPTNR	516/487[a]	487/469[a]
		516/616	

Allergen (*source*, UNIPROT ID)	Peptide	SRM transitions (*m*/*z*) (CE 30 eV)	
		MS^2	MS^3
	EFQQDR	412/403	403/387
		412/290	

[a] *m*/*z* transition monitored for the calculation of the validation parameters

Method validation

Validation of the whole analytical procedure was performed under MS^2 mode on fortified samples of breakfast cereals (mix of cereal flakes) according to Eurachem guidelines.[157] For this purpose, breakfast cereal samples were fortified with different nuts amounts and measurements were carried out by monitoring the most abundant MS/MS transition for each peptide (Table 1). The detection limits (LOD) and the quantitation limits (LOQ) were calculated from the calibration curve as 3 s/slope and 10 s/slope, respectively, where s is the standard deviation of the blank signal obtained by performing 10 independent blank measurements. Linearity was assessed over suitable mg nuts/kg matrix ranges, starting from LOQ values. Precision was evaluated as RSD for each compound in terms of intra-day repeatability and intermediate precision (inter-day repeatability). For this purpose, within day repeatability was evaluated by performing three independent extractions of the matrix fortified with 50 and 100 mg nuts/kg matrix and three LC–MS^2 injections for each extract in the same day; inter-day repeatability was calculated on five days by performing five independent extractions of the matrix fortified with 50 and 100 mg nuts/kg matrix and three LC–MS^2 injections for each extract. Matrix effect was assessed by using the recovery function. The matrix-matched calibration curve was obtained by analyzing the matrix extracts fortified with a mixture of the five nuts at six concentration levels and treated applying the whole analytical procedure. Each level was analyzed three times. The recovery of the protein extraction procedure was evaluated by performing a 6 h extraction at 60 °C on the blank matrix and on the matrix fortified at two different concentration levels (50 and 100 mg nuts/kg matrix). The total protein content was determined by using a Bradford assay.

Results and discussion

In silico selection of biomarker peptides

In this work the proteins that target the five allergen sources were initially selected on the basis of previous experiments and the scientific literature. The following major allergen proteins for the five nuts under investigation were selected: Ana o 2 (cashewnut), Cor a 9 (hazelnut), Pru 1 (almond), Ara h3/4 (peanut), Jug r 4 (walnut). For all the allergens investigated no isomeric forms from the same gene are reported in the database sequences (http://www.uniprot.org/). As for biomarker peptide selection, different criteria, such as absence of missed

cleavages, good ESI sensitivity, no post-translational modification sites and sequence specificity, were considered. Thereby, by analyzing a raw tryptic digest extract from each nut, a subset of peptides was directly identified by the mass spectrometer in a data-dependent acquisition mode to characterize each selected protein with a sequence coverage average of ~35%.

For each targeted protein, those peptides providing good ESI-MS responses and unequivocally identifying the target protein were selected. For this purpose, BLAST (Basic Local Alignment Search Tool; www.ncbi.nml.nih.gov link NCBI BLAST) search was performed (algorithm: blastp; MATRIX PAM 30; GAP COASTS: existence 10, extension 1; DATABASE: non-redundant protein sequences) in order to evaluate the identity of each peptide with all the similar peptides present in the databases. To develop a reliable quantification method, two peptides were selected and monitored for each targeted protein (Table 2.1.1). In the case of the peptides containing a Q or E residue at the N-term, an in-source deamination or dehydratation process was found to occur before trap isolation. In a further step, product-ion LIT measurements were carried out on the biomarker peptides by varying collision energy (from 20 to 35 eV) to select specific SRM transitions for each biomarker peptide. The MS^2 and MS^3 spectra exhibited several fragments of the y- and b-series to cover and confirm their sequences. Attention was paid to the selection of those fragment ions that provide optimal signal intensity and that could discriminate the targeted peptides from other species present in the sample. The definitive assay was constituted of a series of transitions (precursor/fragment ion pairs) in combination with the retention time for each targeted peptide as reported in Table 2.1.1.

Packed versus monolithic column

For MS analysis of complex peptide mixture, suitable separation methods have to be developed to improve resolution, sensitivity and analysis time. With the aim of devising a separation method suitable for the MS detection of the ten biomarker peptides in complex samples, the separation performances of a C18 column packed with 2.6 μm particles, and a C18 monolithic column having the same length and internal diameter were compared. Generally, C18 monolithic columns allow the application of fast gradients at higher flow-rate with lower backpressure, obtaining fast analysis and excellent peak shape.

By analyzing a nut protein aqueous solution with the C18 monolithic column, the LC–IT-MS^2 elution profile (within 8 min) of the peptides resulted to match that observed using the C18 silica particle-packed column (within 9 min) (Figure 2.1.1 and Figure 2.1.2). The chromatographic profile of the ten peptides on the monolithic column showed both excellent peak shape (in-run-peak width (FWHM, average on the ten peptides) = 3.60±0.07 s) and retention time stability (RSD < 2.3%). Also in the case of the C18 packed-particle column, satisfactory results in terms of in-run-peak width (5.10±0.08 s) and retention time variation (RSD < 0.9%) were obtained. As for resolution, the two columns exhibited very

similar values, ranging from 0.7 to 14 for the particle-packed column and from 0.8 to 12 for the monolithic column. The quantification of the tryptic digest on the monolithic column (flow-rate 350 μL min^{-1}) without flow-splitting evidenced approximately a 40% sensitivity reduction (average value for all the peptides) with respect to the particle-packed column (flow-rate 250 μL min^{-1}). As for quantitative results, selectivity of the two columns in terms of matrix effect (i.e. signal enhancement/suppression) was also investigated. For this purpose, an aqueous tryptic digest (*n*=3, *n*=number of independent samples) and a sample tryptic digest (*n*=3) were analyzed. The results evidenced a signal suppression degree ranging from −65% to −2% for the monolithic column for all the peptides, whereas in the case of the C18 particle-packed column the signal variation ranged from −58% to +12%. In particular, by using the particle-packed column three of 10 peptides exhibited a signal enhancement from +5% to +12%. On the basis of these findings, the particle-packed column that provided a rapid LC separation of the analyzed peptides while reducing solvent consumption was selected for further validation studies.

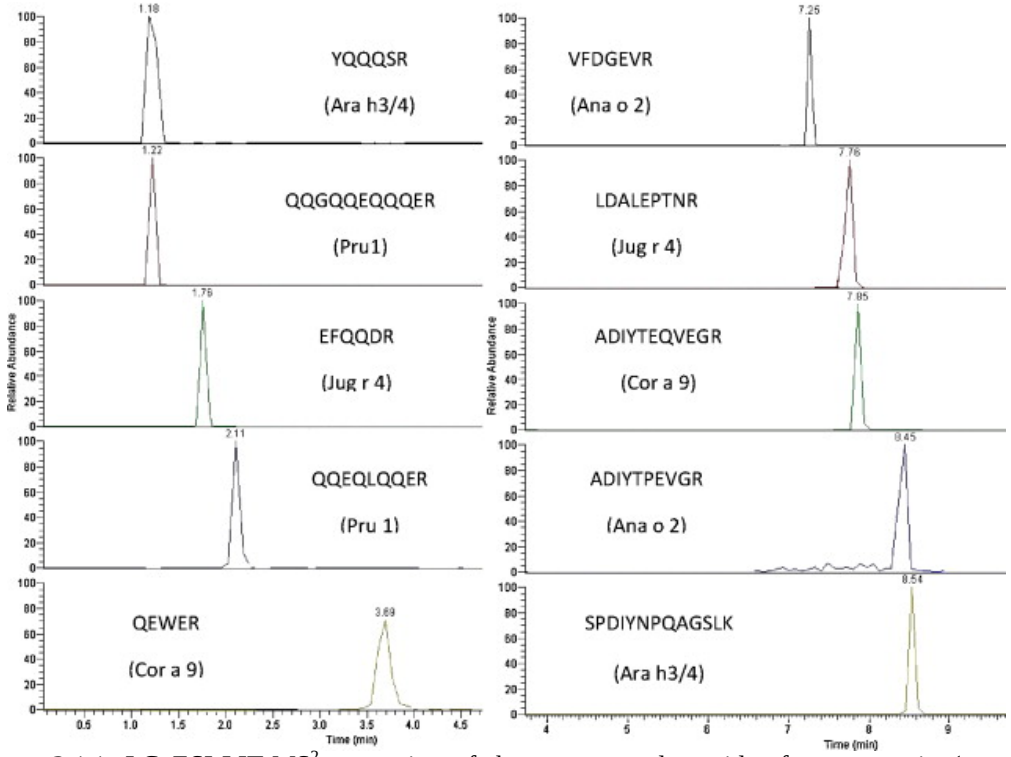

Figure 2.1.1. LC–ESI-LIT-MS^2 separation of the ten targeted peptides from a matrix (cereals) tryptic digest on the C18 particle-packed column (100 mm×2.1mm, 2.6 μm). Blank matrix was fortified with a mixture of the five nuts 0.01% (w/w). Mobile phase: formic acid aqueous solution (0.1%, v/v) / acetonitrile, flow-rate 250 μl min^{-1}, injection volume: 10 μL

LC–MS^2 method validation

The primary goal of this work was to devise a sensitive and robust LC–MS^2 method for the analysis of allergens at trace levels in foods. For this purpose, studies on linearity, trueness, precision, selectivity and recovery were performed. Even if little is known about the minimum concentration level able to provide severe allergy reaction, detection limits between 1 and 100 mg of allergenic protein per kg food are accepted for all the analytical methods.[141] By operating under MS^2 SRM conditions, very good LOD values in the 10–55 mg allergen/kg food were determined from the matrix-matched calibration curves. LOQ values were found in the 37–180 mg allergen/kg food range (Table 2.1.2).

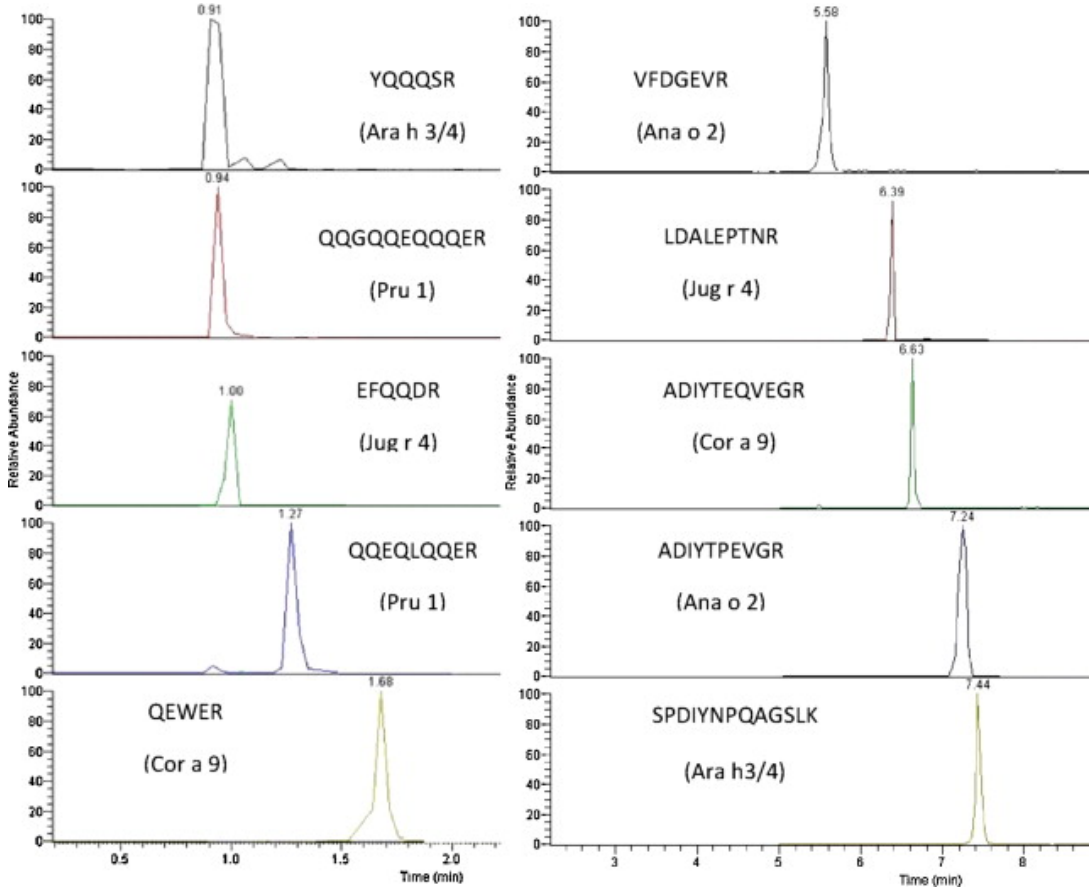

Figure 2.1.2. LC–ESI-LIT-MS^2 separation of the ten targeted peptides from a matrix (cereals) tryptic digest on the C18 monolithic column (100 mm×2.1mm). Blank matrix was fortified with a mixture of the five nuts 0.01% (w/w). Mobile phase: formic acid aqueous solution (0.1%, v/v)/acetonitrile, flow-rate 350 µl min^{-1}, injection volume: 10 µL.

Table 2.1.2. Validation results obtained for the determination of allergens in biscuits under MS^2 acquisition mode. Concentrations are referred to the matrix fortified with a mix of the five nuts (mg nut/kg matrix).

Allergen	Peptide	LOD (mg kg^{-1})	LOQ (mg kg^{-1})	Concentration range (mg kg^{-1})	Linearity $Y=b1(\pm sb1)X$	r^2 (n=21)
Ana o 2	VFDGEVR	14	46	50–500	30,783 (±407)	0.997
Cor a 9	QEWER	30	90	90–1000	8259 (±523)	0.998
Pru 1	QQEQLQQER	17	58	60–500	10,373 (±213)	0.986
Ara h3/4	SPDIYNPQAGSLK	10	37	40–400	32,979 (±1565)	0.998
Jug r 4	LDALEPTNR	55	180	200–1000	3627 (±358)	0.991

Generally, the LC–ESI-MS/MS linear range was explored over one order of magnitude of concentration for all the peptides (Table 2.1.2). After testing significance of the intercept (p value<0.05 at 95% confidence level), linearity was verified by applying the Mandel fitting test. A p value higher than 0.05 demonstrated that the best data fit could be obtained using a first order regression model. Homogeneity of variance of replicates at different concentration levels was proved at 95% confidence level (p>0.05). Method accuracy was then tested both in terms of precision and trueness. Excellent precision in terms of intra-day repeatability was calculated providing RSD% in the 3–10% (n=9) range. The intermediate precision results were found not exceed 15% (n=15), confirming good method precision. As for trueness, a calculation of the recovery function was performed to ascertain the influence of the matrix for the determination of all the peptides under investigation. The slope and the intercept of the recovery functions calculated for the analytes were compared respectively with 1 and 0 by means of a t-test. The t-test performed on the intercept provided a p value at the 95% confidence level higher than 0.05 (p=0.145), demonstrating that the calibration equation is in the $y=b_1x$ form and thus the absence of constant systematic errors. In the case of the slope, since the t-calculated resulted to be higher than the t-tabulated at the 95% confidence level (1.86), it can be inferred that the calibration curve obtained by spiking samples are significantly different from that obtained using standard solutions, except for the VFDGEVR (Ana o 2) peptide. In the case of the SPDIYNPQAGSLK (Ara h3/4) and QEWER (Cor a 9) peptides, a signal enhancement of 12% and 5%, respectively, was observed; in the case of all the other peptides a signal suppression ranging from 11 to 50% was calculated. To overcome matrix effect, matrix-matched calibration curves were built up to perform a label-free quantification method. As for recovery, one batch of breakfast cereals was enriched with a mixture of the five nuts and values ranging from 76±4% to 94±3% were obtained.

Comparison of the LC–MS^2 and the LC–MS^3 methods

By operating under MS^3 SRM conditions, LOD and LOQ of all the peptides except for the allergen Jug r 4 resulted to be higher than those obtained under MS^2 mode (Table 2.1.3). The LC–ESI-MS^3 linear range was established over one order of magnitude of concentration for all the peptides (Table 3). For this purpose,

homogeneity of variance, the significance of the intercept and the best fitting at 95% confidence level were assessed.

Table 2.1.3. Validation results obtained for the determination of allergens in biscuits under MS^3 acquisition mode. Concentrations are referred to the matrix fortified with a mix of the five nuts (mg nut/kg matrix).

Allergen	Peptide	LOD (mg kg^{-1})	LOQ (mg kg^{-1})	Concentration range (mg kg^{-1})	Linearity $Y=b1(\pm sb1)X$	r^2 (n=21)
Ana o 2	VFDGEVR	30	98	100–1000	10,020 (±77)	0.953
Cor a 9	QEWER	35	110	110–1000	7350 (±29)	0.991
Pru 1	QQEQLQQER	25	80	80–1000	5109 (±106)	0.995
Ara h3/4	SPDIYNPQAGSLK	27	90	90–1000	10,178 (±21)	0.988
Jug r 4	LDALEPTNR	50	160	160–1000	2924 (±44)	0.992

Within day repeatability and inter-day repeatability were excellent and ranged from 2 to 13%, and from 5 to 15%, respectively. As for matrix effect, results similar to those obtained under MS^2 mode were obtained in terms of peptides affected by matrix effect. In this case, the signal suppression percentage resulted in the 6% - 28% range, suggesting a slightly reduction in the matrix effects.

Sample analysis

In the last step of the work, the LC–MS^2 and LC–MS^3 methods were applied to a variety of commercial biscuits and breakfast cereal products to evaluate the presence of the hidden allergens under investigation. Among all samples analyzed, under MS^2 mode two of height samples resulted contaminated by traces of almond, hazelnut and peanut (Figure 2.1.3, Table 2.1.4). However, by analyzing the same sample under MS^3 mode the peanut peptide signal was not observed. As for confirmatory purposes, these samples were run under MS^2 and MS^3 product ion scan mode to acquire the whole fragmentation pattern of the targeted peptides, and their identity was univocally verified. In particular, in the case of the peanut peptide, an isobaric interferent was detected demonstrating that MS^3 acquisition mode allows improving analysis selectivity and unequivocally confirming the presence of the peptides found in the samples. The quantitative results are reported in Table 2.1.3.

Analytical results obtained applying the devised method showed that the sample procedure in combination with LC–ESI-LIT-MS^2 and MS^3 analysis of sample extracts is capable of pin-pointing and quantifying the presence of hidden allergens in foods at the levels of interest.

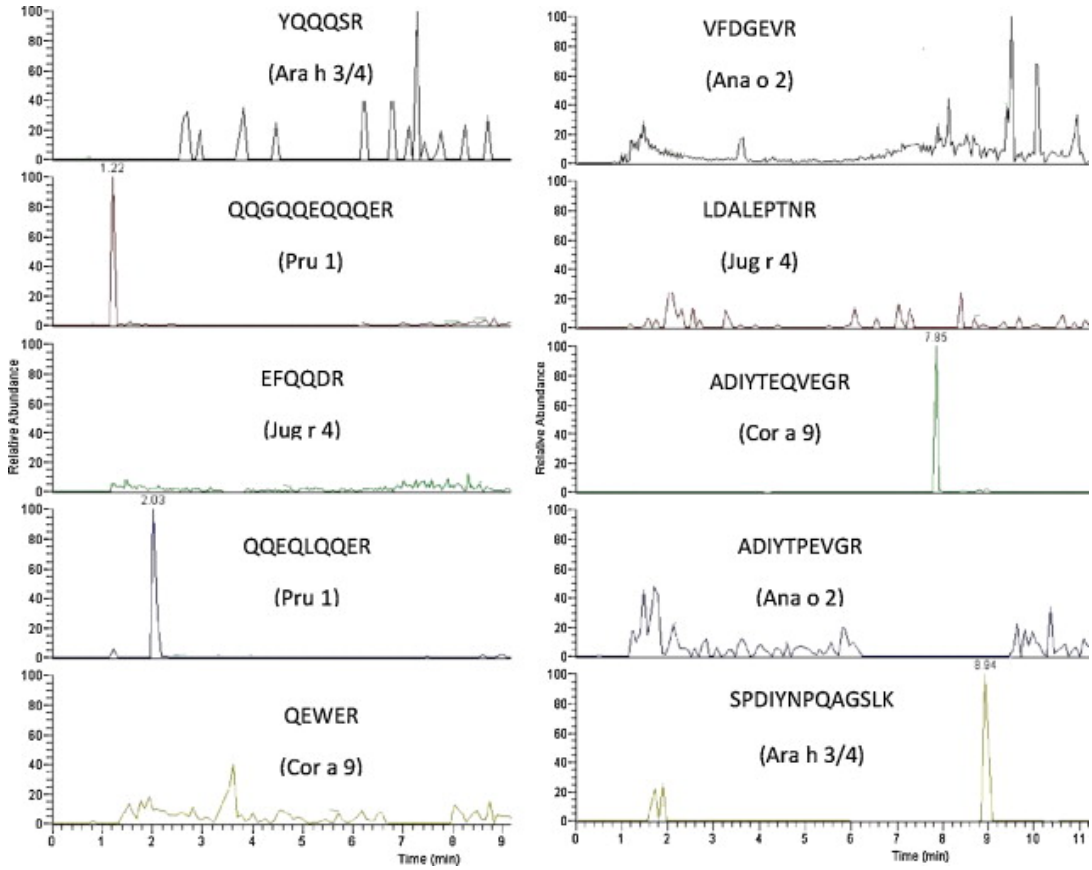

Figure 2.1.3. LC–ESI-LIT-MS^2 separation of the breakfast cereal sample extract on the C18 particle-packed column (100mm×2.1mm, 2.6 μm). Mobile phase: formic acid aqueous solution (0.1%, v/v)/acetonitrile, flow-rate 250 μl min^{-1}, injection volume: 10 μL.

Table 2.1.4. LC–ESI-MS^2 and MS^3 determination of the hidden allergens detected in the food samples investigated (*n*=3).

Sample	**Almond (mg/kg)**		**Hazelnut (mg/kg)**	
	MS^2	**MS^3**	**MS^2**	**MS^3**
Cereal mix with dried fruits	–	–	–	–
Exotic muesli	–	–	–	–
Cornfalkes	–	–	–	–
Muesli with dried fruits	98±12	–	–	–
Natural cereal mix	100±8	117±2	50±5	66±3
Biscuits	–	–	–	–

–, not detected.

Conclusions

A new rapid method for simultaneous detection of five allergens in foods was developed and successfully validated. Two LC columns were evaluated to improve chromatographic performances and the best results in terms of selectivity and sensitivity were obtained using a C18 particle-packed column. By operating under MS^2 conditions, five of the biomarker peptides can be detected quantitatively with LODs from 10 to 50 mg nut/kg matrix and precision from 3 to 15%. Applying the method to 8 commercial samples, the Cor a 9 and Pru 1 hidden allergens were detected at trace level. This study proved the possibility to increase in the future the number of allergens to investigate simultaneously in one single LC–MS^2 run, in order to provide a rapid and selective detection method useful for food control analysis.

Acknowledgments

The project was funded by Laboratorio Regionale SITEIA (PRRIITT Misura 4 “Sviluppo di rete”, Azione A – Laboratori di ricerca e trasferimento tecnologico, DGR n. 1853/07) and by the Italian Ministry for the University and Research (MIUR) with the PNR Project n. RBIP06SXMR “Sviluppo di metodologie innovative per l’analisi di prodotti agroalimentari”.

2.2

A rapid size-exclusion solid phase extraction step for enhanced sensitivity in multi-allergen determination in dark chocolate and biscuits by liquid chromatography tandem mass spectrometry

Introduction

Analytical methods for qualitative and quantitative determinations of food allergens including immunochemical, nucleic acid-based and MS-based methods have been recently reviewed.[141,142,146,158,159] In the last years, the number of applications of MS techniques in this field has considerably increased for unambiguous identification and accurate quantification of proteins and peptides.[146,148,150-153] In this context, our research group successfully proposed analytical methods for the selective determination of hidden allergens in foods by selecting univocal biomarker peptides.[155,160,161] Beyond the accuracy, one of the main advantages of MS-based methods is the possibility of multi-allergen determination by simultaneously monitoring of several food allergens in a single analysis.[160-163] In particular, in our most recent work, we devised a MS-based method capable of investigating simultaneously four lupin allergens in pasta and biscuits in one single liquid chromatography-electrospray-tandem mass spectrometry (LC-ESI-MS^2) run.[161] The food matrix can have a considerable effect on the extraction and determination of allergenic food residues.[164] Chocolate is one of the most challenging food matrices. Indeed, dark chocolate contains a large amount of polyphenolic compounds which can react with food proteins, thus masking the target proteins under investigation. Some commercially available enzyme-linked immunosorbent assay (ELISA) test kits have been used for the analysis of hazelnut and peanut content in dark chocolate samples.[143-145] However, it has to be stated that the most current available commercial ELISA test kits are suitable for qualitative screening but fail for accurate quantitative assays.[143,145]
In this context, taking into account the complexity of dark chocolate matrix and that peanut and tree nuts are among the major food allergens,[165] eliciting the most severe reactions,[166] the scope of the present work was the improvement of sensitivity of the previously devised shot-gun LC-ESI-MS^2 method[160] through the addition of a rapid size-exclusion solid phase extraction-step for sample clean-up, and its application on dark chocolate and biscuit samples for five nut multi-allergen determination. In fact, reliability of the LC-MS analysis strongly depends on the overall quality of the sample extract. The sample treatment protocol was devoted to the analysis of five proteins corresponding to the five most important nut allergens

(Ana o 2, cashewnut; Cor a 9, hazelnut; Pru 1, almond; Jug r 4, walnut; Ara h3/4, peanut). To assess analytical method performance, validation of the method was performed in terms of sensitivity, selectivity, accuracy, recovery, limits of detection and quantification in the food matrices under investigation. The method was then applied for the analysis of nut traces in commercially available commodities.

Materials and methods

Reagents and Chemicals

Water was obtained with a MilliQ element A10 System (S. Francisco, CA, USA). Bicarbonate buffer (pH 8.0), acetonitrile (HPLC purity), trifluoroacetic acid (TFA), formic acid (analytical reagent grade), trypsin from bovine pancreas, dithiothreitol (DTT) and iodoacetamide (IAM) were purchased from Sigma Aldrich (Milan, Italy). Roasted peanuts (*Arachis hypogea*), walnuts (*Juglans regia*), hazelnuts (*Corylus avellana*), almonds (*Prunus dulcis*), cashewnuts (*Anacardium occidentale*), commercial biscuits and dark chocolate were obtained at a local food store. Biscuits and dark chocolates used as blank samples did not report the precautionary label "may contain trace of nuts, milk and soy".

Sample treatment

The protein extracts were prepared by adding 10 mL of 50 mM bicarbonate buffer (pH 8.0) to 1 g of ground sample, and then performing a 6 hour extraction at 60°C. Food extract protein was then reduced (10 mM dithiothreitol, 45 min, 37°C) and alkylated (40 mM iodoacetamide, 45 min, room temperature, dark room). Protein purification by size-exclusion step was performed according to our previous work.[19] More precisely, to purify proteins from the sample extracts the size exclusion columns Bio-Spin 6 (Bio-Rad Laboratories, Milan, Italy) with a 6 kDa exclusion limit were used. Firstly, the column was centrifuged for 2 min in a swinging bucket centrifuge at 1000×g in order to remove the packing buffer and then it was conditioned three times with 500 µL of 50 mM bicarbonate buffer (pH 8.0) and centrifuged for 1 min. One hundred µL of the extract were loaded directly on the column and centrifuged for 4 min. The purified sample (100 µL) was thus collected in a 2.0 mL microcentrifuge tube. Enzymatic digestion was carried out by adding 8 µL of 4 mg mL^{-1} trypsin solution to 100 µL of purified protein extract (protein:enzyme ratio 50:1) and carried out at 50 °C overnight. The digestion reaction was quenched with 2 µL TFA.

LC-MS analytical method

LC separation was carried out on a HPLC system (Thermo Electron Corporation, San Josè, CA, USA) with a flow-rate of 200 µL min^{-1}. A C18 Kinetex (100mm×2.1mm, 2.7 µm particles) (Phenomenex, CA, USA) column thermostated at 25 °C was used. Gradient elution separation was carried out under the following conditions [(A) aqueous formic acid 0.1% solution (*v/v*) and (B) 0.08% (*v/v*) formic

acid in acetonitrile]: solvent B was set at 2% for 2 min, then delivered by a linear gradient from 2% to 25% in 9 min and to 60% in 1 min. Solvent B was maintained at 60% for 1 min before column re-equilibration (7 min).

Mass spectrometer device was an LTQ XL linear ion trap (Thermo Electron Corporation) equipped with a pneumatically assisted ESI interface. The sheath gas (nitrogen, 99.9% purity) and the auxiliary gas (nitrogen, 99.9% purity) were delivered at flow rates of 45 and 5 arbitrary units, respectively. Source conditions were as follows: ESI voltage 3.5 kV, capillary voltage 20 V, tube lens 20 V, capillary temperature 270 °C. In a preliminary step, raw tryptic digest extracts from a mixture of the five nuts under investigation were analysed in data-dependent acquisition (DDA) mode under full scan conditions in the 300-1300 *m/z* mass range and excluding any singly charged species. Collision gas (He) pressure was set at 2.1×10^{-3} mbar in the collision cell, with a collision energy equal to 30 arbitrary units. The product ion spectra obtained from data dependent acquisition were processed using BioWorks 3.3 software (Thermo Electron Corporation) with stringent criteria, against a FASTA database containing only the five proteins selected and specifying iodoacetamine derivative of cysteine (+57) as a fixed modification.

Table 2.2.1. SRM transitions monitored for the five allergen proteins (MS^2 mode, collision energy 30 eV). [a] Transition monitored for the calculation of the validation parameters

Allergen (source, UNIPROT ID)	Peptide	SRM transitions (m/z)
Ana o 2 (Anacardium occidentale, Q8GZP6)	VFGDEVR	412/575a 412/460
	AMTSPLAGR	452/443a 452/701
Cor a 9 (Corylus avellana, Q8W1C2)	QEWER	374/365a 374/490
	ADIYTEQVGR	577/567a 577/689
Pru 1 (Prunus dulcis, Q43607)	QQEQLQQER	594/585a 594/576
	NQIIQVR	436/427a 436/402
Ara h 3/4 (Arachis hypogea, Q8LKN1)	FNLAGNHEQEFLR	526/658a 526/601
	SPDIYNPQAGSLK	695/977a 695/815
Jug r 4 (Juglans regia, Q2TPW5)	LDALEPTNR	515/487a 515/616
	ADIYTEEAGR	563/514a 563/470

From the peptide list generated, two biomarker peptides for each protein were selected with the same criteria used in the previous work,[160] i.e. signal intensity of the most abundant fragment of MS/MS spectrum, no post translational modification sites, absence of missed cleavages and sequence specificity (BLAST

search, *www.blast.ncbi.nlm.nih.gov/Blast.cgi*).Transitions for selected reaction monitoring (SRM) analysis were carefully selected on the basis of sensitivity and selectivity criteria (Table 2.2.1).

Method validation

Validation of the whole analytical method was performed on fortified samples of biscuits and dark chocolate according to Eurachem guidelines.[157] To this aim, food samples were fortified by adding a homogenized mixture of the five ground nuts at different amounts before extraction. To obtain a homogeneous nut mixture, same amounts of the five ground nuts were mixed and spun on a mixer for 30 min, by refrigerating with liquid nitrogen. Measurements were carried out by monitoring the most abundant MS^2 transition for each peptide (Table 2.2.1). The detection limits (LOD) and the quantification limits (LOQ) were calculated from the calibration curve as 3 *s*/slope and 10 *s*/slope, respectively, where *s* is the standard deviation of the blank signal obtained from ten independent blank measurements. Linear dynamic range was investigated starting from LOQ values of each peptide to 10000 mg/kg (ten concentration levels, two replicates for each level). Precision was assessed as RSD% for each compound in terms of intra-day repeatability and inter-day repeatability. For this purpose, the within-day repeatability was evaluated by performing three independent extractions of each matrix fortified with 50 and 100 mg nuts/kg matrix and three LC–MS^2 injections for each extract in the same day. The inter-day repeatability was calculated on five days by performing five independent extractions of the matrix fortified with 50 and 100 mg nuts/kg matrix and three LC–MS^2 injections for each extract. Matrix effect was tested by performing a *t*-test between curves calculated on matrix samples and on standard solutions. Recovery of the whole method was evaluated by analysing in triplicate a matrix fortified sample at two concentration levels, i.e. 5 and 100 mg nuts/kg matrix in the case of biscuits, 50 and 100 mg nuts/kg matrix in the case of dark chocolate, using different batches of nuts and matrices. The recovery was calculated as a ratio in percent (%) of determined and added nut content (= (determined mg nut/kg matrix / added mg nut/kg matrix) ×100).

Results and discussion

Sample treatment and peptide selection

For the analysis of complex matrices as dark chocolate, an efficient sample clean-up step is fundamental for an accurate detection and quantification of trace allergenic proteins. Since chemical and physical matrix properties have significant effect on the extraction efficiency, it is important the use of an extraction and purification procedure applicable for the determination of hidden allergens in most food matrices. For these reasons, with the aim of improving method accuracy and sensitivity in terms of limit of detection and quantification we evaluated the use of a clean-up step by size exclusion chromatography before enzymatic digestion. For

this purpose, we used columns having an exclusion limit of 6 kDa specifically designed to clean protein samples quickly (the process takes about 10 min) in such a way to retain low molecular weight components as carbohydrates and lipids. Furthermore, with the aim of improving the digestion protocol in terms of repeatability and efficiency, protein structures were unfolded by reduction/alkylation steps performed just before enzymatic digestion. The implementation of this sample preparation procedure resulted in a sequence coverage average of about 50%, a greater value with respect to that obtained in the previous work (~35%).[160] On the basis of the new sequence coverage and increased signal intensity, for all allergens except for Cor a 9 it was possible to select some peptides exhibiting higher sensitivity with respect to those chosen in the previous study.[18] It has to be stated that the peptide LDALEPTNR, related to walnut, occurs also in Car i 4, a major allergen in pecan nut. Representative LC–IT-MS^2 chromatograms of the ten targeted peptides from the analysis of a tryptic digest of purified biscuit and chocolate blank matrices fortified with five nut mix are illustrated in Figure 2.2.1 and Figure 2.2.2.

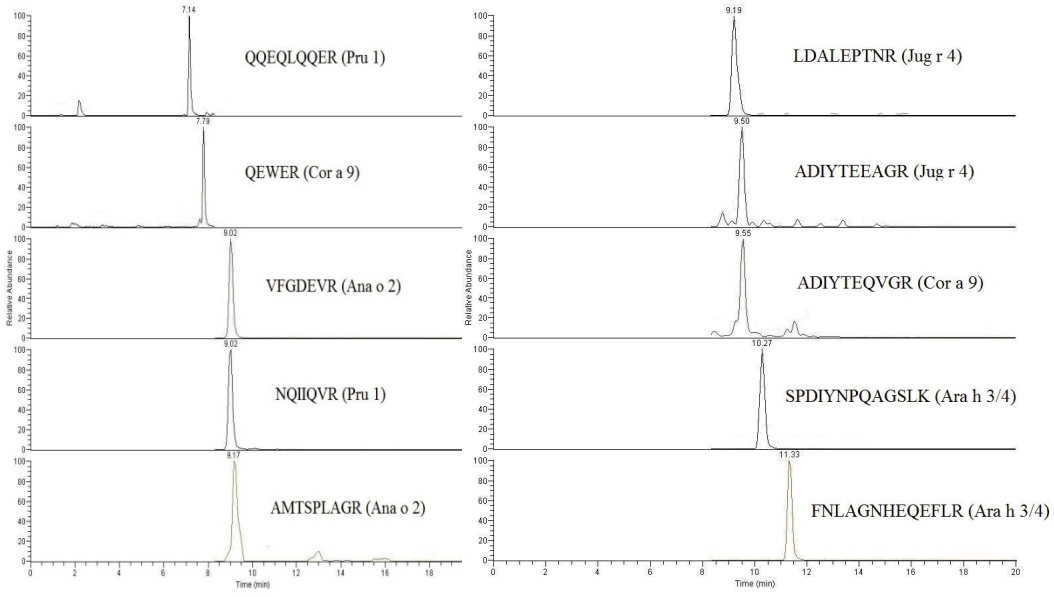

Figure 2.2.1. Selected reaction monitoring LC-ESI-MS^2 chromatograms of the ten targeted peptides from a tryptic digest of a purified biscuit sample. Blank matrix was fortified with a mixture of the five nuts 0.01% (*w/w*)

Method validation

Method validation was carried out in terms of limits of detection and quantification, linear dynamic ranges, accuracy, recovery and selectivity.

As illustrated in Tables 2 and 3, excellent LOD and LOQ values were obtained for each nut. In particular, LODs ranging from 0.1 to 1.3 mg nut/kg for biscuits and

from 5 to 15 mg nut/kg for chocolate were calculated. LOQ values were in the 0.3-4.5 mg nut/kg biscuit and in the 18-50 mg nut/kg chocolate ranges.

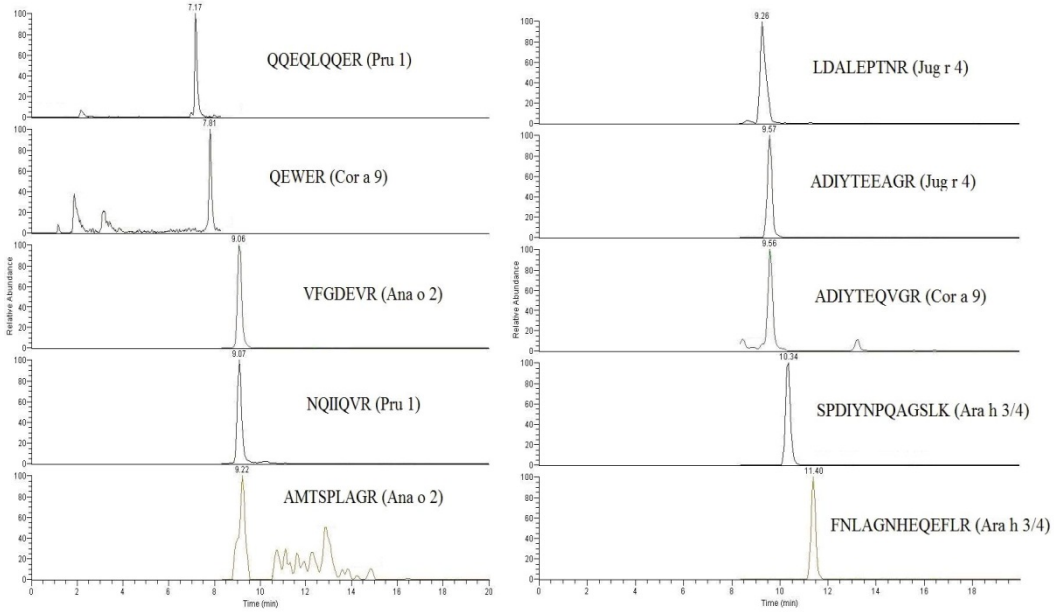

Figure 2.2.2. Selected reaction monitoring LC-ESI-MS^2 chromatograms of the ten targeted peptides from a tryptic digest of a purified dark chocolate sample. Blank matrix was fortified with the five nuts 0.1% (*w/w*)

As expected, for all peptides LOD and LOQ values in chocolate resulted higher of about one order of magnitude than those obtained in biscuits owing to increased complexity of the matrix.

Table 2.2.2. Validation data for the quantitative analysis of nut allergens in biscuits under MS^2 acquisition mode. Concentrations are referred to the matrix fortified with a mix of the five nuts (mg nut/kg matrix)

Allergen	**Peptide**	**LOD (mg kg^{-1})**	**LOQ (mg kg^{-1})**	**Linear dynamic range (mg kg^{-1})**	**Calibration curve Y=b(±sb)X**	**r^2 (n)**
Ana o 2 (cashewnut)	AMTSPLAGR	0.5	1.6	2-10000	170000±8000	0.999 (20)
Cor a 9 (hazelnut)	QEWER	1.3	4.5	5-10000	87000±3000	0.992 (20)
Pru 1 (almond)	NQIIQVR	0.9	3.1	3-10000	206000±8000	0.998 (20)
Ara h 3/4 (peanut)	FNLAGNHEQEFLR	0.1	0.3	0.5-1000	250000±4000	0.999 (18)
Jug r 4 (walnut)	ADIYTEEAGR	0.8	2.6	3-10000	90000±5000	0.998 (20)

Table 2.2.3. Validation data for the quantitative analysis of nut allergens in dark chocolate under MS^2 acquisition mode. Concentrations are referred to the matrix fortified with a mix of the five nuts (mg nut/kg matrix)

Allergen	Peptide	LOD (mg kg^{-1})	LOQ (mg kg^{-1})	Linear dynamic range (mg kg^{-1})	Calibration curve Y=b(±sb)X	r^2 (n)
Ana o 2 (cashewnut)	VFGDEVR	15	50	50-10000	39000±800	0.985 (16)
Cor a 9 (hazelnut)	ADIYTEQVGR	14	49	50-10000	11500±400	0.981 (16)
Pru 1 (almond)	NQIIQVR	9	30	30-10000	50000±1000	0.984 (16)
Ara h 3/4 (peanut)	FNLAGNHEQEF LR	7	25	25-1000	27000±400	0.997 (12)
Jug r 4 (walnut)	LDALEPTNR	5	18	20-10000	15000±700	0.971 (18)

For biscuit samples, linearity was excellent up to four orders of magnitude for all peptides with determination coefficients ($r^2 \geq 0.99$). For chocolate samples, a good linear dynamic range ($r^2 \geq 0.97$) up to three orders of magnitude was achieved. Linearity was demonstrated by variance homogeneity assessment ($p>0.05$) and by applying the Mandel fitting test after calculation of linear curve equations for each targeted peptide; p values greater than 0.01 allowed to confirm that the quadratic model was not significantly better than the linear one. In addition, no significant intercepts confirmed the absence of constant systematic errors at a confidence level of 95%. Good results were obtained also for method precision, intra-day precision ranging between 3 and 11% (n=9). For inter-day precision RSD% values lower than 19% (n=75) were always obtained.

To verify matrix effect, systematic proportional errors were calculated with a *t*-test by comparing calibration curve slopes obtained for the aqueous tryptic digests and the matrix tryptic digests ($p<0.05$). For both types of matrix, significant ion suppression was observed from matrices to standard solutions in terms of a decrease of curve slopes. In the case of biscuits, a reduction in sensitivity from 6 to 33% with respect to the aqueous tryptic digest was evidenced. On the other hand, in the case of dark chocolate a stronger suppression effect was observed, with a lack of sensitivity in the range of 16-58% owing to the increased complexity of the matrix compared to biscuits. Hence, to overcome matrix effect matrix-matched calibration curves were built up to perform a label-free quantification method. Method recoveries obtained in the case of biscuits were in the 84(±6)-106(±4)% range at the low and high fortification level. Similarly, recoveries from chocolate were found to vary between 98(±5) and 108(±6)% at the 50 and 100 mg nuts/kg matrix spiking level, respectively.

Enhanced performances of the new approach were evaluated by comparing it to the previous one[18] in terms of quality parameters. For all nuts values of both

LODs and LOQs lower of at least one order of magnitude were obtained in biscuits, with the advantage to detect and quantify five allergenic proteins at very low concentration levels in the same chromatographic run. On the basis of these findings, it can be inferred that the introduction of the size exclusion purification step resulted to be helpful both for allergen detectability and for linearity, since a wider linear range of response was observed.

Sample analysis

In the final part of the work, an important step was represented by sample analysis. The successfully validated method was applied to evaluate the presence of allergens of the five nuts under investigation in different brands of biscuits and dark chocolate samples. In particular, the applicability of the method was tested following two approaches: the first had the final aim of ascertaining possible discrepancies between allergen content and food allergen labelling in positive samples; the second one had the final goal of investigating presence of hidden nut allergens in samples not including peanuts or tree nuts as ingredients. In all the cases, the identification criteria were retention time and comparison of fragmentation spectra between sample and an aqueous extract. For the first purpose, nut contents were estimated in two biscuit and in two chocolate samples having nuts as declared ingredients. As can be seen from Table 2.2.4, the quantitative results are in excellent agreement with the labelled values, proving the reliability and the trueness of the method. Examples of separation of the targeted peptides in a hazelnut-biscuit and a hazelnut-chocolate extract are depicted in Figure 2.2.3 and Figure 2.2.4, respectively.

Table 2.2.4. LC-ESI-MS^2 determination of the hazelnut content in the food samples investigated (n=3)[a]

	Hazelnut (%)	
Samples	Calculated content	Declared label content
Hazelnut-biscuit (Brand 1)	1.7±0.1	1.8
Hazelnut-biscuit (Brand 2)	0.42±0.04	0.5
Hazelnut-dark chocolate (Brand 3)	20±3	20
Hazelnut-dark chocolate (Brand 4)	23±4	23

[a] n = number of independent samples

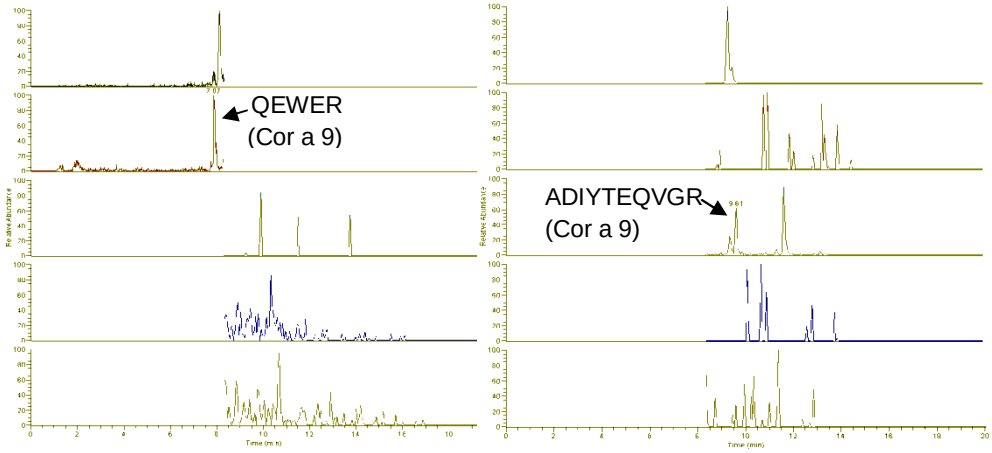

Figure 2.2.3. Selected reaction monitoring LC-ESI-MS^2 chromatograms of the ten targeted peptides in hazelnut-biscuit (brand 1)

For the second purpose, the potentiality of the method for trace multi-allergens detection was proved by analysing five biscuits and five dark-chocolates of different brands among commercially available products that do not include peanuts or tree nuts as ingredients. All the biscuit samples resulted to be negative, whereas two of the five dark chocolate samples under investigation resulted positive to hazelnut (Table 2.2.5, Figure 2.2.5).

Table 2.2.5. LC-ESI-MS^2 determination of hidden allergens (%) in the food samples investigated (n=3)[a,b]

	Cashewnut	Hazelnut	Almond	Peanut	Walnut
Biscuit sample					
A	-	-	-	-	-
B	-	-	-	-	-
C	-	-	-	-	-
D	-	-	-	-	-
E	-	-	-	-	-
Dark-chocolate sample					
F	-	-	-	-	-
G	-	0.07±0.01	-	-	-
H	-	-	-	-	-
I	-	0.15±0.03	-	-	-
L	-	-	-	-	-

[a] n = number of independent samples
[b] -, not detected

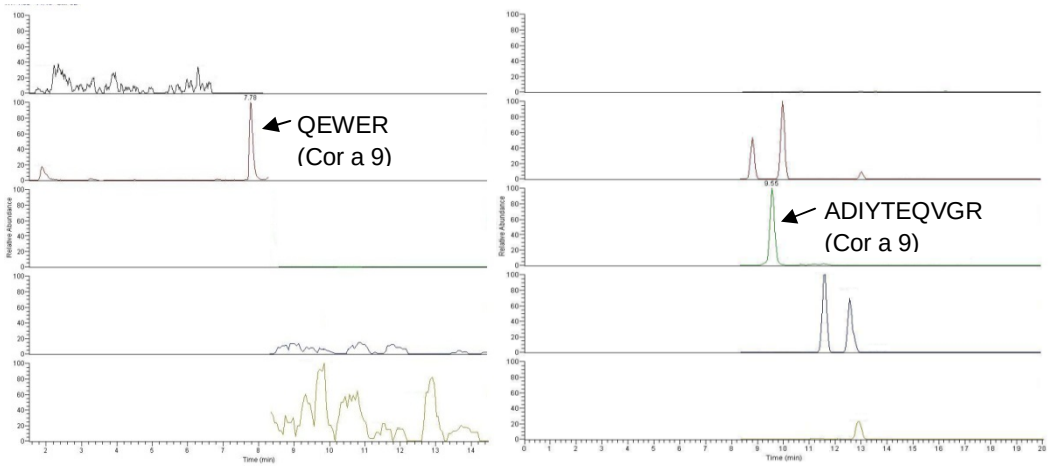

Figure 2.2.4. Selected reaction monitoring LC-ESI-MS^2 chromatograms of the ten targeted peptides in hazelnut-dark chocolate (brand 3)

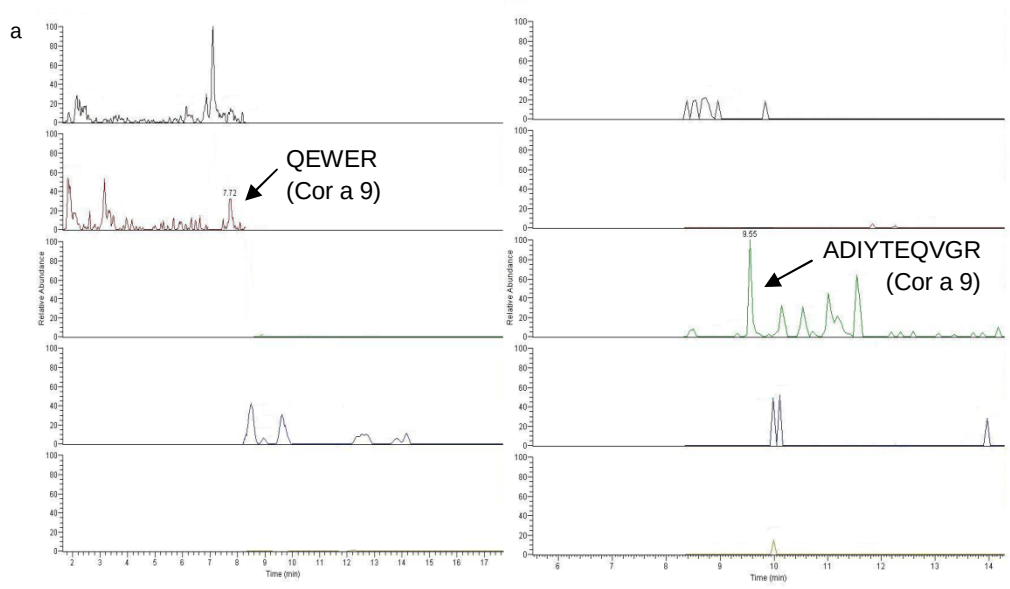

Figure 2.2.5 depicts the chromatographic separation of a chocolate sample showing signals corresponding to both the hazelnut peptides monitored. Figure 2.2.5b and Figure 2.2.5c illustrate this result for the product ion mass spectrum of the precursor ion at m/z 577 of the ADIYTEQVGR peptide. A good correspondence of the spectra (14/23 fragment ions) with those recorded by analysing a hazelnut extract allows us to confirm the presence of hazelnut traces in the analysed sample.

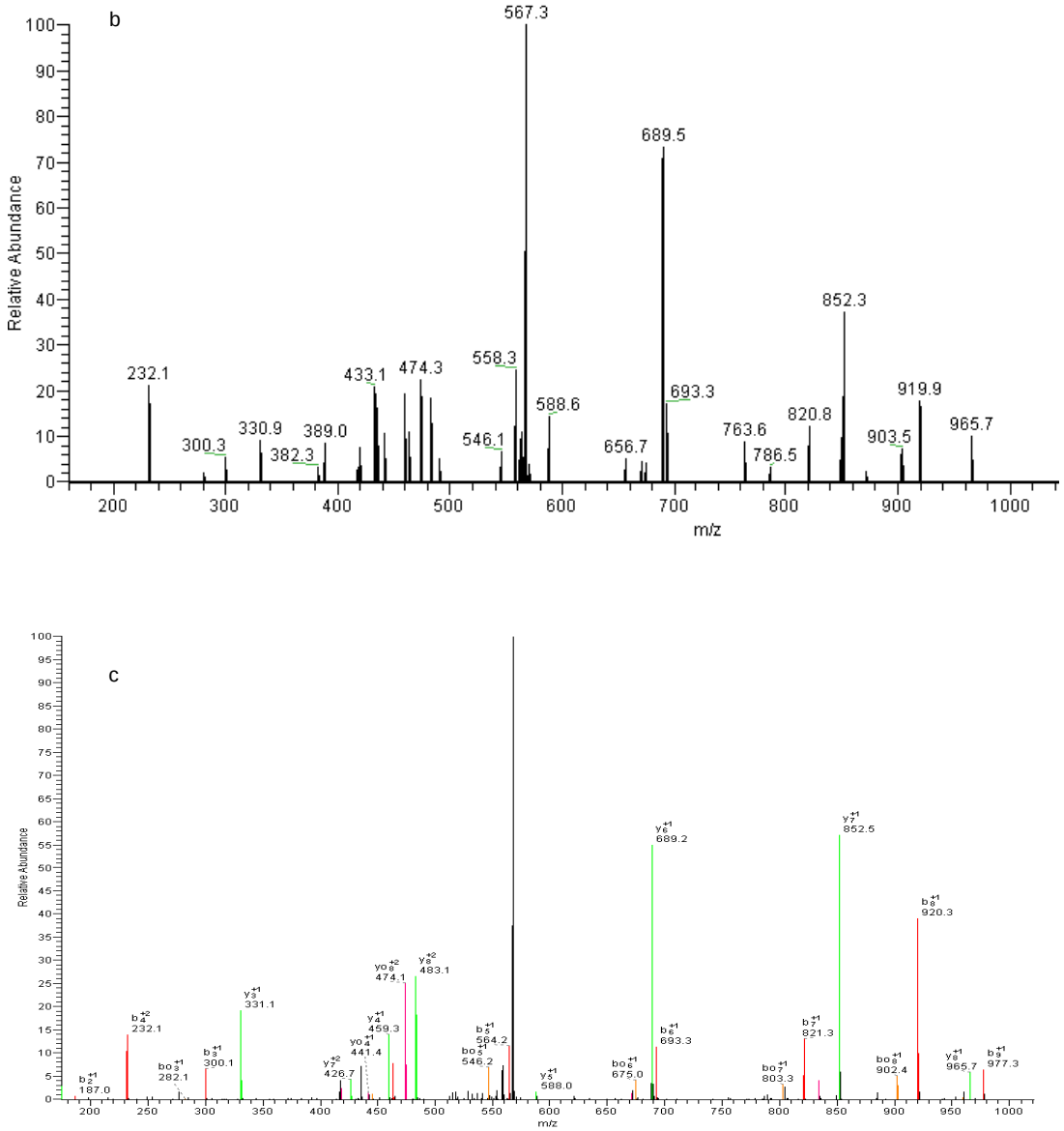

Figure 2.2.5. (a) Selected reaction monitoring LC-ESI-MS^2 chromatograms of the ten targeted peptides in a dark chocolate sample not including peanuts or tree nuts in the ingredient label (sample G). (b) Product ion mass spectrum of the precursor ion at *m/z* 577 corresponding to the signal at 9.55 min, assigned to the hazelnut ADIYTEQVGR peptide. (c) BioWorks-matched product ion mass spectrum of the precursor ion at *m/z* 577, which was attributed by the software to the ADIYTEQVGR peptide (the base peak in the mass spectrum at *m/z* 567 corresponds to the loss of water from the doubly charged precursor ion)

Conclusions

The determination of hidden allergens at trace levels in a complex food sample as dark chocolate requires the application of efficient extraction procedures and accurate analytical methods. This work demonstrated the potentiality of the size exclusion-based sample treatment able to efficiently clean-up complex food extracts for the sensitive detection of hidden food allergens. The sample treatment proposed proved effective in determining a significant improvement both in protein sequence coverage for peptide-based biomarker discovery related to food allergies and in sensitivity of the multi-allergen LC-MS^2 method, fully taking advantage of the highly selective SRM analysis. Thanks to the very low limits of detection and quantification reached, the extended linearity range and the rapidity of the analysis, this method could be proposed for strict allergen quality controls of both the final products and the production lines for food manufacturers in order to protect consumer health and safety.

Acknowledgements

The authors acknowledge funding support from the interdepartmental research center on food safety and technology SITEIA.PARMA of the Parma Technopole (Emilia-Romagna High Technology Network) and from the Italian Ministry for the University and Research (MIUR) with the PNR Project n. RBIP06SXMR “Sviluppo di metodologie innovative per l’analisi di prodotti agroalimentari”.

References

(1) Fenn, J. B.; Mann, M.; Meng, C. K.; Wong, S. F.; Whitehouse, C. M. *Science* **1989**, *246*, 64.

(2) Karas, M.; Bachmann, D.; Hillenkamp, F. *Anal Chem* **1985**, *57*, 2935.

(3) Laiko, V. V.; Baldwin, M. A.; Burlingame, A. L. *Anal Chem* **2000**, *72*, 652.

(4) Venter, A.; Nefliu, M.; Cooks, R. G. *Trac-Trend Anal Chem* **2008**, *27*, 284.

(5) Takats, Z.; Wiseman, J. M.; Gologan, B.; Cooks, R. G. *Science* **2004**, *306*, 471.

(6) Morris, H. R.; Panico, M.; Barber, M.; Bordoli, R. S.; Sedgwick, R. D.; Tyler, A. *Biochemical and biophysical research communications* **1981**, *101*, 623.

(7) Benninghoven, A. *Phys Status Solidi* **1969**, *34*, K169.

(8) Badu-Tawiah, A.; Cooks, R. G. *J Am Soc Mass Spectr* **2010**, *21*, 1423.

(9) Bereman, M. S.; Muddiman, D. C. *J Am Soc Mass Spectr* **2007**, *18*, 1093.

(10) De Hoffmann, E.; Stroobant, V. *Mass spectrometry: principle and applications; Wiley VCH* **2007**.

(11) Shin, Y. S.; Drolet, B.; Mayer, R.; Dolence, K.; Basile, F. *Anal Chem* **2007**, *79*, 3514.

(12) Qiu, B.; Luo, H. *J Mass Spectrom* **2009**, *44*, 772.

(13) Nefliu, M.; Smith, J. N.; Venter, A.; Cooks, R. G. *J Am Soc Mass Spectr* **2008**, *19*, 420.

(14) Myung, S.; Wiseman, J. M.; Valentine, S. J.; Takats, Z.; Cooks, R. G.; Clemmer, D. E. *J Phys Chem B* **2006**, *110*, 5045.

(15) Gao, L.; Li, G. T.; Cyriac, J.; Nie, Z. X.; Cooks, R. G. *J Phys Chem C* **2010**, *114*, 5331.

(16) Grimm, R. L.; Beauchamp, J. L. *J Phys Chem B* **2005**, *109*, 8244.

(17) Takats, Z.; Wiseman, J. M.; Cooks, R. G. *J Mass Spectrom* **2005**, *40*, 1261.

(18) Cotte-Rodriguez, I.; Takats, Z.; Talaty, N.; Chen, H. W.; Cooks, R. G. *Anal Chem* **2005**, *77*, 6755.

(19) Kertesz, V.; Ford, M. J.; Van Berkel, G. J. *Anal Chem* **2005**, *77*, 7183.

(20) Wiseman, J. M.; Ifa, D. R.; Song, Q. Y.; Cooks, R. G. *Angew Chem Int Edit* **2006**, *45*, 7188.

(21) Hu, L. C.; Shea, K. J. *Chem Soc Rev* **2011**, *40*, 688.

(22) Hench, L. L.; West, J. K. *Chem Rev* **1990**, *90*, 33.

(23) Attia, S. M.; Wang, J.; Wu, G. M.; Shen, J.; Ma, J. H. *J Mater Sci Technol* **2002**, *18*, 211.

(24) Brinker, C. J.; Scherer, G. W. *Sol-Gel Science: The Physics and Chemistry of Sol-Gel Processing. Academic Press* **1990**.

(25) Klein, L. C. *Sol-Gel Optics: Processing and Applications. Springer Verlag* **1994**.

(26) Ulman, A. *Chem Rev* **1996**, *96*, 1533.

(27) Bigelow, W. C.; Pickett, D. L.; Zisman, W. A. *J Colloid Sci* **1946**, *1*, 513.

(28) Nuzzo, R. G.; Allara, D. L. *J Am Chem Soc* **1983**, *105*, 4481.

(29) Plueddemann, E. P. *Journal of Adhesion* **1970**, *2*.

(30) Pape, P. G.; Plueddemann, E. P. *Journal of Adhesion Science and Technology* **1991**, *5*, 842.

(31) Osterholtz, F. D.; Pohl, E. R. *Journal of Adhesion Science and Technology* **1992**, *6*, 127.

(32) Duchet, J.; Chabert, B.; Chapel, J. P.; Gerard, J. F.; Chovelon, J. M.; JaffrezicRenault, N. *Langmuir* **1997**, *13*, 2271.

(33) Brzoska, J. B.; Benazouz, I.; Rondelez, F. *Langmuir* **1994**, *10*, 4367.

(34) Witucki, G. L. *J Coating Technol* **1993**, *65*, 57.

(35) Roumeliotis, P.; Unger, K. K. *Journal of Chromatography* **1978**, *149*, 211.

(36) Fadeev, A. Y.; McCarthy, T. J. *Langmuir* **2000**, *16*, 7268.

(37) Mcgovern, M. E.; Kallury, K. M. R.; Thompson, M. *Langmuir* **1994**, *10*, 3607.

(38) Bigelow, W. C.; Pickett, D. L.; Zisman, W. A. *J Coll Sci Imp U Tok* **1946**, *1*.

(39) Maoz, R.; Sagiv, J. *J Colloid Interf Sci* **1984**, *100*

(40) Takats, Z.; Wiseman, J. M.; Cooks, R. G. *J Mass Spectrom* **2005**, *40*, 1261.

(41) Ifa, D. R.; Jackson, A. U.; Paglia, G.; Cooks, R. G. *Anal Bioanal Chem* **2009**, *394*, 1995.

(42) Cheng, S. C.; Lin, Y. S.; Huang, M. Z.; Shiea, J. *Rapid Commun Mass Spectrom* **2010**, *24*, 203.

(43) Wu, C.; Qian, K.; Nefliu, M.; Cooks, R. G. *J Am Soc Mass Spectrom* **2010**, *21*, 261.

(44) Manicke, N. E.; Kistler, T.; Ifa, D. R.; Cooks, R. G.; Ouyang, Z. *J Am Soc Mass Spectrom* **2009**, *20*, 321.

(45) Green, F. M.; Stokes, P.; Hopley, C.; Seah, M. P.; Gilmore, I. S.; O'Connor, G. *Anal Chem* **2009**, *81*, 2286.

(46) Ifa, D. R.; Manicke, N. E.; Rusine, A. L.; Cooks, R. G. *Rapid Commun Mass Spectrom* **2008**, *22*, 503.

(47) Kennedy, J. H.; Wiseman, J. M. *Rapid Commun Mass Spectrom* **2010**, *24*, 309.

(48) Paglia, G.; Ifa, D. R.; Wu, C.; Corso, G.; Cooks, R. G. *Anal Chem* **2010**, *82*, 1744.

(49) Wu, C.; Ifa, D. R.; Manicke, N. E.; Cooks, R. G. *Analyst* **2010**, *135*, 28.

(50) Wiseman, J. M.; Ifa, D. R.; Song, Q.; Cooks, R. G. *Angew Chem Int Ed Engl* **2006**, *45*, 7188.

(51) Wiseman, J. M.; Ifa, D. R.; Venter, A.; Cooks, R. G. *Nat Protoc* **2008**, *3*, 517.

(52) Kertesz, V.; Van Berkel, G. J.; Vavrek, M.; Koeplinger, K. A.; Schneider, B. B.; Covey, T. R. *Anal Chem* **2008**, *80*, 5168.

(53) Watrous, J.; Hendricks, N.; Meehan, M.; Dorrestein, P. C. *Anal Chem* **2010**, *82*, 1598.

(54) Chipuk, J. E.; Gelb, M. H.; Brodbelt, J. S. *Anal Chem* **2010**, *82*, 16.

(55) Pasilis, S. P.; Kertesz, V.; Van Berkel, G. J. *Anal Chem* **2007**, *79*, 5956.

(56) Volny, M.; Venter, A.; Smith, S. A.; Pazzi, M.; Cooks, R. G. *Analyst* **2008**, *133*, 525.

(57) Mahltig, B.; Audenaert, F.; Bottcher, H. *J Sol-Gel Sci Techn* **2005**, *34*, 103.

(58) Pilotek, S.; Schmidt, H. K. *J Sol-Gel Sci Techn* **2003**, *26*, 789.

(59) Ameduri, B.; Boutevin, B.; Moreau, J. J. E.; Moutaabbid, H.; Man, M. W. C. *J Fluorine Chem* **2000**, *104*, 185.

(60) Lin, Y. S.; Chen, Y. C. *Anal Chem* **2002**, *74*, 5793.

(61) Wei, Y.; Yeh, J. M.; Jin, D. L.; Jia, X. R.; Wang, J. G.; Jang, G. W.; Chen, C. C.; Gumbs, R. W. *Chem Mater* **1995**, *7*, 969.

(62) Wu, S. J. *Polym Sci Part C* **1971**, *34*, 19.

(63) Feher, F. J., T.A. Budzichowski *J. Organomet. Chem.* **1989**, *373*, 153.

(64) Degarmo, E. P., J.T. Black, R.A. Kohser *Materials and Processes in Manufacturing (9th ed.)*, 2003.

(65) Komori, Y.; Nakashima, H.; Hayashi, S.; Sugahara, Y. *J Non-Cryst Solids* **2005**, *351*, 97.

(66) Zerda, T. W.; Hoang, G. *J Non-Cryst Solids* **1989**, *109*, 9.

(67) Schmidt, H.; Kaiser, A.; Rudolph, M.; Lentz, A.; Science of cercamic chemical processing, W., NY, p.87 **1986**.

(68) Penna, A.; Elviri, L.; Careri, M.; Mangia, A.; Predieri, G. *Anal Bioanal Chem* **2011**, *400*, 1515.

(69) Feher, F. J.; Newman, D. A.; Walzer, J. F. *J Am Chem Soc* **1989**, *111*, 1741.

(70) Feher, F. J.; Budzichowski, T. A.; Blanski, R. L.; Weller, K. J.; Ziller, J. W. *Organometallics* **1991**, *10*, 2526.

(71) Prabakar, S.; Assink, R. A.; Raman, N. K.; Myers, S. A.; Brinker, C. J. *J Non-Cryst Solids* **1996**, *202*, 53.

(72) Cordes, D. B.; Lickiss, P. D.; Rataboul, F. *Chem Rev* **2010**, *110*, 2081.

(73) Tiddy, G. J. T. *Phys. Rep.* **1980**, *57*.

(74) Bunker, B. C.; Carpick, R. W.; Assink, R. A.; Thomas, M. L.; Hankins, M. G.; Voigt, J. A.; Sipola, D.; de Boer, M. P.; Gulley, G. L. *Langmuir* **2000**, *16*, 7742.

(75) Brandriss, S.; Margel, S. *Langmuir* **1993**, *9*, 1232.

(76) Parikh, A. N.; Liedberg, B.; Atre, S. V.; Ho, M.; Allara, D. L. *J Phys Chem-Us* **1995**, *99*, 9996.

(77) Allara, D. L.; Parikh, A. N.; Rondelez, F. *Langmuir* **1995**, *11*, 2357.

(78) Legrange, J. D.; Markham, J. L.; Kurkjian, C. R. *Langmuir* **1993**, *9*, 1749.

(79) Parikh, A. N.; Allara, D. L.; Azouz, I. B.; Rondelez, F. *J Phys Chem-Us* **1994**, *98*, 7577.

(80) Doudevski, I.; Schwartz, D. K. *J Am Chem Soc* **2001**, *123*, 6867.

(81) Rozlosnik, N.; Gerstenberg, M. C.; Larsen, N. B. *Langmuir* **2003**, *19*, 1182.

(82) Krasnoslobodtsev, A. V.; Smirnov, S. N. *Langmuir* **2002**, *18*, 3181.

(83) Leitner, T.; Friedbacher, G.; Vallant, T.; Brunner, H.; Mayer, U.; Hoffmann, H. *Mikrochim Acta* **2000**, *133*, 331.

(84) Powell, C. J. *The Physical Basis for Quantitative Surface Analysis by Auger Electron Spectroscopy* **1978**.

(85) Scofield, J. H. *J. Electron Spectrosc. Relat. Phenom.* **1976**, *8*, 129.

(86) Reilman, R. F.; Msezane, A.; Manson, S. T. *J. Electron Spectrosc. Relat. Phenom.* **1976**, *8*, 389.

(87) Seah, M. P. D., W. A. *Surf. Interface Anal.* **1979**, *1*, 2.

(88) Tanuma, S.; Powell, C. J.; Penn, D. R. *Surf Interface Anal* **1991**, *17*, 911.

(89) Tanuma, S.; Powell, C. J.; Penn, D. R. *Surf Interface Anal* **2003**, *35*, 268.

(90) Chen, J. J.; Struk, K. N.; Brennan, A. B. *Langmuir* **2011**, *27*, 13754.

(91) Nishino, T.; Meguro, M.; Nakamae, K.; Matsushita, M.; Ueda, Y. *Langmuir* **1999**, *15*, 4321.

(92) Can, K.; Ozmen, M.; Gurfidan, L.; Gubbuk, I. H.; Kaymak, E.; Ersoz, M.; Ozbek, Z.; Capan, R. *J Optoelectron Adv M* **2010**, *12*, 1552.

(93) Cras, J. J.; Rowe-Taitt, C. A.; Nivens, D. A.; Ligler, F. S. *Biosens Bioelectron* **1999**, *14*, 683.

(94) Singh, J.; Whitten, J. E. *J Phys Chem C* **2008**, *112*, 19088.

(95) Stevens, M. J. *Langmuir* **1999**, *15*, 2773.

(96) Yokota, K.; Takai, K.; Enoki, T. *Nano Lett* **2011**, *11*, 3669.

(97) Senkevich, J. J.; Mitchell, C. J.; Yang, G. R.; Lu, T. M. *Langmuir* **2002**, *18*, 1587.

(98) Beurer, E.; Venkataraman, N. V.; Rossi, A.; Bachmann, F.; Engeli, R.; Spencer, N. D. *Langmuir* **2010**, *26*, 8392.

(99) Wagner, C. D.; Moulder, J. F.; Davis, L. E.; Riggs, W. M.; Handbook of X-ray photoelectron spectroscopy, P.-E. C., Physical Electronics Division, 1978.

(100) Wagner, C. D.; Passoja, D. E.; Hillery, H. F.; Kinisky, T. G.; Six, H. A.; Jansen, W. T.; Taylor, J. A. *Journal of Vacuum Science and Technology* **1982**, *21*, 933.

(101) Hu, M.; Noda, S.; Tsuji, Y.; Okubo, T.; Yamaguchi, Y.; Komiyama, H. *J Vac Sci Technol A* **2002**, *20*, 589.

(102) Zhang, Y. F.; Liao, L. S.; Chan, W. H.; Lee, S. T.; Sammynaiken, R.; Sham, T. K. *Phys Rev B* **2000**, *61*, 8298.

(103) Wang, X. J.; Hu, W. C.; Ramasubramaniam, R.; Bernstein, G. H.; Snider, G.; Lieberman, M. *Langmuir* **2003**, *19*, 9748.

(104) Hozumi, A.; Ushiyama, K.; Sugimura, H.; Takai, O. *Langmuir* **1999**, *15*, 7600.

(105) Storp, S. *Spectrochim Acta B* **1985**, *40*, 745.

(106) Semak, B. S.; van der Marel, C.; Tougaard, S. *Surf Interface Anal* **2002**, *33*, 238.

(107) Costa, A. B.; Cooks, R. G. *Chem Phys Lett* **2008**, *464*, 1.

(108) Venter, A.; Sojka, P. E.; Cooks, R. G. *Anal Chem* **2006**, *78*, 8549.

(109) Frankevich, V.; Nieckarz, R. J.; Sagulenko, P. N.; Barylyuk, K.; Zenobi, R.; Levitsky, L. I.; Agapov, A. Y.; Perlova, T. Y.; Gorshkov, M. V.; Tarasova, I. A. *Rapid Commun Mass Sp* **2012**, *26*, 1567.

(110) Kaftan, F.; Kofronova, O.; Benada, O.; Lemr, K.; Havlicek, V.; Cvacka, J.; Volny, M. *J Mass Spectrom* **2011**, *46*, 256.

(111) Wood, M. C.; Busby, D. K.; Farnsworth, P. B. *Anal Chem* **2009**, *81*, 6407.

(112) Zivolic, F.; Zancanaro, F.; Favretto, D.; Ferrara, S. D.; Seraglia, R.; Traldi, P. *J Mass Spectrom* **2010**, *45*, 411.

(113) Seraglia, R.; Molin, L.; Isak, I.; Traldi, P. *Eur J Mass Spectrom* **2012**, *18*, 195.

(114) Owens, D. K.; Wendt, R. C. *J Appl Polym Sci* **1969**, *13*.

(115) Yu, S.; Dekker, M.; Polymer Interface and Adhesion, N., 1982.

(116) Reed, J.; Singer, E.; Kresbach, G.; Schwartz, D. C. *Anal Biochem* **1998**, *259*, 80.

(117) Spori, D. M.; Drobek, T.; Zurcher, S.; Spencer, N. D. *Langmuir* **2010**, *26*, 9465.

(118) Clarke, T. A.; Rizkall, E. N. *Chem Phys Lett* **1976**, *37*, 523.

(119) Serway, R. A.; Principles of Physics (2nd ed.), F. W., Texas, Saunders College Publications (1998).

(120) Mudarra, M.; Diaz-Calleja, R.; Belana, J.; Canadas, J. C.; Diego, J. A.; Sellares, J.; Sanchis, M. J. *Polymer* **2001**, *42*, 1647.

(121) Smith, D. P. H. *Ieee T Ind Appl* **1986**, *22*, 527.
(122) Taylor, G. I.; Mcewan, A. D. *Journal of Fluid Mechanics* **1965**, *22*, 1.
(123) Haddad, R.; Sparrapan, R.; Eberlin, M. N. *Rapid Commun Mass Sp* **2006**, *20*, 2901.
(124) Hirabayashi, A.; Sakairi, M.; Koizumi, H. *Anal Chem* **1994**, *66*, 4557.
(125) Green, F. M.; Stokes, P.; Hopley, C.; Seah, M. P.; Gilmore, I. S.; O'Connor, G. *Anal Chem* **2009**, *81*, 2286.
(126) Ranc, V.; Havlicek, V.; Bednar, P.; Lemr, K. *Eur J Mass Spectrom* **2008**, *14*, 411.
(127) Taylor, G. I. *J Fluid Mech* **1965**, *2*, 1.
(128) Mukherjee, S.; Ren, J. H. *J Am Soc Mass Spectr* **2010**, *21*, 1720.
(129) Lim, C.; Bashford, D.; Karplus, M. *J Phys Chem-Us* **1991**, *95*, 5610.
(130) Marsh, J. R.; Weiss, P. J. *Assoc. Office of Anal. Chem.* **1967**, *50*, 457.
(131) Bann, B.; Miller, S. A. *Chem Rev* **1957**, *58*.
(132) Jouyban, A. *Handbook of Solubility Data for Pharmaceuticals, CRC Press* **2009**.
(133) Badu-Tawiah, A.; Bland, C.; Campbell, D. I.; Cooks, R. G. *J Am Soc Mass Spectr* **2010**, *21*, 572.
(134) Douglass, K. A.; J., S.; W.R., B.; Venter, A. R. *J Am Soc Mass Spectr* **2012**, *23*, 1896.
(135) Ortolani, C.; Ispano, M.; Scibilia, J.; Pastorello, E. A. *Allergy* **2001**, *56*, 5.
(136) Anibarro, B.; Seoane, F. J.; Mugica, M. V. *J Invest Allerg Clin* **2007**, *17*, 168.
(137) *European Commission, Off. J. Eur. Union, L 109* **2000**.
(138) *European Commission, Off. J. Eur. Union, L 308* **2003**.
(139) *European Commission, Off. J. Eur. Union, L 368* **2006**.
(140) Bindslev-Jensen, C.; Briggs, D.; Osterballe, M. *Allergy* **2002**, *57*, 741.
(141) Kirsch, S.; Fourdrilis, S.; Dobson, R.; Scippo, M. L.; Maghuin-Rogister, G.; De Pauw, E. *Anal Bioanal Chem* **2009**, *395*, 57.
(142) Schubert-Ullrich, P.; Rudolf, J.; Ansari, P.; Galler, B.; Fuhrer, M.; Molinelli, A.; Baumgartner, S. *Anal Bioanal Chem* **2009**, *395*, 69.
(143) Hurst, W. J.; Krout, E. R.; Burks, W. R. *J Immunoass Immunoch* **2002**, *23*, 451.
(144) Pele, M.; Brohee, M.; Anklam, E.; Van Hengel, A. J. *Food Addit Contam* **2007**, *24*, 1334.
(145) Poms, R. E.; Agazzi, M. E.; Bau, A.; Brohee, M.; Capelletti, C.; Norgaard, J. V.; Anklam, E. *Food Addit Contam* **2005**, *22*, 104.
(146) Monaci, L.; Visconti, A. *Trac-Trend Anal Chem* **2009**, *28*, 581.

(147) Weber, D.; Raymond, P.; Ben-Rejeb, S.; Lau, B. *J Agr Food Chem* **2006**, *54*, 1604.

(148) Shefcheck, K. J.; Callahan, J. H.; Musser, S. M. *J Agr Food Chem* **2006**, *54*, 7953.

(149) Chassaigne, H.; Norgaard, J. V.; Hengel, A. J. *J Agric Food Chem* **2007**, *55*, 4461.

(150) Kerkaert, B.; Mestdagh, F.; De Meulenaer, B. *Food Chem* **2010**, *120*, 580.

(151) Kuppannan, K.; Albers, D. R.; Schafer, B. W.; Dielman, D.; Young, S. A. *Anal Chem* **2011**, *83*, 516.

(152) Monaci, L.; van Hengel, A. J. *J Chromatogr A* **2008**, *1192*, 113.

(153) Monaci, L.; Losito, I.; Palmisano, F.; Visconti, A. *J Chromatogr A* **2010**, *1217*, 4300.

(154) Careri, M.; Elviri, L.; Maffini, M.; Mangia, A.; Mucchino, C.; Terenghi, M. *Rapid communications in mass spectrometry : RCM* **2008**, *22*, 807.

(155) Careri, M.; Elviri, L.; Lagos, J. B.; Mangia, A.; Speroni, F.; Terenghi, M. *J Chromatogr A* **2008**, *1206*, 89.

(156) Careri, M.; Costa, A.; Elviri, L.; Lagos, J. B.; Mangia, A.; Terenghi, M.; Cereti, A.; Garoffo, L. P. *Anal Bioanal Chem* **2007**, *389*, 1901.

(157) *The Fitness for Purpose of Analytical Methods: A Laboratory Guide to Method Validation and Related Topics, Eurachem Guide, 1st English edition 1.0, LGC (Teddington) Ltd., http://www.eurachem.org/.* **1998**.

(158) Sancho, A. I.; Hoffmann-Sommergruber, K.; Alessandri, S.; Conti, A.; Giuffrida, M. G.; Shewry, P.; Jensen, B. M.; Skov, P.; Vieths, S. *Clin Exp Allergy* **2010**, *40*, 973.

(159) Sancho, A. I.; Mills, E. N. C. *Regul Toxicol Pharm* **2010**, *58*, S42.

(160) Bignardi, C.; Elviri, L.; Penna, A.; Careri, M.; Mangia, A. *J Chromatogr A* **2010**, *1217*, 7579.

(161) Mattarozzi, M.; Bignardi, C.; Elviri, L.; Careri, M. *J Agric Food Chem* **2012**.

(162) Heick, J.; Fischer, M.; Popping, B. *J Chromatogr A* **2011**, *1218*, 938.

(163) Ansari, P.; Stoppacher, N.; Rudolf, J.; Schuhmacher, R.; Baumgartner, S. *Anal Bioanal Chem* **2011**, *399*, 1105.

(164) Taylor, S. L.; Nordlee, J. A.; Niemann, L. M.; Lambrecht, D. M. *Anal Bioanal Chem* **2009**, *395*, 83.

(165) Luccioli, S. *Curr Opin Allergy Cl* **2012**, *12*, 323.

(166) Eller, E.; Hansen, T. K.; Bindslev-Jensen, C. *Ann Allerg Asthma Im* **2012**, *108*, 332.

Aknowledgements

I would like to express my warmest gratitude to:
Prof. Maria Careri for giving me the opportunity to work in her research lab and supervising me during my PhD;
Prof. Nicholas D. Spencer and Prof. Antonella Rossi for hosting me to work in their research lab at the ETH in Zurich and for their great scientific support;
Dr Maura Crobu, Dr Lucio Isa, Dr Vikrant Naik, Giovanni Cossu, Andrea Arcifa, Clément Cremmel, Giacomo Fontani, Ang Li, Cathrein Hueckstaedt and all other LSST members for their scientific and personal support.
Thanks are also due to Dr Monica Mattarozzi, Dr Vincenzo Verdolino, Chiara Bignardi and Marco Milioli.